Spontaneous and stimulated emission from quasifree electrons

A. Friedman and A. Gover

Tel Aviv University, Ramat Aviv, Israel 69978
*and Science Applications International Corporation, 1710 Goodridge Drive, P.O. Box 1303, McLean, Virginia 22102**

G. Kurizki

Department of Chemistry, Weizmann Institute, Rehovot, Israel

S. Ruschin

Tel Aviv University, Ramat Aviv, Israel 69978

A. Yariv

Sackle Institute of Advanced Study, Tel Aviv University, Ramat Aviv, Israel 69978
and California Institute of Technology, Pasadena, California 91125†

This article presents a unified formulation and review of an extensive class of radiation effects and devices based on free or quasifree electrons. The effects and devices reviewed include slow-wave radiators [such as Čerenkov, Smith-Purcell, and TWT (traveling-wave tube) effects and devices], periodic bremsstrahlung radiators [such as undulator radiation, magnetic bremsstrahlung FEL's (free-electron lasers), and coherent bremsstrahlung in the crystal lattice], and transverse-binding radiators [such as the CRM (cyclotron resonance maser) and channeling radiation]. Starting from a general quantum-electrodynamic model, both quantum and classical effects and operating regimes of these radiation devices are described. The article provides a unified physical description of the interaction kinematics, and presents equations for the characterization of spontaneous and stimulated radiative emission in these various effects and devices. Universal relations between the spontaneous and stimulated emission parameters are revealed and shown to be related (in the quantum limit) to Einstein relations for atomic radiators and (in the classical limit) to the relations derived by Madey for magnetic bremsstrahlung FEL for on-axis radiative emission. Examples for the application of the formulation are given, estimating the feasibility of channeling radiation x-ray laser and optical regime Smith-Purcell FEL, and deriving the gain equations of magnetic bremsstrahlung FEL and CRM for arbitrary electron propagation direction, structure (wiggler) axis, and radiative emission angle.

CONTENTS

I. Introduction 472
II. Kinematic Considerations 473
  A. The case of transversely discrete states: Intrabranch (longitudinal) transitions 476
  B. Finite-length homogeneous broadening 477
  C. The classical limit 477
  D. Interbranch (transverse states) transitions 479
  E. Multiphoton emission 482
  F. The transition from the quantum to the classical regime 484
  G. The case of transversely continuous states 486
  H. The case of transversely discrete states: Combined longitudinal and transverse transitions 487
III. Transition Rates Calculation 489
  A. A first-order perturbation analysis 489
  B. The transition rate calculation for different electron transverse states 492
    1. The transversely discrete (quantum) case 492
    2. The transversely continuous (inherently quantum) case 493
    3. The transversely continuous classical case 494
  C. The relativistic regime 496
  D. Calculation of the matrix element and homogeneous broadening line-shape function for various radiation schemes 498
  E. The transition rate calculation 502
  F. The longitudinal classical limit 506
IV. Spontaneous and Stimulated Emission 508
  A. Radiant intensity and gain 508
  B. The longitudinal classical limit in the homogeneous broadening regime 511
  C. Inhomogeneous broadening and Einstein relations 512
  D. Relations between spontaneous and stimulated emission in the inhomogeneous broadening regime 515
V. Conclusion and Examples 518
  A. Estimating a Smith-Purcell free-electron laser gain 519
  B. Estimating a channeling radiation free-electron laser gain 520
  C. General (off-axis) gain equations for the magnetic bremsstrahlung free-electron laser and cyclotron resonance maser 520
Appendix A: The Cyclotron Resonance Maser Energy Levels 522
Appendix B: The Classical Limits of an Electron Wave Packet 522
  1. Transverse classical limit 523
Appendix C: A Detailed Derivation of the Transition Rate Equation for Various Cases of Transverse States 523
  1. The transversely discrete (quantum) case 523
  2. The transversely continuous (inherently quantum) case 524
  3. The transversely continuous classical case 525
Appendix D: Second Quantization of the Klein-Gordon Equation 526
Appendix E: First-Order Expansion of the Emission and Absorption Detuning Parameters 528

*Present address.

†Permanent address.

Appendix F: The Recoil Parameter and its Symmetry Properties 529
Appendix G: The Inhomogeneous Broadening Regime and Hole-Burning Effect 531
Appendix H: Einstein Relations between Spontaneous and Stimulated Emission 532
References 534

I. INTRODUCTION

The goal of this paper is to present a unified formulation for characterizing spontaneous and stimulated radiation emission parameters of quasifree electrons. By the term quasifree electrons we refer to electrons propagating in electromagnetic field configurations in which the electrons are unbound at least in one dimension, and thus occupy a continuum of quantum states in this dimension (the propagation direction). Specifically we apply the formulation to problems in which the fields that the propagating electron experiences are either uniform or periodic in the propagation (z) dimension. In these cases the longitudinal quantum states are continuous (if the structure is considered infinitely long) and characterized by the electron wave number $k_z = p_z/\hbar$, where p_z is the electron axial momentum.

There is a large number of spontaneous and stimulated emission radiation effects that fit the above definition. These radiation effects and devices were previously classified into three classes (Gover and Yariv, 1978a; Pantell, 1980).

(1) Slow-wave radiators: These produce radiation effects in which the electrons pass through a structure in which electromagnetic wave components can propagate with a phase velocity slower than the speed of the electrons (and thus, in general, slower than the speed of light c). The electrons in these structures are basically free, and only the radiation field is perturbed. This class includes radiation effects such as Čerenkov radiation (Jelly, 1958; Coleman and Enderby, 1960; Ulrich, 1967; Piestrup *et al.*, 1973; Felch *et al.*, 1981; Kimura *et al.*, 1982; Von Laven *et al.*, 1982), Smith-Purcell radiation (Smith and Purcell, 1953; Salisbury, 1970; Bachheimer, 1972; Van den Berg, 1973; Burdette and Hughes, 1976; Gover *et al.*, 1984), and coherent transition radiation (Chu *et al.*, 1980, 1981; Piestrup and Finman, 1983; Datta and Kaplan, 1985), and devices such as the Traveling-Wave Amplifier (a microwave electron tube; see Pierce, 1950) and the Orotron (a 20-mm-wavelength tube; see Rusin and Bogomolov, 1969; Mizuno *et al.*, 1973; Korneyenkov and Shestopalov, 1977; Wortman *et al.*, 1981). Such radiation effects were also considered with semiconductor carriers propagating in structures with periodic perturbation of the index of refraction (Solimar and Ash, 1966; Sumi, 1966; Gover *et al.*, 1974; Gover and Yariv, 1975).

(2) Periodic bremsstrahlung radiators: These produce radiation effects in which the electron propagates in a structure where it is subjected to a *spatially* periodic force throughout its traversal along the free propagation dimension. This class includes radiation effects such as synchrotron undulator radiation (Motz, 1951; Kincaid, 1977) and coherent bremsstrahlung in the crystal lattice (Uberal, 1956; Walker *et al.*, 1975; Kurizki and McIver, 1982; Spence *et al.*, 1983), and stimulated emission devices such as the magnetic bremsstrahlung free-electron laser (Elias *et al.*, 1976; Deacon *et al.*, 1977), the Ubitron microwave tube (Philips, 1960) and their electrostatic analogues (Bekefi and Shefer, 1979; Gover, 1980a). Such radiation effects can also take place with semiconductor carriers in superlattice structures (Tsu and Esaki, 1973). Similar radiation effects can also take place when the periodic force that operates on the electron is time varying. These include spontaneous and stimulated Compton (Thompson) scattering of intense radiation waves off an accelerated electron beam (Pantell *et al.*, 1968). However, in the more restrictive context of this paper we will exclude these cases.

(3) Transverse binding radiators: These produce radiation effects in which the electron propagates in a structure where a transverse (perpendicular to the direction of propagation) binding force is operating on it. The electron thus oscillates in the transverse dimensions and is "free" in the axial direction. Included in this category are radiation effects such as the cyclotron resonance maser (Twiss, 1958; Schneider, 1959) and channeling radiation in a crystal lattice (Kumakhov, 1976; Terhune and Pantell, 1977), and radiation devices such as the Gyrotron microwave tube (Hirshfield and Wachtel, 1964; Hirshfield and Granatstein, 1977). Such radiation effects are also possible with drifting semiconductor carriers in an axial magnetic field (Fassum and Ancker-Johnson, 1973).

The purpose of this paper is to reveal the basic common quantum-electrodynamical features of all these radiation schemes. This interest is motivated by the significant developments in the field of free-electron lasers research. Since every spontaneous emission radiation effect can be turned, in principle, into a stimulated emission device, revelation of the common features of the various radiation effects and the relations between their spontaneous and stimulated emission may help in the invention and development of new free-electron lasers, including possible developments in such attractive wavelength regimes as the x-ray and vuv (very ultraviolet) regimes.

One of the goals of this paper is to derive the general relations between spontaneous and stimulated emission of radiation in quasifree-electron radiation effects. In most cases the spontaneous emission parameters can either be calculated with less difficulty than the stimulated emission parameters or be measured experimentally. Consequently, such relations can be useful for estimating the feasibility of stimulated emission devices on the basis of the known (calculated or measured) spontaneous emission parameters of any given radiation effect.

That there exists a basic relation between the spon-

taneous and stimulated emission of every radiation effect is a fundamental result of quantum electrodynamics (Feynman, 1961) and was stated even before the modern development of QED by Einstein (Haken, 1981). However, the application of Einstein relations to the estimation of the stimulated emission gain of various quasifree-electron radiation schemes is not straightforward. Extension of Einstein relations to account for certain free-electron radiation processes is described in Bekefi's book (Bekefi, 1966). More recently, simple classical relations between spontaneous and stimulated emission of free electrons in a magnetic bremsstrahlung free-electron laser scheme were derived by Madey (1979) and were shown later to have wider range validity than originally assumed (Krinsky *et al.*, 1982; Kroll, 1982). One of the goals of this paper is to extend these relations to all kinds of quasifree-electron radiation schemes and to describe their quantum and classical limits in a unified manner.

Although most of the radiation effects mentioned above can be analyzed classically in their practical regimes of operation, a full quantum-electrodynamical model is used here to describe both the electron wave function and the electromagnetic field, the reason being that in the quantum-electrodynamic theory the connection between spontaneous and stimulated emission is straightforward. We later take the classical limit to obtain the corresponding relation between spontaneous and stimulated emission of classical radiation devices.

Extensive work was carried out recently on quantum-mechanical analysis of the magnetic bremsstrahlung free-electron lasers (Madey, 1971; Elias *et al.*, 1976; McIver and Federov, 1979; Becker, 1980; Stenholm and Bambini, 1981; Bosco *et al.*, 1983; Dattoli, 1983), even though this type of laser would operate in the quantum regime only under very strenuous conditions (supposedly in the x-ray regime; see Gea-Banacloche *et al.*, 1983; Gover, 1984; Renieri, 1984). Few works were published on the quantum treatment of stimulated emission in slow-wave structures (Dekker, 1977; Soln, 1981; Becker and McIver, 1982). Channeling radiation is usually treated quantum mechanically in the transverse dimensions (Pantell and Alguard, 1979), and sometimes also in the longitudinal dimension (Beloshitskii and Kumakhov, 1978; Kurizki and McIver, 1984). The three-dimensional quantum-mechanical model that will be employed in this paper is more general than in the previous works. It describes in a unified way the various radiation schemes listed above in various operating regimes, permitting arbitrary mutual orientation of the structure axis, electron propagation direction, and radiative emission direction. We do not treat, however, any photon statistics and quantum coherence aspects of the radiation (Bonifacio, 1980; Becker and McIver, 1983; Dattoli *et al.*, 1985).

We note that the stimulated emission gain regimes considered here are only the homogeneously and inhomogeneously broadened low gain tenuous beam gain regimes (Gover and Sprangle, 1981). Collective effects, high gain, and large signal saturation regimes are not considered here. The units used in this paper are rationalized SI units. The interacting charge is assumed in all cases to be an electron of charge $-e$. In radiation schemes utilizing positrons (or holes in a semiconductor), the only transformation necessary is $-e \rightarrow e$.

II. KINEMATIC CONSIDERATIONS

A considerable amount of understanding and a full description of the radiation wavelength conditions can be gained from mere kinematic considerations. Before embarking on a detailed solution of the interaction dynamics, we will exploit kinematic considerations in order to derive important relations for the radiation parameters of quasifree-electron radiation effects.

It is well known that a free electron in an infinite free space can never radiate, since the conservation of energy and momentum conditions

$$\mathcal{E}_{\mathbf{k}_i} - \mathcal{E}_{\mathbf{k}_f} = \hbar\omega \ , \tag{2.1}$$

$$\mathbf{k}_i - \mathbf{k}_f = \mathbf{q} \ , \tag{2.2}$$

cannot be satisfied simultaneously in such a transition. Here

$$\mathbf{p} = \hbar\mathbf{k} \tag{2.3}$$

and

$$\mathcal{E}_{\mathbf{k}} = c\sqrt{(\hbar\mathbf{k})^2 + (mc)^2} \tag{2.4}$$

are the electron momentum and energy, respectively, i represents initial, f represents final, and $\mathbf{q}$ is the radiation wave vector, $|\mathbf{q}| = \omega/c$.

The principles of all the radiation effects and FEL (free-electron laser) devices listed above are based on perturbing the energy or wave number (momentum) of the electron or the radiation wave in such a way that the energy and momentum conservation laws (and possibly other conservation or selection rules) are satisfied in the radiative emission process. In the slow-wave radiation effects this is made possible by increasing the wave number $\mathbf{q}$ by one of two means: (a) propagating the radiation in a dielectric matter with a refractive index $n > 1$ (as in the Čerenkov effect), (b) propagating the wave in an axially periodic structure where the structure endows the *radiation wave* components with "crystal" momentum $mk_w\hat{e}_z$, where $k_w = 2\pi/\lambda_w$, $m = \pm 1, \pm 2, \ldots$, and λ_w is the period of the periodic structure. The crystal-momentum-assisted radiative emission and absorption processes are depicted in Fig. 1(a) for $m = 1$. The periodic bremsstrahlung radiation effects are based on endowing "crystal momentum" $mk_w\hat{e}_z$ to the *electron wave* by propagating the electron in a force field that is axially periodic. Emissive radiative transition can take place then via an electron wave component with increased wave number in the final state ($m > 0$) or a decreased wave number in the initial state ($m < 0$). See Fig. 1(b) in which an $m = \pm 1$ example is depicted. The transverse

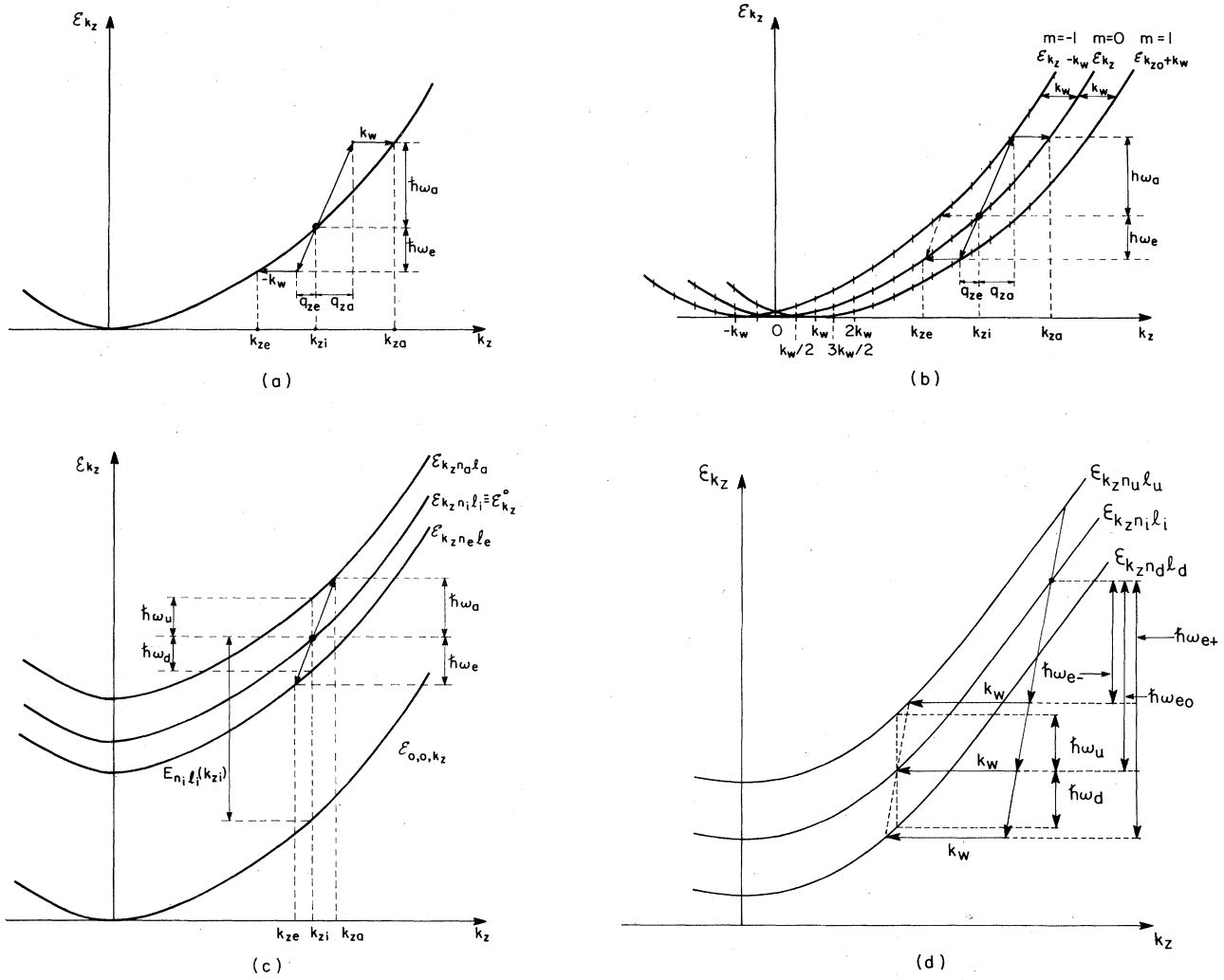

FIG. 1. $\mathcal{E}-k_z$ diagrams and radiative transitions.

confinement radiation effects are based on transitions of electrons from energy branches corresponding to higher transverse energy states to energy branches corresponding to lower transverse energy states for cases of emission, and, *vice versa,* in cases of absorption [see Fig. 1(c)]. A combined case in which radiation processes involving both interbranch transitions and an exchange of longitudinal crystal momentum are depicted in Fig. 1(d).

It should be noted that Fig. 1 is only an illustration of a one-dimensional (z) model, which is easier to display. We will discuss later the three-dimensional case. The curve in Fig. 1(a) represents in the case of an entirely free electron the hyperbolic k_z dependence of the energy dispersion curve (2.4). The energy dispersion curves in Figs. 1(b) and 1(c) are also nearly hyperbolic, but they are modified by the respective static periodic force or transverse binding force in which the electron propagates.

In a structure with periodic boundaries in the z dimension the *electromagnetic field* modes assume the Floquet form (Collin, 1960),

$$\mathbf{A}(\mathbf{r})=\sum_{m=-\infty}^{\infty}\mathbf{A}_m(\mathbf{r}_\perp)\exp[i(q_z+mk_w)z]\ . \tag{2.5}$$

In such structures the interaction between the electron and the electromagnetic wave can be mediated via one of the components (space harmonics) of Eq. (2.5) with $m>0$, which have an increased wave number and thus can satisfy the momentum conservation equation (2.2). In a structure that applies a periodic potential on the electron along the propagation direction (z), it is the *electron wave* function that satisfies the Floquet theorem

$$\psi(\mathbf{r})=\sum_{m=-\infty}^{\infty}\Psi_m(\mathbf{r}_\perp)\exp[i(k_z+mk_w)z]\ . \tag{2.6}$$

This is a special case of the Bloch theorem for an electron

wave function in a one-dimensional "crystal" lattice. The interaction in this case is due to the space harmonics of the electron wave function (2.6), which are endowed with excess crystal momentum in the initial or final states and thus can satisfy the conservation of momentum condition (2.2). The electron energy dispersion curve in a periodic structure is a Brillouin diagram, and the electron radiative transition can be described, as illustrated in Fig. 1(b), as an interband transition in which the electron makes a transition into a lower (higher) energy passband in a lower (higher) Brillouin zone for the cases of emission (absorption), respectively (Gover and Yariv, 1978a). For simplicity we assumed in Fig. 1(b) that the periodic perturbation is weak enough, so that the energy dispersion curve looks as if the free-space energy curve displaced infinite times by mk_w in the k_z direction. We assume that the electron energy is away from the forbidden bands (which are not shown in the diagram, but are marked by short vertical lines), and we only show parts of the Brillouin zones that correspond to $k_{z_i}>0$ and $m=-1,0,1$.

The transverse binding radiation schemes are based on structures where an axially uniform transverse confining potential operates on the electron. Due to the axial translation symmetry and the transverse confinement, the electron is characterized by a continuous axial wave number k_z (eigenvalue of the axial momentum operator) and by a set of discrete transverse quantum numbers n,l:

$$\psi_{n,l,k_z}(\mathbf{r})=\Psi_{n,l,k_z}(\mathbf{r}_\perp)\exp(ik_z z)\ , \tag{2.7}$$

where

$$H\psi_{n,l,k_z}(\mathbf{r})=\mathcal{E}_{n,l,k_z}\psi_{n,l,k_z}(\mathbf{r})\ . \tag{2.8}$$

We may define the transverse energy $E_{n,l}(k_z)$ as the incremental energy relative to the fundamental transverse quantum numbers branch $\mathcal{E}_{0,0,k_z}$,

$$\mathcal{E}_{n,l,k_z}=\mathcal{E}_{0,0,k_z}+E_{n,l}(k_z)\ . \tag{2.9}$$

In the particular case that the Hamiltonian is separable into a term that depends only on the transverse coordinates and one that depends only on the longitudinal coordinates, the transverse energy $E_{n,l}$ is independent of k_z, each energy branch is displaced from its neighbors by a fixed amount independent of the abscissa coordinate, and they are all parallel to each other in the $\mathcal{E}-k_z$ diagram plane. This is the case in the nonrelativistic electron limit of an axially uniform structure, where $H_{el}=H(\mathbf{r}_\perp)-(\hbar^2/2m)\partial^2/\partial z^2$. A well-known example for such a case is an electron in an axial magnetic field (Landau, 1930). In the nonrelativistic limit the transverse energy branches (Landau levels) are equispaced with a uniform k_z-independent spacing: $\Delta E=\hbar\omega_c$. The cyclotron frequency is $\omega_c=eB/(mc)$. In the relativistic regime the energy-level spacings are not equal and are k_z dependent.

Figure 1(c) illustrates a section of the multiple-transverse energy branches diagram of a transverse binding electron radiation scheme. We point out that, contrary to the other two types of schemes, the transitions in the latter case become possible due to modification of the *energy* conservation condition (2.1) instead of the *momentum* conservation condition (2.2). The electron is capable of performing a radiative transition with a small change in its axial momentum. It is capable of emitting (absorbing) the large photon energy by making a transition to a lower (higher) transverse energy branch for the cases of emission or absorption, respectively.

In addition to these three radiation schemes, any combination of these is also possible. For instance, an electron that is channeling in the crystal lattice between crystalline planes may emit channeling radiation due to the transverse binding potential applied on it in the channel. However, it may at the same time also emit coherent bremsstrahlung radiation due to the axial periodic potential applied on it when traversing through periodic crystal planes (Kurizki and McIver, 1982; Spence *et al.*, 1983). It may also emit Smith-Purcell-type radiation due to the effect on the radiation wave of the dielectric constant modulation along the crystal lattice periodicity (Gover and Yariv, 1978a). The energy diagram in this case is a combination of Figs. 1(a), 1(b), and 1(c), and its illustration would be quite elaborate [a simple special case is depicted in Fig. 1(d)]. In general, any electron state needs to be characterized by two transverse discrete quantum numbers n,l, an axial quantum number m (corresponding to the space harmonic number or Brillouin-zone number), and a continuous-state wave number k_z. In the slow-wave radiation mechanism the radiative process involves transitions in which $(n_i,l_i,m_i)=(n_f,l_f,m_f)$, and the excess momentum that is produced in the radiative transition is imparted by a slow space harmonic of the radiation field. In the pure bremsstrahlung radiation mechanism $(n_i,l_i)=(n_f,l_f)$ and $m_i\neq m_f$. In the pure transverse binding radiation mechanism $m_i=m_f$ and $(n_i,l_i)\neq(n_f,l_f)$. In the most general case (Kurizki and McIver, 1982) $(n_i,l_i m_i)\neq(n_f,l_f,m_f)$. In all cases $k_{zi}\neq k_{zf}$, and the electron imparts some of its axial momentum to the radiation field.

In considering the kinematics of the various radiation schemes, we will distinguish between cases in which the electron transverse quantum numbers are discrete (as in the channeled electron example) and cases in which the transverse quantum numbers are continuous. Except for the channeled electron and the cyclotron resonance maser examples, in most radiation schemes and FEL's the large transverse dimensions of the structure warrant a model of continuous transverse states. Nevertheless, we choose to start our discussion with the analysis of the case of transversely discrete states, since it can be described in terms of simple two-dimensional planar diagrams and is thus easier to visualize. We will generalize the discussion later to the case of transversely continuous states. It should be noted though that most quantum treatises of the FEL, which were previously published, assume that all the fields are transversely infinite and

transversely uniform, and that the electron transverse wave number does not change in the transition (pure axial recoil). Such an assumption is equivalent to a case model of transversely discrete states.

A. The case of transversely discrete states: Intrabranch (longitudinal) transitions

The most general radiative transition in the case of transversely discrete states is limited by the conservation of energy and longitudinal momentum conditions:

$$\mathcal{E}_{k_{zi},n_i,l_i}-\mathcal{E}_{k_{zf},n_f,l_f}=\pm\hbar\omega \ , \tag{2.10}$$

$$k_{zi}-k_{zf}=q_z+mk_w \ , \tag{2.11}$$

assuming that other possible conservation or selection rules for transition between the two transverse states (such as angular momentum and parity conservation) are satisfied. We first analyze the schemes of slow-wave and bremsstrahlung radiation effects. In both of these schemes $(n_i,l_i)=(n_f,l_f)$, and hence all the energy curves in Figs. 1(a) and 1(b) correspond to a single transverse quantum numbers branch, which we define as

$$\mathcal{E}^0_{k_z}\equiv\mathcal{E}_{k_z,n_i,l_i} \ . \tag{2.12}$$

Such transitions will be termed intrabranch or longitudinal transitions.

For simplicity we assume in all cases interaction via the first-order space harmonic ($m=1$). The general case can always be restored by substituting $k_w\rightarrow mk_w$. An exception is the case of Čerenkov radiation, where the entire formulation still applies with $k_w=0$. The conservation of energy and longitudinal momentum conditions, in the emission and absorption radiative processes which are displayed in Figs. 1(a) and 1(b), are then given by

$$\mathcal{E}^0_{k_{zi}}-\mathcal{E}^0_{k_{ze}}=\hbar\omega_e \ , \tag{2.13}$$

$$k_{zi}-k_{ze}=q_{ze}+k_w \ , \tag{2.14}$$

$$\mathcal{E}^0_{k_{za}}-\mathcal{E}^0_{k_{zi}}=\hbar\omega_a \ , \tag{2.15}$$

$$k_{za}-k_{zi}=q_{za}+k_w \ , \tag{2.16}$$

where $q_{ze}\equiv q_z(\omega_e)$, $q_{za}\equiv q_z(\omega_a)$.

We assume that the electromagnetic dispersion relation $q_z(\omega)$ and the electron energy dispersion relation $\mathcal{E}^0_{k_z}$ are known. Hence Eqs. (2.13) and (2.14) constitute a set of equations that define uniquely the photon emission frequency ω_e, and similarly Eqs. (2.15) and (2.16) define the photon absorption frequency ω_a.

In the classical limit $\hbar\rightarrow 0$ the two sets of equations [(2.13), (2.14) and (2.15), (2.16)] can be solved by first-order Taylor expansion of $\mathcal{E}^0_{k_{ze}}=\mathcal{E}^0_{k_{zi}-q_{ze}-k_w}$, $\mathcal{E}^0_{k_{za}}=\mathcal{E}^0_{k_{zi}+q_{za}+k_w}$ around k_{zi}. This produces for both emission and absorption the same radiation condition

$$\omega_e\approx\omega_a\approx v_{gz}(q_{z0}+k_w)\equiv\omega_0 \ , \tag{2.17}$$

where

$$v_{gz}\equiv\frac{1}{\hbar}\frac{\partial\mathcal{E}^0_{k_z}}{\partial k_z}\bigg|_{k_{zi}} \tag{2.18}$$

is the electron group velocity (electron classical velocity).

Since $q_{z0}=q_z(\omega_0)$, we need to use an explicit equation for the electromagnetic dispersion relation in order to obtain an explicit equation for the radiation frequency ω_0. We distinguish between two different electromagnetic structures. If the electromagnetic wave structure (or resonator) is forcing quantization of the electromagnetic transverse wave number $\mathbf{q}_\perp$ (as is the case in a waveguide), then

$$\mathbf{q}(\omega)=\mathbf{q}_\perp+\hat{e}_z q_z(\omega) \ . \tag{2.19}$$

(Here we assumed the case of most relevance, one in which the waveguide axis is along the electron propagation direction.) In other electromagnetic structures, which correspond to most practical realizations of Smith-Purcell radiation, synchrotron undulator radiation (or bremsstrahlung FEL's), and other radiation schemes, the electromagnetic dispersion function is the free-space relation

$$\mathbf{q}(\omega)=\hat{e}_q\frac{\omega}{c} \ . \tag{2.20}$$

In both cases we may write

$$q_z(\omega)=\frac{\omega}{c}\cos\Theta_{\mathbf{q}} \ , \tag{2.21}$$

where $\Theta_{\mathbf{q}}\equiv\cos^{-1}(\hat{e}_{\mathbf{q}}\cdot\hat{e}_z)$ in the second case and $\Theta_{\mathbf{q}}$ is the waveguide mode "zigzag angle" in the first case. Equation (2.21), when substituted in Eq. (2.17), produces the following radiation condition:

$$\omega_0=\frac{v_{gz}\mathbf{k}_w}{1-\beta_{gz}\cos\Theta_{\mathbf{q}}} \ . \tag{2.22}$$

It is instructive to note that Eq. (2.22) produces directly the Smith-Purcell (1953) radiation condition

$$\lambda=\frac{\lambda_w}{m}(\beta_{gz}^{-1}-\cos\Theta_q) \ , \tag{2.23}$$

where we restored the higher-order harmonics case by substituting $k_w\rightarrow mk_w$. Equation (2.22) is also the radiation condition of the synchrotron undulator radiation effect (Motz, 1951; Kincaid, 1977) and can be viewed as the Doppler-shifted frequency of the undulating electron, which in its average motion rest frame oscillates at a frequency $\omega_0'=\gamma_z\mathbf{k}_z v_w$ (Jackson, 1975). The well-known FEL radiation condition (Gover and Sprangle, 1981)

$$\lambda=\frac{\lambda_w}{2\gamma_z^2} \tag{2.24}$$

can also be directly derived from Eq. (2.22) by substituting $\Theta_{\mathbf{q}}=0$, $\beta_{gz}\approx 1$, and $\gamma_z\equiv(1-\beta_{gz}^2)^{-1/2}$. For completion we also point out that, in the case when the radiation wave propagates in a uniform dielectric matter, the

right-hand sides of Eqs. (2.20) and (2.21) should be multiplied by the material refraction index n. The Čerenkov radiation condition is then obtained directly from Eq. (2.17) by substituting $k_w=0$:

$$n(\omega_0)\cos\Theta_q=\frac{1}{\beta_{gz}} , \tag{2.25}$$

which is the well-known Čerenkov radiation condition.

B. Finite-length homogeneous broadening

In a finite interaction length L the axial momentum conservation conditions (2.14) and (2.16) do not need to be satisfied exactly. The allowed deviations are of the order of $\pm\pi/L$:

$$| k_{zi}-k_{ze}-q_z-k_w | <\frac{\pi}{L} , \tag{2.26}$$

$$| k_{za}-k_{zi}-q_z-k_w | <\frac{\pi}{L} . \tag{2.27}$$

Thus, instead of the unique definition of the emission and absorption frequencies ω_e,ω_a set by the respective sets of Eqs. (2.13), (2.14) and (2.15), (2.16), we obtain emission and absorption lines with center frequencies ω_e,ω_a and frequency linewidths $\Delta\omega_L$ defined by (2.13), (2.26) and (2.15), (2.27), respectively [see the upper curve of Fig. 2(a) and Fig. 3]. The finite-length-limited linewidth $\Delta\omega_L$ is the lower bound for the bandwidth of the free-electron laser emission curve. We will discuss in subsequent sections also additional mechanisms of homogeneous broadening (e.g., electron collisions) and inhomogeneous broadening (e.g., electron energy spread) that can only increase the emission linewidth beyond this fundamental limit.

To obtain the equation for the FWHM (full width at half maximum) linewidth of the emission and absorption lines, respectively, we expand again (2.13) and (2.15) to first order in $\hbar$, as we did in the case of (2.17). This time, however, the expansion is carried out at frequencies $\omega_e\pm\Delta\omega_L/2$ and final wave numbers $k_{ze}\pm(\Delta q_z/2+\pi/L)$, where $\Delta q_z\equiv q_z(\omega_e+\Delta\omega_L/2)-q_z(\omega_e-\Delta\omega_L/2)$ (see Fig. 3):

$$\mathcal{E}^0_{k_{zi}}-\mathcal{E}^0_{k_{ze}}\pm\frac{d}{dk_z}\mathcal{E}^0_{kz}\,|_{k_z=k_{ze}}\left[\frac{\Delta q_z}{2}+\frac{\pi}{L}\right]=\hbar\omega_e\pm\frac{\Delta\omega_L}{2} .$$

Using Eq. (2.13), this produces

$$\Delta\omega_L=v_{gz}\left[\Delta q_z+\frac{2\pi}{L}\right] , \tag{2.28}$$

where in this case

$$v_{gz}\equiv\frac{1}{\hbar}\frac{d}{dk_z}\mathcal{E}^0_{k_z}\,|_{k_z=k_{ze}} . \tag{2.29}$$

A similar result is obtained also for the absorption linewidth, except that in this case v_{gz} is evaluated at $k_z=k_{za}$. However, in practice, and certainly when the classical limit applies, we may substitute $v_{gz}\,|_{k_{ze}}\approx v_{gz}\,|_{k_{za}}\approx v_{gz}\,|_{k_{zi}}$, and Eq. (2.28) is applicable for both the emission and absorption linewidths with v_{gz} defined by (2.18). In fact, in this case Eq. (2.28) could be derived directly by differentiation of (2.17).

In order to obtain an explicit equation for $\Delta\omega_L$, the dispersion relation $q_z(\omega)$ needs to be differentiated and expressed in terms of $\Delta\omega_L$: $\Delta q_z=(dq_z/d\omega)\Delta\omega_L$. Here we need to distinguish between the dispersion relations (2.19) and (2.20), which now produce somewhat different results. In the first case we obtain

$$\Delta\omega_L=\frac{v_{gz}}{1-v_{gz}/v_{\rm gr}}\frac{2\pi}{L} , \tag{2.30}$$

where $v_{\rm gr}\equiv d\omega/dq_z$ is the group velocity of the radiation mode. In the second case,

$$\Delta\omega_L=\frac{v_{gz}}{1-\beta_{gz}\cos\Theta_q}\frac{2\pi}{L} . \tag{2.31}$$

This last relation can be written with the aid of Eq. (2.22) in the simple form

$$\frac{\Delta\omega_L}{\omega_0}=\frac{\lambda_w}{L}=\frac{1}{N_w} , \tag{2.32}$$

which is well known in the conventional FEL theory (Madey, 1971; Gover and Sprangle, 1981). N_w is the number of periods along the interaction region. This result is independent of the kind of periodic structure used and the emission direction.

For completion we also give the equation for the finite-length linewidth of the Čerenkov radiation:

$$\Delta\omega_L=\frac{v_{gz}}{1-v_{gz}[n'(\omega_0)+1]\cos\Theta_q}\frac{2\pi}{L} . \tag{2.33}$$

This is obtained by differentiating $q_z(\omega)=n(\omega)(\omega/c)\cos\Theta_q$ for a fixed radiation direction Θ_q, and substituting in Eq. (2.28).

C. The classical limit

There is clearly a significant qualitative difference between the limit

$$\Delta\omega_L\ll|\omega_a-\omega_e|\equiv|\delta\omega| , \tag{2.34}$$

called the inherently quantum limit, and the opposite limit

$$\Delta\omega_L\gg|\omega_a-\omega_e|\equiv|\delta\omega| , \tag{2.35}$$

called the classical limit. In the first case the emission and absorption lines are well separated [upper curve in Fig. 2(a)], while in the second case they are largely overlapping. However, even in the latter case the line centers are displaced by a small but nonvanishing interval, and the two processes do not exactly cancel each other. Consequently, the net stimulated emission line shape, which is proportional to the difference between the emission

and absorption line functions, is proportional in this case to the derivative of the emission line-shape function [lower curve in Fig. 2(a); see also Madey, 1971].

We observed before that in the classical limit $\hbar \to 0$, one obtains $\omega_e \approx \omega_a \approx \omega_0$. This is why we identify (2.35) as the classical limit condition and (2.34) as the inherently quantum-mechanical limit condition. In the first case (the quantum regime), the net stimulated emission line-shape function depends separately on the values of the emission and absorption line-center frequencies ω_e, ω_a, which are quantum ($\hbar$ dependent) parameters. In the second case (the classical regime), the net emission line-shape function is only characterized by ω_0 and $\Delta\omega_L$, which are both independent of $\hbar$. The net gain, however, is still proportional then to the line-centers frequency spacing $\delta\omega \equiv \omega_a - \omega_e$, which results from the differentiation of the emission and absorption line functions difference. The lines spacing parameter $\delta\omega$ is proportional to $\hbar$, but this dependence cancels out when the net stimulated emission rate or the gain parameter is calculated (as will be shown later in Secs. III.F and IV.B). The evaluation of the line-centers spacing parameter $\delta\omega$ is, however, important not only for identifying the regime of operation (classical or quantum), but also for a quantitative evaluation of the net stimulated emission (gain) when the classical condition (2.35) is satisfied. Detailed computation of the stimulated emission gain in the classical limit for different free-electron radiation devices will be given in Sec. IV, utilizing the equations for $\delta\omega$, which we subsequently derive in the present section.

In order to express the line-centers spacing parameter in terms of the device parameters, we now compute ω_e, ω_a to first order in $\hbar$ by a second-order expansion of (2.13) and (2.15) in terms of $\hbar$. This results in

$$\omega_e = \omega_0 - \tfrac{1}{2}\delta\omega \ , \tag{2.36}$$

$$\omega_a = \omega_0 + \tfrac{1}{2}\delta\omega \ , \tag{2.37}$$

where

$$\delta\omega \equiv \omega_a - \omega_e = (\mathcal{E}^0_{k_{zi}+q_{za}+k_w} - \mathcal{E}^0_{k_{zi}-q_{ze}-k_w} - 2\mathcal{E}_{ki})/\hbar$$
$$= v_{gz}(q_{za} - q_{ze}) + \frac{\hbar}{m^*_{\parallel}}(q_{z0}+k_w)^2 \ . \tag{2.38}$$

Here $q_{z0} \equiv q_z(\omega_0)$, v_{gz} is defined in (2.18) in terms of the first-order derivative of $\mathcal{E}_k$, and $m^*_{\parallel}$ is the longitudinal

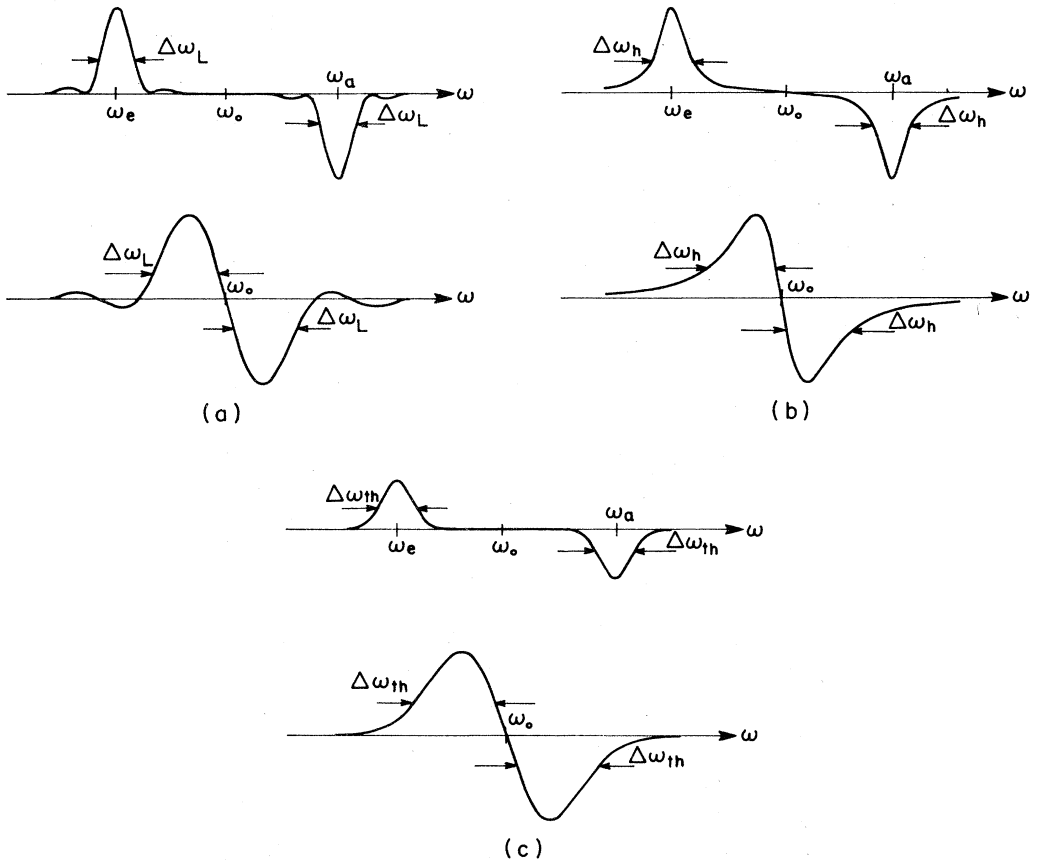

FIG. 2. Line-shape functions in the quantum (upper curve) and classical (lower curve) regimes, and the corresponding definitions of the linewidth parameters $\Delta\omega_L$, $\Delta\omega_h$, and $\Delta\omega_{\rm th}$.

effective mass defined by

$$\frac{1}{m_{\parallel}^*}=\frac{1}{\hbar^2}\frac{d^2\mathcal{E}_{k_z}}{dk_z^2}\bigg|_{k_{zi}} . \tag{2.39}$$

For the two different optical dispersion relations (2.19) and (2.20), the respective spacings between the absorption and emission line centers are derived by substitution into (2.38), resulting in, correspondingly,

$$\delta\omega=\omega_a-\omega_e=\frac{\hbar\omega_0^2}{m_{\parallel}^* v_{gz}^2}\frac{1}{1-v_{gz}/g_{gr}} , \tag{2.40}$$

$$\delta\omega=\omega_a-\omega_e=\frac{\hbar\omega_0^2}{m_{\parallel}^* v_{gz}^2}\frac{1}{1-v_{gz}\cos\Theta_q/c} , \tag{2.41}$$

where we also made use of Eq. (2.17).

By dividing Eqs. (2.40) and (2.41) by (2.30) and (2.31), respectively, we obtain a general equation for both cases

$$\frac{\omega_a-\omega_e}{\Delta\omega_L}=\frac{\hbar\omega_0}{m_{\parallel}^* v_{gz}^2}\frac{\omega_0 L}{2\pi v_{gz}} . \tag{2.42}$$

The first factor on the right-hand side is the ratio of photon energy to twice the classical kinetic energy of a particle with mass $m_{\parallel}^*$. The second factor is the number of electromagnetic oscillations within the interaction length transit time L/v_{gz}. The classical limit (2.35) can be written in terms of (2.42),

$$\frac{\omega_a-\omega_e}{\Delta\omega_L}=\frac{\hbar\omega_0}{m_{\parallel}^* v_{gz}^2}\frac{\omega_0 L}{2\pi v_{gz}}\ll 1 . \tag{2.43}$$

The ratio (2.42) and the classical limit condition (2.43) may be written in various cases in alternate forms. In the case of Eq. (2.21), we may substitute ω_0 from (2.22) and obtain

$$\frac{\omega_a-\omega_e}{\Delta\omega_L}=\frac{1}{1-\beta_{gz}\cos\Theta_q}\frac{\hbar\omega_0}{m_{\parallel}^* v_{gz}^2}N_w\ll 1 , \tag{2.44}$$

where $N_w\equiv L/\lambda_w$ is the number of periods along the periodic structure (wiggler).

We note that the derived expressions for $\delta\omega/\Delta\omega_L$ have a somewhat wider validity than just for the case of transversely discrete states for which they were derived. The analysis so far is independent of the dispersion relation of the electron $\mathcal{E}_{k_z}$, and only assumes that the momentum conservation condition is satisfied in the longitudinal dimension [see Eqs. (2.14) and (2.16)]. Such a situation can occur also in examples of continuous transverse states under conditions where the electron quantum recoil effect is purely longitudinal. An example such as this, which is analyzed in greater detail in the next section, is the Smith-Purcell effect observed under conditions in which the radiation wave vector has no lateral components (the emission is in a plane that includes the electron trajectory and the normal to the grating). This is also the case under conditions of arbitrary emission angle under the "magnetized plasma approximation" (Gover and Sprangle, 1981). In the Smith-Purcell radiation case, as in all other slow-wave radiation schemes, the electron is entirely free, and its dispersion relation is given by (2.4) with $\mathbf{k}_\perp=0$. The longitudinal effective mass (2.39) can then be expressed explicitly as

$$m_{\parallel}^*=\gamma^3 m . \tag{2.45}$$

Another case of transverse continuous states to which we can still apply the *longitudinally constrained* recoil expressions derived in this section is the case of the magnetic bremsstrahlung FEL, for conditions when the electron propagates along the wiggler axis [zero canonical momentum (Sprangle and Smith, 1980)] and the radiative emission is on axis ($\Theta_q=0$). In this case

$$\mathcal{E}_{k_z}^0=c\sqrt{(mc)^2+(\hbar k_z)^2+(e\,\mathbf{A}_w)^2} , \tag{2.46}$$

where $\mathbf{A}_w$ is the transverse vector potential of the wiggler, and the longitudinal effective mass (2.39) is found to be

$$m_{\parallel}^*=\gamma_z^2\gamma m \tag{2.47}$$

[instead of (2.45)]. The expression for the parameter $\delta\omega/\Delta\omega_L$ (and subsequently the classical limit condition) for the bremsstrahlung FEL is then found by substituting (2.47) and $\Theta_q=0$ in (2.44):

$$\frac{\omega_a-\omega_e}{\Delta\omega_L}=\frac{1+\beta_{gz}}{\beta_{gz}^2}\frac{\hbar\omega_0}{\gamma mc^2}N_w . \tag{2.48}$$

This equation is in full agreement with the conventional classical limit condition, which was derived earlier for FEL's in the highly relativistic beam limit ($\beta_{gz}\to 1$) (Philips, 1960; Kurizki and McIver, 1982). Equation (2.48) indicates that it may be easier to observe quantum effects with nonrelativistic beams. Note, however, that this equation is only valid under the particular conditions for which there is no transverse momentum transfer (recoil). In the general case (namely, when the radiative emission is off axis) the model for transversely discrete states cannot be used to describe the FEL. To obtain an equation for the classical limit parameter of FEL's in the general case, a model for transversely continuous states must be used, as is done further on in Sec. II.G.

D. Interbranch (transverse states) transitions

We now consider the case of transversely discrete states for transitions between pure transverse states. In this case the energy and momentum conservation conditions are satisfied with Eqs. (2.10) and (2.11), where $(n_i,l_i)\neq(n_f,l_f)$ and $m=0$ (or there is no longitudinal periodic structure at all).

For simplicity we consider emissive and absorptive transitions only between adjacent branches as shown in Fig. 1(c). Substituting $m=0$ and the definition (2.9) in Eqs. (2.10) and (2.11), we get instead of (2.13)–(2.16) the following two sets of equations, which define the emission

and absorption line frequencies, respectively,

$$\mathcal{E}^0_{k_{zi}} - \mathcal{E}^0_{k_{ze}} = \hbar(\omega_e - \omega_d) , \tag{2.49}$$

$$k_{zi} - k_{ze} = q_{ze} , \tag{2.50}$$

$$\mathcal{E}^0_{k_{za}} - \mathcal{E}^0_{k_{zi}} = \hbar(\omega_a - \omega_u) , \tag{2.51}$$

$$k_{za} - k_{zi} = q_{za} , \tag{2.52}$$

where $\mathcal{E}^0_{k_{zi}}$ is defined in (2.12) and

$$\omega_d = [E_{n_i l_i}(k_{zi}) - E_{n_e l_e}(k_{ze})]/\hbar , \tag{2.53}$$

$$\omega_u = [E_{n_a l_a}(k_{za}) - E_{n_i l_i}(k_{zi})]/\hbar . \tag{2.54}$$

To obtain the emission and absorption line frequencies in the classical limit $\hbar \to 0$, we expand $\mathcal{E}^0_{k_{ze}}$ and $\mathcal{E}^0_{k_{za}}$ to first order in $\hbar$ around k_{zi} in a manner similar to that used to derive (2.17) and (2.22). For both electromagnetic dispersion relations (2.19) and (2.20), this results in

$$\omega_{e0} = \frac{\omega_d}{1 - \beta_{gz}\cos\Theta_q} , \tag{2.55}$$

$$\omega_{a0} = \frac{\omega_u}{1 - \beta_{gz}\cos\Theta_q} . \tag{2.56}$$

In Eqs. (2.55) and (2.56) ω_d, ω_u are calculated to zero order in the longitudinal quantum recoil. Since to this order one can equate $E_{n_f l_f}(k_{zf}) = E_{n_f l_f}(k_{zi})$, Eqs. (2.53) and (2.54) define $\hbar\omega_d, \hbar\omega_u$ as the *vertical* spacings between the initial and final branches (lower and upper, respectively) at $k_z = k_{zi}$, as shown in Fig. 1(c).

Equation (2.55) may be compared for instance, with the emission frequency conditions calculated for channeling radiation (Pantell and Alguard, 1979) and for cyclotron resonance emission (Schneider, 1959). In the first case ω_d and ω_u are usually different, though one may consider a special case applicable mostly for positrons channeling, in which they are nearly equal (degenerate). If an harmonic binding potential is assumed in that case, then $\omega_u = \omega_d = \omega_{h0}/\gamma^{1/2} \equiv \omega_h$, where $\omega_{h0} \equiv (k_1/m)^{1/2}$ and k_1 is the spring constant of the harmonic potential (Pantell and Alguard, 1979). In the second example, the CRM (cyclotron resonance maser), the branches spacing is nearly degenerate: $\omega_u = \omega_d = \omega_{c0}/\gamma \equiv \omega_c$, where $\omega_{c0} \equiv (eB_0/mc)^{1/2}$ [see Eq. (A3) in Appendix A] and ω_c is the Lorentz-covariant cyclotron frequency. In both of these examples the emission and absorption line centers ω_{e0}, ω_{a0} are degenerate in the classical limit and are given by

$$\omega_0 = \omega_{e0} = \omega_{a0} = \frac{\omega_{h,c}}{1 - \beta_{gz}\cos\Theta_q} . \tag{2.57}$$

In many cases one is interested mainly in forward emission ($\Theta_q = 0$) and highly relativistic beams, for which stronger emission at higher (Doppler-shifted) frequency is obtained. In this case the emission and absorption frequencies (2.55) and (2.56) are given by

$$\omega_{e0,a0} = (1 + \beta_{gz})\gamma_{gz}^2 \omega_{d,u} \approx 2\gamma_{gz}^2 \omega_{d,u} . \tag{2.58}$$

In the specific examples of degenerate transverse transitions considered above, the degenerate forward emission and absorption frequencies are

$$\omega_0 = (1 + \beta_{gz})\gamma_{gz}^2 \omega_{h,c} \approx 2\gamma_{gz}^2 \omega_{h,c} . \tag{2.59}$$

This demonstrates the known scaling laws of positron channeling and cyclotron resonance forward emission frequencies, which at relativistic beam energies scale as $\gamma^{3/2}$ and γ, respectively.

For calculating the finite-length homogeneous broadening of the emission and absorption lines of transverse binding free-electron radiators, we allow an uncertainty in the axial momentum conditions (2.26) and (2.27), with $k_w = 0$. The previous equations for the linewidths (2.28)–(2.31) are applicable then without change. The relative linewidth of the emission and absorption lines can be found for case (2.20) (free-space radiation modes) by dividing (2.31) by (2.55) or (2.56), resulting in the simple equation

$$\frac{\Delta\omega_L}{\omega_{e0,a0}} = \frac{2\pi v_{gz}}{L\omega_{d,u}} . \tag{2.60}$$

This has the simple interpretation as the reciprocal of the number of natural transverse oscillation periods ($2\pi/\omega_{u,d}$) during the transit time (L/v_{gz}), which has the same meaning as Eq. (2.32) for the periodic structure radiators.

The inherently quantum-mechanical and the classical regimes are defined for the transverse binding radiators by the same conditions [see (2.34) and (2.35)] that we used for the slow-wave and bremsstrahlung radiators. However, contrary to the previous case, the difference between the emission (ω_e) and absorption (ω_a) line frequencies is not only a consequence of the curvature of the energy dispersion $\mathcal{E}_{kz}$ as a function of k_z (longitudinal quantum effect), but is also a result of the difference in the energy branches spacing $\omega_u \neq \omega_d$ (transverse quantum effect), as illustrated in Fig. 1(c). Thus the second-order expansion of $\mathcal{E}^0_{k_{ze}}, \mathcal{E}^0_{k_{za}}$ in (2.49) and (2.51) results in

$$\omega_e = \omega_d + v_{gz} q_{ze} - \frac{1}{2}\frac{\hbar}{m_\parallel^*} q_{ze}^2 , \tag{2.61}$$

$$\omega_a = \omega_u + v_{gz} q_{za} + \frac{1}{2}\frac{\hbar}{m_\parallel^*} q_{za}^2 , \tag{2.62}$$

$$\omega_a - \omega_e = \omega_u - \omega_d + v_{gz}(q_{za} - q_{ze}) + \frac{\hbar}{2m_\parallel^*}(q_{ze}^2 + q_{za}^2) , \tag{2.63}$$

instead of (2.38). For the optical dispersion relation (2.20), one obtains instead of (2.41)

$$\omega_a - \omega_e = \frac{\omega_u - \omega_d + \dfrac{\hbar}{2m_\parallel^*}(q_{ze}^2 + q_{za}^2)}{1 - v_{gz}\cos\Theta_q/c} . \tag{2.64}$$

Dividing by Eq. (2.31), we find that the classical limit condition (2.35) is

$$\frac{\omega_a-\omega_e}{\Delta\omega_L}=\left[\omega_u-\omega_d+\frac{\hbar}{2m_{\parallel}^*}(q_{ze}^2+q_{za}^2)\right]\frac{L}{2\pi v_{gz}}\ll 1 \ . \tag{2.65}$$

In many types of radiation effects (as in channeling radiation from electrons; see Andersen *et al.*, 1983), the energy branches are not necessarily equispaced ($\omega_u\neq\omega_d$), and they are determined by the particular (nonharmonic) transverse binding potential. In these cases the third (longitudinal recoil) term in the parentheses of Eq. (2.65) is usually negligible, and the classical limit is reached due to finite-length broadening only if the radian frequency bandwidth due to the transit time $\Delta\omega=2\pi/(L/v_{gz})$ is larger than $\omega_u-\omega_d$. There are other cases, such as the cyclotron resonance maser and planar channeling radiation from positrons, which can be characterized by a nearly harmonic confining potential, for which the energy branches are almost equispaced ("degenerate spacing"); see Andersen *et al.*, 1983). One needs to be careful in these cases and note that ω_u and ω_d are *not* exactly the vertical spacing frequencies between the neighboring branches (2.53) and (2.54). Furthermore, when calculating the emission and absorption frequencies to first order in $\hbar$, the dispersion of $\omega_u(k_z),\omega_d(k_z)$ (the dependence of the branches spacing on the initial wave number k_{zi}) may not be neglected.

This is indeed the case in the cyclotron resonance maser. Except for the limit of longitudinally nonrelativistic electrons $\beta_z\rightarrow 0$ (for which case the Landau-level spacing $\hbar\omega_c$ is nondispersive), the dependence of ω_u and ω_d on both the longitudinal wave number k_{zi} and the transverse-state (Landau-level) number must be considered (to first order in $\hbar$). The expansion of $\omega_u-\omega_d$ to first order in $\hbar$ is carried out for this case in Appendix A.[1] The result is

$$\delta\omega=\omega_a-\omega_e=\frac{\hbar\omega_{c0}^2}{mc^2\gamma^3}\left[\frac{1}{\gamma_z^2}\frac{\cos^2\Theta_q}{(1-\beta_z\cos\Theta_q)^2}-2\beta_z\frac{\cos\Theta_q}{1-\beta_z\cos\Theta_q}-1\right] . \tag{2.66}$$

Dividing by (2.31), we find the classical limit parameter (2.65) of the cyclotron resonance radiation to be

$$\frac{\omega_a-\omega_e}{\Delta\omega_L}=-\frac{\sin^2\Theta_q}{1-\beta_z\cos\Theta_q}\frac{\hbar\omega_{e0}}{\gamma^3mc^2}\frac{\omega_{c0}L}{2\pi v_{gz}} . \tag{2.67}$$

The arbitrary emission angle equations for the frequency line spacing and classical limit parameters (2.66) and (2.67) are useful for understanding the physical mechanism in devices based on the cyclotron resonance radiation effect. These include various FEL-type devices such as the quasioptical CRM (Sprangle *et al.*, 1981), the CARM (Bratman *et al.*, 1983), and the axial magnetic field (wigglerless) FEL (Ride and Colson, 1979; Gell *et al.*, 1982; Fruchtman and Friedland, 1983). As we indicated in the previous section, the small signal gain of the radiation device is proportional to $\delta\omega$.[2] We can thus relate the different terms in the equations for $\delta\omega$ to the physical mechanisms dominating the gain of these devices.

We can trace the origin of the different terms in Eq. (2.66) to three geometrical sources, which correspond to the last three terms in the second-order expansion in (A4). The third term originates from the relativistic mass effect that lifts off the vertical spacing "degeneracy" (equality) between adjacent Landau levels due to the relativistic mass effect (Schneider, 1959). The first term results from the curvature of the energy dispersion curve and the change in the electron wave number due to photon emission (longitudinal recoil). This is an entirely classical gain mechanism, which was proposed first by Weibel (1959), and is identical to the longitudinal recoil gain mechanism in the interbranch transition FEL devices discussed in the previous section. The second term is a new mixed contribution term, which expresses the second-order change in the electron energy due to both longitudinal recoil and transverse-state (Landau-level) transition.

The different terms in the CRM stimulated emission can also be given classical interpretation, as was shown by Chu and Hirshfield (1978). The third term can be related to an azimuthal electron bunching effect, and the first term results from the longitudinal bunching. The mixed term was omitted in that derivation, but it can be easily restored in a fully relativistic classical derivation. It represents the mixed process of azimuthal bunching, due to an axial force, and longitudinal bunching, due to a transverse force. This process is intrinsically relativistic. Consequently the mixed term [second term in Eq. (2.66)] is non-negligible at relativistic electron energies and vanishes at nonrelativistic energies.

It is instructive to compare the CRM line spacing Eqs. (2.66) and (2.67) to the corresponding equation for intra-

[1]For derivation of $\delta\omega$ corresponding to the analogous problem of planar channeling radiation of positrons, see Kurizki and McIver (1985).

[2]We must restrict our conclusion only to devices operating in the low gain regime under conditions in which the electron performs a large number of oscillations (turns) along the interaction length. As will be shown in Sec. III.H, when this condition is not satisfied, extra terms may appear that are not proportional to $\delta\omega$ (these gain terms are not proportional to the derivative of the spontaneous line-shape function, and scale as the interaction length squared instead of the cubic power scaling of the principal term). Consequently, the conclusions drawn in the rest of this section bear limited applicability to some "short" device embodiments of gyrotron and quasioptical CRM.

branch transitions (and the conventional FEL). See Eqs. (2.41) and (2.42). The first observation is that the sign of $\delta\omega$ is opposite in these two cases. This means that the line-shape functions [Fig. 2(a), for both the quantum and classical limits] are inverted relative to each other in the two different cases. The nonrelativistic mass instability effect and the longitudinal bunching effect tend to cancel each other, but the relativistic mass effect is dominant in all emission directions, keeping the sign of $\delta\omega$ negative, except at $\Theta_q=0$, for which $\delta\omega=0$.

The vanishing of $\delta\omega$ and consequently of the gain at $\Theta_q=0$, as is evident from Eq. (2.67), is an important conclusion in the consideration of various FEL-type cyclotron resonance radiation devices, which are proposed for operation at optical frequencies with high-energy electron beams and "long" interaction lengths [axial magnetic field FEL (Ride and Colson, 1979; Gell *et al.*, 1982), wigglerless FEL (Fruchtman and Friedland, 1983), CARM (Bratman *et al.*, 1983), etc.]. In all of these cases small signal gain terms proportional to L^3 are not to be expected for forward radiative emission where $\Theta_q=0$ (for which the analysis is usually done), and the highest-order linear gain term scales in this case, such as L^2. Equation (2.67) suggests that L^3 scaling gain may be obtained with radiation angles (or guided mode zigzag angles), which are at the edge of the spontaneous emission radiative cone $\Theta\lesssim 1/\gamma_z$. For a long interaction length, this gain may be possibly higher than the on-axis gain.

For nonrelativistic electrons the mixed term in Eq. (2.66) always vanishes, and the total stimulated emission can indeed be expressed as the result of pure transverse and longitudinal contributions. We note that even in this limit, the relativistic mass effect is dominant and $\delta\omega$ is always negative. The longitudinal recoil [first term in (2.66)] then only subtracts from the gain. Its negative contribution reduces to zero at transverse emission conditions $\Theta_q\approx\pi/2$. This explains why low electron energy radiative devices, like the quasioptical CRM and the gyrotron,[3] operate predominantly at radiative emission angle vertical or nearly vertical to the magnetic axis. However, in some of these devices the interaction length is short, and gain terms that scale like L^2 may be required to be included for full characterization of the radiation device (Sprangle *et al.*, 1981; Kreischer and Temkin, 1983).

Similar analysis to the one given here for the CRM can be carried out to obtain the conditions for the classical and quantum-mechanical regimes, and to evaluate the linewidth spacing and gain of other transverse binding radiation effects at arbitrary radiation angles. An important example is channeling radiation with an harmonic confining potential [detailed analysis of channeling radiation and its quantum and classical limits can be found in Beloshitskii and Kumakhov (1978)]. Another example is the quadrupole wiggler FEL (Levush *et al.*, 1985), which is a proposed magnetic focus transverse binding force device that can be viewed as an optical version of the "strophotron" (Agdur, 1961) microwave tube.

E. Multiphoton emission

As illustrated in Fig. 3 we usually have for all intrabranch radiative transitions $\omega_e<\omega_a$, because the curvature of the energy dispersion curve is usually positive. This fact gave rise to net gain, as explained before, because it displaces the emission and absorption line centers by a finite amount (however small).

We also notice that due to the monotonous increase of the energy dispersion curve slope, the solution of the energy and momentum conservation conditions (2.13) and (2.14) for a given k_w produces ever decreasing emission line-center frequency as $\mathcal{E}_i$ decreases. Thus an electron at k_{zi}, which makes a spontaneous emission transition, emitting a photon at frequency ω, within a linewidth $\Delta\omega_e$ centered around ω_e, may sometimes make another transition, emitting spontaneously another photon at frequency ω' within a linewidth $\Delta\omega'_e$ centered around $\omega'_e=\omega_e-\delta\omega$, where

$$\delta\omega\equiv\omega_a-\omega_e \tag{2.68}$$

is the same quantum recoil frequency shift calculated in the previous sections [given, for instance, by Eq. (2.42)]. If the electron emits yet another photon, its energy is reduced further and its spontaneous emission line center shifts further toward low frequencies. This spontaneous multiphoton emission effect is not realized in most practical FEL devices and effects, which would generally emit an average of a fraction of a photon per electron. Multi-

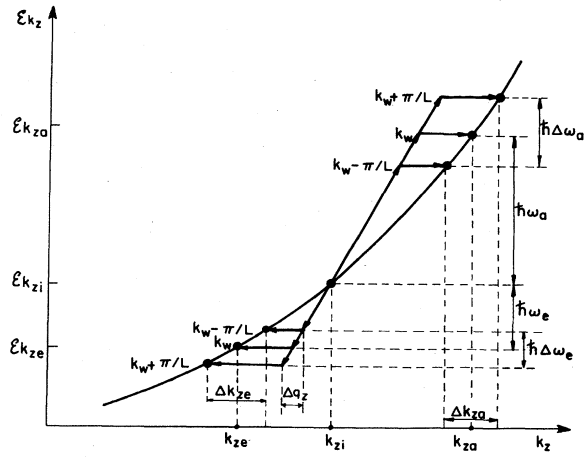

FIG. 3. Finite-length homogeneous broadening caused by an uncertainty $\pm\hbar\pi/L$ in the momentum conservation condition.

[3]Gyrotrons operate with near cutoff waveguide modes for which the "zigzag propagation angle" is nearly vertical (Lau *et al.*, 1981) and quasioptical masers operate with an open cavity radiation mode with propagation direction perpendicular to the magnetic field axis **z** (Sprangle *et al.*, 1981).

photon spontaneous emission is possible, though, in principle, with strong, long wiggler FEL's. It was discussed (see Madey and Deacon, 1977 and Gover, 1983) as a possible theoretical noise saturation mechanism in x-ray FEL's.

Another multiphoton emission effect may take place in stimulated emission.[4] In this case, however, the emitted photons must all be at the same frequency ω of the amplified radiation field. To permit emission of a photon of frequency ω, this frequency must be within the emission linewidth $\omega_e - \Delta\omega_L/2 < \omega < \omega_e + \Delta\omega_L/2$. Since after one photon emission the emission line center reduces to $\omega_e' = \omega_e - \delta\omega$, a second photon emission at frequency ω is possible only if $\omega_e - \delta\omega - \Delta\omega_L/2 < \omega < \omega_e - \delta\omega + \Delta\omega_L/2$, which can be satisfied only if the emission linewidth is larger than the momentum recoil shift—$\Delta\omega_L > \delta\omega$. With similar arguments we find out that in order for a single electron to be able to emit $N_{\rm ph}$ photons of frequency ω in a cascade process, the condition $\Delta\omega_L > N_{\rm ph}\delta\omega$ must be satisfied. We conclude that an upper limit estimate for the number of photons that can be emitted by stimulated emission by a single electron is

$$(N_{\rm ph})_{\rm sat} = \frac{\Delta\omega_L}{\delta\omega} = \frac{\Delta\omega_L}{\omega_a - \omega_e} . \tag{2.69}$$

The stimulated multiphoton emission process is illustrated in Fig. 4. In order to keep emitting at the same photon frequency ω, the crystal momentum imparted by the recoiling electron has to increase gradually from k_w up to its maximum value limited by the finite-length momentum uncertainty $k_w + \pi/L$. We note that to obtain the maximum photons emission number given by Eq. (2.69), which is the saturation photon emission number, it is necessary that $\omega_0 > \omega > \omega_0 - \delta\omega/2$, and that the stimulated emission rate will be strong enough to reach saturation within the interaction range. Note also that the quasilinear gain physical picture given here is a simplification of a complex process and is only useful for crude estimates. In the full saturation process, multiphoton stimulated absorption always takes place simultaneously with the emission in a complex process involving cascade occupation of increasing and decreasing numbers states (McIver and Federov, 1979; Becker, 1980).

The above semiquantitative discussion of the saturation mechanism in a finite-length homogeneously broadened FEL also leads to an estimate for the saturation energy extraction efficiency of the quasifree-electron stimulated radiation emission device (FEL):

$$\eta = \frac{(N_{\rm ph})_{\rm sat}\hbar\omega}{\mathcal{E}_k} = \frac{\hbar\omega}{\mathcal{E}_k}\frac{\Delta\omega_L}{\omega_a - \omega_e} . \tag{2.70}$$

When $\Delta\omega_L$ and $\omega_a - \omega_e$ are substituted from Eqs. (2.31) and (2.41) and $m_\parallel^*$ from Eq. (2.47), one obtains

$$\eta = \beta_z^3\gamma_z^2\frac{\lambda}{L} . \tag{2.71}$$

This equation agrees well with previous estimates of the power extraction efficiency in FEL's (Gover and Sprangle, 1981). In the highly relativistic limit of the magnetic bremsstrahlung FEL (2.24), it reduces to the known equation (Sprangle and Smith, 1980) $\eta = 1/(2N_w)$. Rigorously the extraction efficiency of the FEL must be determined in a nonlinear gain calculation (which is outside the scope of the present model), and would be expected to be a function of the FEL input power. Equations (2.70) and (2.71) signify the maximum possible efficiency that can be achieved in a uniform interaction region of length L. That is assuming that the device is tuned to operate within the positive gain curve in the small signal regime, and the input power is increased until saturation is reached at the end of the interaction region.

A comparison of (2.34) and (2.35) to (2.69) leads to the conclusion that the quantum regime is always characterized by single photon emission (per electron), while the classical regime is characterized by the *possibility* of multiphoton emission. Note, however, that even though (2.69) indicates that $N_{\rm ph} \gg 1$ in the classical regime, this number of photons is emitted only if saturation is reached. Typically $(N_{\rm ph})_{\rm sat}$ photons of the order of thousands is emitted per electron in saturated magnetic bremsstrahlung FEL oscillators (Elias *et al.*, 1976). However, below saturation fewer photons than $(N_{\rm ph})_{\rm sat}$

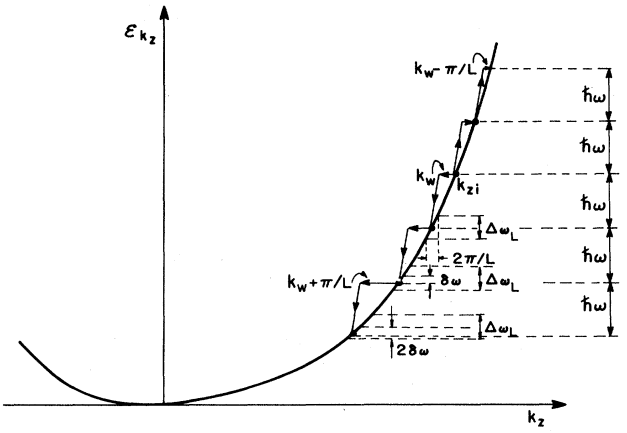

FIG. 4. Multiphoton stimulated emission and absorption process by a quasifree electron.

[4]Both the spontaneous and stimulated multiphoton emission effects that we discuss here are simple demonstrations of the fact that classical oscillators, such as radio antenna or a microwave tube, can emit, either spontaneously or by stimulation, many photons. This should be distinguished from the use of the term "multiphoton process" in connection with atomic ionization by intense laser fields (Bucksbaum *et al.*, 1987), where quantum effects remain even in the "multiphoton absorption" process.

(even less than 1 on the average) may be emitted even in the classical regime, if the amplified radiation signal power is small enough.

We point out that the entire discussion of this section, which referred to intrabranch radiative transition schemes [with the exception of Eq. (2.71), which was evaluated specifically for the case of the magnetic bremsstrahlung FEL], applies without change also to interbranch radiative schemes. This is correct on the condition that the spacings between the branches are nearly degenerate.

F. The transition from the quantum to the classical regime

We have described the radiation from quasifree electrons in the case of transversely discrete states as quantum-mechanical electronic transitions between the longitudinal continuous states. The initial and final longitudinal states k_z, between which the electronic transitions take place, are well-defined quantum mechanically in the long interaction length (quantum) limit (2.34). In this limit the spacing between the emission and absorption lines, $\delta\omega$ [see upper curve of Fig. 2(a)], which is a $\hbar$-dependent quality, is considerably larger than the linewidth (which is $\hbar$ independent). For this reason we consider (2.34) as the condition for the longitudinally quantum-mechanical regime. In the opposite limit (2.35), the characteristic parameters of the net stimulated emission curve [lower curve of Fig. 2(a)] are not a function of $\hbar$, and therefore we consider it to be the classical regime limit. We also proved that in the quantum limit only single photon emission is possible, while in the classical limit multiphoton emission is possible.

An alternative definition for the quantum and classical regimes was suggested by Renieri (1984). This definition can be restated in a more general way as follows. The electron operates in the finite-length homogeneously broadened classical regime if throughout the entire interaction length L its axial position can be quantum mechanically localized with an accuracy better than the wavelength of the electromagnetic force wave with which it interacts. In the opposite limit the electron operates in the longitudinally quantum-mechanical regime (Fig. 5). The interacting electromagnetic force wave is the ponderomotive force in the case of bremsstrahlung FEL's, and is the slow electromagnetic field component in the case of slow-wave FEL's (Gover and Sprangle, 1981). In either case it is given by $\lambda_{pm}=2\pi/(q_z+k_w)$, with $k_w=0$ in the case of Čerenkov FEL. Renieri's classical limit condition is derived in Appendix B, resulting in (B9),

$$\frac{\hbar L}{2\pi m_{\parallel}^{*} v_{gz}}(q_z+k_w)^2 \ll \pi \ , \tag{2.72}$$

which can also be written in the practical form

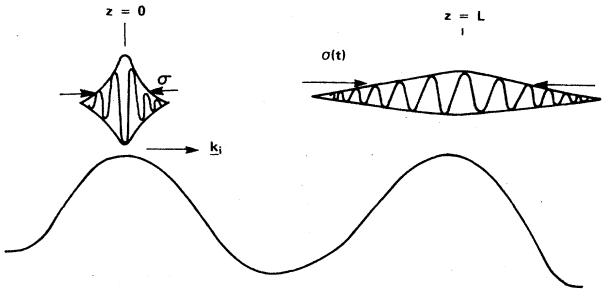

FIG. 5. Longitudinal electron wave packet in the longitudinal quantum limit at the beginning and end of the interaction region. The longitudinal variation of the electromagnetic force (ponderomotive wave) is shown for comparison.

$$\frac{\lambda_{pm}^2}{L} > \frac{1}{\pi}\frac{\lambda_c}{\gamma_z^2\gamma\beta_z} = \frac{7.8\times10^{-3}\ \text{Å}}{\gamma_z^2\gamma\beta_z} \ , \tag{2.73}$$

where $\lambda_c=\hbar/(mc)=2.4\times10^{-2}$ Å is the Compton wavelength.

Although Renieri's quantum regime criterion and the criterion of nondegeneracy of the emission and absorption lines ("large longitudinal recoil") refer to quite different physical aspects of the interaction, it is found that they take place at almost the same parameters regime. Condition (2.72) is identical with (2.43) except for a numerical factor. This interesting result is taken advantage of in the following discussion. It is instructive to point out that a full quantum-mechanical description of a particle requires a quantum wave packet. In general, it is necessary to justify the common practice of using a single harmonic plane wave to describe the particle in a quantum-mechanical analysis of electron radiation problems. Moreover, we point out that the single wave approximation is not valid in certain problems as in FEL's with prebunched electron beams (Schnitzer and Gover, 1985), where a full wave packet should be used in order to describe properly the electron.

In the next sections we derive significant quantitative conclusions from the transition from the quantum to the classical limit. This requires careful examination of the assumptions made in the quantum-mechanical analysis. We make the following observations.

(1) In the quantum analysis we usually assume a single longitudinal state function [(2.6) or (2.7)] in order to describe the electron. This approach is legitimate in the inherently quantum-mechanical regime (2.34), because, as we show in Appendix B, in this regime any electron wave packet will spread very fast into a width much larger than λ_{pm}, and throughout most of the interaction length will behave indeed as an infinite-length single state harmonic wave function of wave number k_z. However, in the opposite (classical) limit (2.35), using a single state wave function to describe the electron quantum mechanically, as is usually done (Madey, 1971; McIver and Federov, 1979; Becker, 1980; Stenholm and Bambini, 1981; Bosco *et al.*, 1983; Dattoli and Reinieri, 1983;

Gover, 1984),[5] is not always correct. The most general quantum description of the electron should be done by means of a wave packet [see Eq. (B6)], which keeps the information on the position (phase) of the well-localized electron particle relative to the wave. Indeed, such an approach would be essential in problems where the electron phase is important, as in the prebunched FEL (Schnitzer and Gover, 1985). Since we will relate in the present work only to FEL's with electrons arriving at random phase, the use of the single longitudinal state wave-function quantum description (2.7) is acceptable, even if we intend later on to take the classical limit, (2.35). The quantum-mechanical uncertainty in the axial position of an electron described by a single longitudinal state wave function (2.7) is equivalent to averaging over the electron's initial phases (entry times) in a classical analysis.

(2) In the classical regime [see (2.35)] multiphoton emission is possible. Only a multiphoton emission quantum analysis will describe correctly the FEL in the entire small signal classical regime (McIver and Federov, 1979; Becker, 1980). However, it is still correct to use a single photon emission analysis (as we will do in the next section) even in the classical limit, as long as we limit the signal wave input down to assure that the energy of the radiation emitted per one electron is less than $\hbar\omega$. It was shown elsewhere (McIver and Federov, 1979; Becker, 1980) that a full multiphoton emission model does not change the results obtained from a single photon emission analysis.

(3) We note that Renieri's quantum limit condition refers only to the longitudinal dimension. This can be used only for intrabranch transitions in radiation schemes with transversely discrete quantum states, or when the problem is uniform in the transverse dimensions. For completion one should identify also the possibility of a transverse quantum regime, which can take place in the case of transversely continuous states. This inherently quantum regime is obtained when there is no way to describe the electron with a wave packet of finite transverse dimensions, so that the electron wave diffraction effect along the entire interaction length remains negligible. More specifically, the wave-packet transverse dimensions do not expand beyond the extent of the electromagnetic field transverse variation parameter (e.g., the reciprocal transverse wave number, or in the case of Smith-Purcell radiation, the transverse decay length). If we are in this inherent transversely quantum regime [Fig. 6(a)], it is correct to use a plane wave to describe the electron. However, if we want to describe the electron quantum mechanically in a way that is also correct in the transversely classical limit, we must use a transverse wave packet, since in this limit the electron

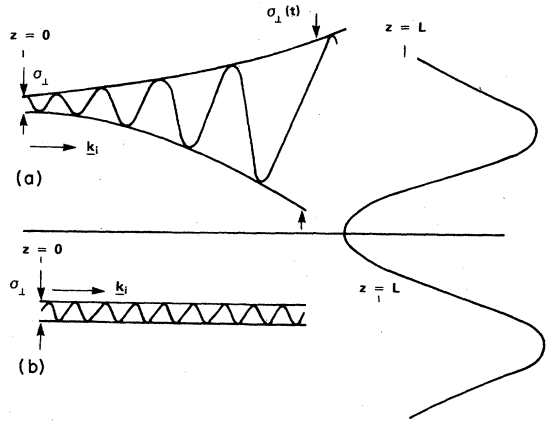

FIG. 6. Transverse electron wave-packet diffraction along the interaction region, compared with the transverse variation of the electromagnetic force.

transverse coordinates can be localized well enough along the entire interaction length [Fig. 6(b)] and thus be affected by the radiation field variation. The field variation experienced in the transverse classical limit by a localized electron along its classical trajectory is deterministic and can be used in the interaction calculation (as we later demonstrate in Sec. III.B.3). Appropriate precautions for carrying out correctly a quantum-mechanical analysis in the transverse dimensions are taken in the next section in the transverse quantum and classical analyses (Sec. III.B) in line with the present observation.

The parametric conditions for the inherent transverse quantum and classical limits are described in Appendix B. The transverse dimension of the electron is estimated to be the minimal width of the transverse wave packet for which the wave diffraction expansion within the interaction length L is still moderate. For an electron characterized by the de Broglie wave number $\lambda_{DB}=\hbar/\bar{p}$, this minimum width is $\sqrt{\lambda_{DB}L/\pi}$. We note that the relevant momentum for the calculation of the de Broglie wavelength is the average axial momentum $\bar{p}=\gamma m\bar{v}$ (which is different from the total momentum $p=\gamma mv$ when the electron is subjected to an intense transverse quiver).

The dimension of the transverse variation of the radiation and wiggler fields, to which the electron wave-packet width needs to be compared, is different for various free-electron radiation effects. In the case of free-space propagation we may distinguish between two different situations. (1) The wave propagates at an angle to the electron, in which case the relevant parameter characterizing the transverse variation of the radiation field is $2\pi/q_\perp=\lambda/\sin\Theta_q$ (also applicable to waveguide modes with Θ_q representing the "zigzag" angle). (2) The radiation wave beam propagates coaxially with the electron, and its diffraction limited minimum transverse dimension is given by $\sqrt{\lambda L/\pi}$. In the first case the transverse classical limit condition is found to be

[5]See an extensive bibliography on quantum treatises of magnetic bremsstrahlung FEL's in Elias *et al.*, 1976.

$$\frac{\lambda^2}{L\sin^2\Theta_q} > \frac{1}{\pi}\frac{\lambda_c}{\beta\gamma} = \frac{7.8\times10^{-3}\ \text{Å}}{\beta\gamma} \tag{2.74}$$

and in the second case

$$\lambda > \frac{\lambda_c}{\beta\gamma} = \frac{2.4\times10^{-2}}{\beta\gamma} . \tag{2.75}$$

In the language of accelerator physics, $\lambda_{\rm DB}=\lambda_c/(\beta\gamma)$ can be interpreted as the "emittance" (Lawson, 1977) of a single electron, fundamentally limited by the quantum uncertainty principle $\Delta p_\perp \Delta r_\perp \approx \hbar$. In this interpretation λ_c is equivalent to the "normalized emittance" of a single electron, and Eq. (2.75) is analogous to the classical condition at which an electron beam, interacting with a radiation beam, can be treated as a filamentary current with zero emittance.

When considering typical parameters of magnetic bremsstrahlung FEL's one can verify that in most practical situations both the longitudinal [Eq. (2.73)] and the transverse [Eqs. (2.74) and (2.75)] classical limits are difficult to violate. There is some interest in operating a FEL in the quantum regime, stemming from fundamental research motivation (Gea-Banacloche *et al.*, 1983). Equations (2.73)–(2.75) suggest that the quantum regime may be easier to attain in schemes utilizing nonrelativistic electrons. We also note that in order to observe quantum effects, one should satisfy strenuous conditions on the electron beam quality parameters in addition to operating in a parameter regime that is excluded by one of the classical conditions (2.73)–(2.75). See Gover (1983).

G. The case of transversely continuous states

Only in particular emission directions and when symmetry considerations or selection rules dictate it, will the emission process involve electronic transitions into only one transverse state. In general, when calculating the probability for photon emission, one should consider all possible electronic transitions. In the limit when a large number of transverse states are involved in the radiative transitions (which is certainly the case when the electron is unbound in the transverse dimensions), it would be appropriate to assume a model of transversely continuous states. Thus, contrary to the case considered before, the electron may recoil in the radiative process in an arbitrary direction (both longitudinal and transverse) and its final state is selected from a three-dimensional continuum.

The simplest examples to consider are those in which the electrons and the radiation propagate in transversely uniform (laminated) periodic structures, as is the case in many of the radiation effects and devices under consideration, as, for instance, in magnetic bremsstrahlung FEL (Elias *et al.*, 1976), coherent bremsstrahlung (Uberal, 1956; Walker *et al.*, 1975), and coherent transition radiation (Piestrup and Finman, 1983). In all of these cases $\mathcal{E}_{\mathbf{k}}$ is given by Eq. (2.4), and the emission and absorption frequencies are determined by the energy conservation condition (2.1) and the momentum conservation condition (2.2) modified by the crystal momentum $\mathbf{k}_w = k_w \hat{e}_z$. This can be written explicitly in the form

$$\mathcal{E}_{\mathbf{k}_i} - \mathcal{E}_{\mathbf{k}_e} = \hbar\omega_e , \tag{2.76}$$

$$\mathbf{k}_i - \mathbf{k}_e = \mathbf{q}_e + \mathbf{k}_w , \tag{2.77}$$

$$\mathcal{E}_{\mathbf{k}_a} - \mathcal{E}_{\mathbf{k}_i} = \hbar\omega_a , \tag{2.78}$$

$$\mathbf{k}_a - \mathbf{k}_i = \mathbf{q}_a + \mathbf{k}_w , \tag{2.79}$$

which modifies the set (2.13)–(2.16) by the inclusion of the transverse momentum conservation condition.

Expansion of $\mathcal{E}_{\mathbf{k}_e}$ and $\mathcal{E}_{\mathbf{k}_a}$ to first order in $\hbar$ around k_i produces a result similar to that of (2.17),

$$\omega_a \approx \omega_e \approx \mathbf{v}_g\cdot(\mathbf{q}_0+\mathbf{k}_w) \equiv \omega_0 , \tag{2.80}$$

where

$$\mathbf{v}_g \equiv \frac{1}{\hbar}\frac{\partial \mathcal{E}_{\mathbf{k}}}{\partial \mathbf{k}} . \tag{2.81}$$

With the optical dispersion relation (2.20) (free-space radiation modes), the radiation condition is

$$\omega_0 = \frac{\mathbf{v}_g\cdot\mathbf{k}_w}{1-\beta_g\cdot\hat{e}_{\mathbf{q}}} . \tag{2.82}$$

This is identical to Eq. (2.22) when $\mathbf{v}_g = \hat{e}_z v_{gz}$.

In the case considered now (of a laminated periodic structure), the finite-length homogeneous broadening effect is derived from (2.26) and (2.27), assuming exact satisfaction of the transverse momentum conservation conditions $\mathbf{k}_{i_\perp} - \mathbf{k}_{e_\perp} = \mathbf{q}_{e_\perp}$, $\mathbf{k}_{a_\perp} - \mathbf{k}_{i_\perp} = \mathbf{q}_{a_\perp}$. This results in

$$\Delta\omega_L = \mathbf{v}_g\cdot\left[\Delta\mathbf{q} + \frac{2\pi}{L}\hat{e}_z\right] , \tag{2.83}$$

and using (2.20),

$$\Delta\omega_L = \frac{v_{gz}}{1-\beta_g\cdot\hat{e}_{\mathbf{q}}}\frac{2\pi}{L} . \tag{2.84}$$

The well-known fractional linewidth equation $\Delta\omega_L/\omega_0 = 1/N_w$ [Eq. (2.32)] is straightforwardly derived for the present case by taking the ratio between (2.84) and (2.82).

The quantum-mechanical shift between the emission and absorption lines is found from second-order expansion of $\mathcal{E}_{\mathbf{k}_e}, \mathcal{E}_{\mathbf{k}_a}$ in terms of $\hbar$ around $\mathbf{k}_i$. Instead of (2.41), we obtain, using (2.20),

$$\omega_e = \omega_0 - \tfrac{1}{2}\delta\omega , \tag{2.85}$$

$$\omega_a = \omega_0 + \tfrac{1}{2}\delta\omega , \tag{2.86}$$

$$\delta\omega = \omega_a - \omega_e = \frac{\hbar}{1-\beta_g\cdot\hat{e}_{\mathbf{q}}}\sum_{i,j=1}^{3}\left[\frac{1}{m^*}\right]_{ij}(\mathbf{q}_0+\mathbf{k}_w)_i(\mathbf{q}_0+\mathbf{k}_w)_j , \tag{2.87}$$

where

$$\left[\frac{1}{m^*}\right]_{ij}=\frac{1}{\hbar^2}\frac{\partial^2\mathscr{E}_{\mathbf{k}}}{\partial k_i\partial k_j}\ , \tag{2.88}$$

with k_i,k_j $(i,j=1,2)$ being transverse continuous wave numbers related to the transverse momentum $\mathbf{p}_\perp=\hbar\mathbf{k}_\perp$, and $k_3\equiv k_z$ is the longitudinal wave number. The classical limit condition (2.35) now reads

$$\frac{\omega_a-\omega_e}{\Delta\omega}=\frac{\hbar L}{2\pi v_{gz}}\sum_{i,j=1}^{3}(\mathbf{q}_0+\mathbf{k}_w)_i\left[\frac{1}{m^*}\right]_{ij}(\mathbf{q}_0+\mathbf{k}_w)_j\ll 1, \tag{2.89}$$

and the maximum number of stimulated emission photons $(N_{\rm phq})_{\rm sat}$ that can be emitted at direction $\hat{e}_{\mathbf{q}}$ is given by the inverse of (2.89).

Equation (2.89) can be made more explicit when we substitute the effective-mass tension elements [calculated for the energy dispersion relation (2.4)]:

$$\left[\frac{1}{m^*}\right]_{i\neq j}=-\frac{\beta_i\beta_j}{\gamma m},\quad \left[\frac{1}{m^*}\right]_{i=j}=\frac{1}{\gamma\gamma_i^2 m}\ , \tag{2.90}$$

where $\gamma_i=(1-\beta_i^2)^{-1/2}$. We can also substitute [using (2.20) and (2.80) with $\mathbf{k}_w=k_w\hat{e}_z$] $(\mathbf{q}_0+\mathbf{k}_w)_{i\neq z}=(\omega_0/c)\cos\Theta_i$, $(\mathbf{q}_0+\mathbf{k}_w)_z=(\omega_0/c)\beta_z^{-1}$. For the case in which the electron motion is aligned with the wiggler axis z: $\boldsymbol{\beta}=\beta\hat{e}_z$, the mass tensor becomes diagonal:

$$(1/m^*)_{i\neq j}=0\ ,$$
$$(1/m^*)_{xx,yy}=(\gamma m)^{-1}\ ,$$
$$(1/m^*)_{zz}=(\gamma_z^2\gamma m)^{-1}\ ,$$

and Eq. (2.89) simplifies into

$$\frac{\omega_a-\omega_e}{\Delta\omega_L}=[(\gamma_z\beta_z)^{-2}-\sin^2\Theta]\frac{\hbar\omega_0}{\gamma mc^2}\frac{\omega_0 L}{2\pi v_z}\ll 1\ ; \tag{2.91}$$

using the radiation condition (2.82),

$$\frac{\omega_a-\omega_e}{\Delta\omega_L}=\frac{(\gamma_z\beta_z)^{-2}-\sin^2\Theta}{1-\beta_z\cos\Theta}\frac{\hbar\omega_0}{\gamma mc^2}N_w\ll 1\ . \tag{2.92}$$

Note that Eqs. (2.91) and (2.92) reduce into the corresponding Eqs. (2.43) and (2.44) of the transverse discrete states in the limit $\Theta=0$. This justifies the use of a one-dimensional "longitudinal recoil" model for various radiation schemes (such as the magnetic bremsstrahlung FEL), even though they are really characterized by transverse continuous states. However, the difference between Eqs. (2.91) and (2.92) and the corresponding Eqs. (2.43) and (2.44) for $\Theta\neq 0$ indicates that the neglect of the transverse recoil in the calculation of gain in such devices is not always correct, and it may result in a significant error unless $\Theta\ll(\beta_z\gamma_z)^{-1}$. In Sec. V we will take advantage of the more general classical limit parameters, Eqs. (2.91) and (2.92), in order to calculate the gain of the magnetic bremsstrahlung FEL and the cyclotron resonance maser at a general off-axis emission angle.

A known radiation effect that is a good example for the present formulation of transversely continuous states is the coherent bremsstrahlung radiation effect (Uberal, 1956; Walker *et al.*, 1975; Kurizki and McIver, 1982; Spence *et al.*, 1983). It also demonstrates well the transition from the case of transverse continuous states to the case of transverse discrete states. The periodic structure in which the electron (or positron) propagates is the crystal lattice. The periodic structure wave number that it experiences is $k_w=|\mathbf{G}|$, where $\mathbf{G}$ is any reciprocal-lattice vector of the crystal lattice. If the kinetic energy of the electron motion in any direction is much larger than the binding potential energy of the crystal, then the electron in the crystal can be considered free in all dimensions, characterized by continuous transverse and longitudinal states, and its group velocity and mass tensor are the same as in free space [as given in Eq. (2.90) above]. If the electron (positron) propagates at a small angle relative to a crystal channel, and its kinetic energy perpendicular to the channel is only slightly above the binding energy of the channel, then even though the particles occupy a continuum of transverse states, their energy dispersion relation may deviate significantly from the free-space dispersion (2.4). In such a case explicit knowledge of the band diagram in the solid is necessary in order to calculate the mass tensor (2.88) and the group velocity (2.81). Alternatively, it may be necessary in such a case to solve for the emission and absorption frequencies by exact solution of the energy-momentum conservation conditions (2.76)–(2.79) with the given dispersion relation of the transverse energy bands (Kurizki and McIver, 1985). When the transverse energy of the electron (positron) is smaller than the binding energy of the crystal channel, the electron will occupy transversely bound (channeling) discrete states. The radiation processes in this case are better described in terms of transverse discrete states in Secs. II.A, II.D, and the next section.

H. The case of transversely discrete states: Combined longitudinal and transverse transitions

In Sec. II.A we considered purely longitudinal (intrabranch) radiative transitions. In Sec. II.D we considered transitions between pure transverse states (interbranch transitions). For the sake of completeness we briefly discuss in this section the synergistic case, in which the transitions are between branches of different transverse quantum numbers and at the same time involve a transfer of longitudinal crystal momentum. These transitions are still controlled by the energy and momentum conservation conditions (2.10) and (2.11), where $(n_i,l_i)\neq(n_f,l_f)$ and $m_i\neq m_f$.

There are a few radiation effects for which the mixed transitions case is of interest. One example is the combined transverse and longitudinal transitions in FEL schemes, which consists of an axial magnetic field superposed by a periodically modulated transverse or longitu-

dinal magnetic field (McMullin and Bekefi, 1981; Grossman *et al.*, 1983; Shraga *et al.*, 1986). Another example is the betatron oscillation in magnetic bremsstrahlung FEL with a long wiggler. This transverse oscillation results from a transverse quadrupole focusing force produced by the wiggler or superposed on it. In both cases the transverse oscillations generate in the radiative emission spectrum sideband lines superposed on the high-frequency lines associated with the periodicity.

In this section we will briefly examine the kinematics of the combined longitudinal and transverse transitions case through the example of coherent bremsstrahlung radiation by transversely bound (channeled) electrons (or positrons) in the crystal lattice. A channeled electron (or positron) experiences simultaneously the transverse binding potential of the channel potential and the longitudinal periodic electrostatic potential produced by the periodic arrangement of the crystal atoms along the channel. The radiation wave is also affected by the periodic refraction index modulation of the same period (Gover and Yariv, 1978a; Kurizki and McIver, 1982) (photon umklapp or Smith-Purcell mechanism), though this mechanism is believed to produce a much smaller radiation effect (Andersen *et al.*, 1983; Kurizki and McIver, 1984, 1985). Consequently the high-frequency coherent bremsstrahlung spectrum that is attributed to crystal momentum-transfer processes between continuous states can be superposed with the channeling radiation frequencies in mixed longitudinal-transverse transitions. The frequencies associated with different transverse transitions of the same longitudinal momentum transfer k_w value should give rise to satellites ("sidebands") about the purely longitudinal k_w peak. These combined spectrum characteristics were proposed and analyzed in previous publications (Kurizki and McIver, 1982, 1984, 1985), and may have been observed experimentally (Andersen, 1986). New coherent bremsstrahlung experiments with very low energy e-beams recently pioneered by Spence *et al.* (1983) give hope that the expected satellites spectrum may be revealed if measurement could be carried out with high enough spectral resolution.

The energy diagram needed for a full description of the mixed transitions case is a combination of Figs. 1(a), 1(b), and 1(c). This combination (describing the combined channeling-Smith-Purcell-bremsstrahlung processes) is difficult to represent graphically. In order not to obscure the picture, we show in Fig. 1(d) only a simplified diagram, which is essentially a combination of diagrams 1(a) and 1(c) describing the combined channeling radiation-photon umklapp process. Since the kinematic considerations of the photon umklapp (Smith-Purcell-type emission) and coherent bremsstrahlung types of interactions are the same, and since the index of refraction modulation period is the same as the electric potential modulation, the radiation frequencies equations that we derive from Fig. 1(d) apply also to the coherent bremsstrahlung process. For simplicity we show in Fig. 1(d) only the radiative emission process and ignore absorptive transitions. It is assumed that the intrabranch radiation frequency ω_0 [see Eq. (2.22)], which is associated only with the crystal momentum transfer, is much larger than the interbranch (pure transverse-states transition) frequencies given by Eqs. (2.55) and (2.56). This is indeed the case in coherent bremsstrahlung of channeled electrons in which

$$v_z k_w \gg \omega_{a,u} \ , \tag{2.93}$$

so the transitions between channeling states will normally form satellites on the coherent bremsstrahlung lines spectrum. In Fig. 1(d) $\omega_u(\omega_d)$ are the vertical energy spacings between the initial energy branch and any higher (lower) branch of the channeling states. The periodic structure wave number is $k_w = 2\pi/\lambda_w$, where λ_w is the lattice constant in the channeling direction.

Inspection of Fig. 1(d) leads to the conclusion that the satellite transition frequencies, which are the general solutions of Eqs. (2.10) and (2.11), are just the beat frequencies of the pure intrabranch and interbranch transitions frequencies. The combination of Eqs. (2.22), (2.36), (2.41), (2.55), and (2.56) results in the satellites frequencies:

$$\omega_{e\pm} = \frac{v_{gz} k_w - \hbar\omega_0^2/(2m_{\parallel}^* v_{gz}^2) \pm \omega_u^d}{1 - \beta_{gz}\cos\Theta_{\mathbf{q}}} \ . \tag{2.94}$$

The center line frequency ω_{e0} is found from this equation by substituting $\omega_u^d = 0$. In the derivation of this equation we neglected the quantum recoil correction to the interbranch (transverse) transition frequencies, and calculated the longitudinal quantum recoil shift of the lines [second term in the numerator of Eq. (2.94)] to first order in $\hbar$. This approximation is valid at low energies (below few MeV for electron channeling radiation). At high energies the recoil effect may have to be calculated to higher order in $\hbar$ or evaluated by exact solution of Eqs. (2.13), (2.14), (2.4), and (2.21), if the line frequencies are to be evaluated at an accuracy better than the satellite spacing [third term in the numerator of Eq. (2.94)]. See Kurizki and McIver (1985).

The finite-length homogeneous broadening of the satellite emission lines will be similar to the broadening of the center line $\Delta\omega_L$ [see Eq. (2.31)]. If this broadening mechanism is dominant in determining the emission linewidths, as in the experiment of Andersen and McIver (1981), then the condition for resolving the satellites from the center line is

$$\omega_{u,d} > \frac{2\pi v_{gz}}{L} \tag{2.95}$$

Considering that $\omega_{u,d}$ decreases as a function of beam energy (in the harmonic potential model applicable to positrons, $\omega_{u,d} \approx \omega_{h0}/\gamma^{1/2}$, whereas for electrons $\omega_{u,d} \approx \omega_{h0}/\gamma^{1/3}$), one would expect to be able to observe the satellites spectrum in combined channeling-coherent bremsstrahlung experiments with low energy (up to few MeV). For typical values (Andersen and McIver, 1981) of $\hbar\omega_d \approx 100$ eV (obtained for electrons channeled along

the 110 or 100 plane in Si) and crystal thickness $L > 0.5$ μm, for which $\hbar(2\pi v_{gz}/L) \approx 2.5$ eV, condition (2.95) is well satisfied. We conclude that if the coherent bremsstrahlung spectrum would be measured with high spectral resolution under the same conditions as Andersen's channeling radiation experiment, the satellites structure could possibly be resolved.

III. TRANSITION RATES CALCULATION

In order to obtain a quantitative measure of the spontaneous and stimulated radiative power emission in the various radiation schemes considered here, one should embark on the dynamical analysis of the interaction process and solve the quantum-mechanical equations (at least perturbatively, as in this work). Since we are interested in both spontaneous and stimulated emissions, and particularly in the relation between them, it is advantageous to start from a quantum-electrodynamical model where both the electrons and the radiation field are described quantum mechanically, and both spontaneous and stimulated emission are treated with the same formulation.

As we pointed out in the Introduction, the electrons occupy a continuum of quantum states, at least in the longitudinal dimension. On the other hand, the photon occupation states, which describe the radiation field, are discrete. A first step in calculating the spontaneous and stimulated emission parameters is to derive the transition rate, which in our model is the rate at which the radiation mode photon occupation state $|\nu+1\rangle$ grows, when starting from a state $|\nu\rangle$ (emission), or the rate at which state $|\nu-1\rangle$ grows, starting from $|\nu\rangle$ (absorption). In the linear regime the net photon emission rate is the growth rate of the state $|\nu+1\rangle$ minus the growth rate of the state $|\nu-1\rangle$. The spontaneous emission rate into a given mode $\mathbf{q}$ is found by setting $\nu_{\mathbf{q}}=0$ in the equation for the emission rate. This can be transformed into an equation for spontaneous emission spectral radiant intensity when going to the large cavity limit where the radiation modes form a continuum (as we will do in Sec. IV). The stimulated emission net gain of a given mode can then be straightforwardly derived in terms of the difference between emission and absorption rates. It is calculated here in the limit of single photon emission absorption.

The model we just described suggests the use of Fermi's golden rule to calculate the transition rates (Schiff, 1971). However, caution must be exercised, since in some radiation schemes application of Fermi's rule may lead to erroneous results. We therefore start from a first principle first-order perturbation analysis of the electron-photon wave equations, and find that in some cases, as in the classical case of transversely continuous states, a modified version of Fermi's golden rule should be used.

We start by deriving a general first-order perturbation procedure for quantum states with two subsets of quantum numbers, one of which is discrete. This is applied to the case in which the continuous subset refers to electron states that are solutions for Schrödinger's equation in a general wiggler field, and the discrete subset refers to the occupation number states of a quantized radiation field. Since in most radiation schemes of interest the electron is relativistic, this model, which relies on the Schrödinger equation, is not satisfactory. We thus extend it in Sec. III.C to the relativistic regime by reducing the Klein-Gordon equation into a Schrödinger-type form. The use of Dirac equation formulation can be avoided since, in general, spin effects are negligible.

A. A first-order perturbation analysis

The combined Hamiltonian of the electron and radiation field in the nonrelativistic limit is (Marcuse, 1980)

$$H=\frac{(-i\hbar\nabla+e\,\mathbf{A})^2}{2m}-eV+\sum_{\mathbf{q}\sigma}\hbar\omega_q(\hat{a}^{\dagger}_{\mathbf{q}\sigma}\hat{a}_{\mathbf{q}\sigma}+\tfrac{1}{2}) , \quad (3.1)$$

where $\hat{a}^{\dagger}_{\mathbf{q}\sigma},\hat{a}_{\mathbf{q}\sigma}$ are the creation and annihilation operators of mode $\mathbf{q}\sigma$, $\mathbf{q}$ is the spatial mode index, σ is the polarization index, and ω_q is the frequency of this mode. We substitute $\mathbf{A}=\mathbf{A}_w+\mathbf{A}_s$, $V=V_w+V_s$ where $\mathbf{A}_w$ and V_w are vector and scalar potentials of a general wiggler, and $\mathbf{A}_s$ is the radiation mode vector and scalar potentials. Neglecting the second-order term in $\mathbf{A}_s$ the Hamiltonian can be written as the sum of an unperturbed Hamiltonian (H_0) and a perturbation Hamiltonian (H'), which is first order in the radiation field, $\mathbf{A}_s$, where

$$H_0=H_{0\,\mathrm{el}}+H_{0\,\mathrm{field}}=\frac{(-i\hbar\nabla+e\,\mathbf{A}_w)^2}{2m}-eV_w+\sum_{\mathbf{q}\sigma}\hbar\omega_{\mathbf{q}}(\hat{a}^{\dagger}_{\mathbf{q}\sigma}\hat{a}_{\mathbf{q}\sigma}+\tfrac{1}{2}) , \quad (3.2)$$

$$H'\equiv\frac{e}{m}\hat{\mathbf{A}}_s\cdot(-i\hbar\nabla+e\,\mathbf{A}_w) . \quad (3.3)$$

Since the quantized radiation fields are the sourceless cavity modes, we may assume a transverse gauge with $\nabla\cdot\mathbf{A}_s=0$, $V_s=0$, for which case the use we made in (3.3) of the commutation relation $[\nabla,\hat{\mathbf{A}}_s]=0$ is justified. If the radiation field quantization is carried out on traveling radiation modes in the Schrödinger picture, then the vector potential operator can be presented as (Bjorken and Drell, 1965)

$$\hat{\mathbf{A}}_s=\sum_{\mathbf{q}\sigma}[\tilde{\mathbf{A}}_{s_{\mathbf{q}\sigma}}(\mathbf{r})\hat{a}_{\mathbf{q}\sigma}+\tilde{\mathbf{A}}^{*}_{s_{\mathbf{q}\sigma}}\hat{a}^{\dagger}_{\mathbf{q}\sigma}] , \quad (3.4)$$

where $\tilde{\mathbf{A}}_{s_{\mathbf{q}\sigma}}(\mathbf{r})$ is the phasor of the classical field of mode $\mathbf{q}\sigma$:

$$\mathbf{A}_{s_{\mathbf{q}\sigma}}(\mathbf{r},t)\equiv\mathrm{Re}[\tilde{\mathbf{A}}_{s_{\mathbf{q}\sigma}}(\mathbf{r})\exp(-i\omega t)] ,$$

$\tilde{\mathbf{A}}_{s_{\mathbf{q}\sigma}}(\mathbf{r})$ is a single mode in an arbitrary set of orthogonal eigenmodes and is normalized in a finite volume V to

$$\int_V \tilde{\mathbf{A}}_{s_{q\sigma}}(\mathbf{r})\cdot\tilde{\mathbf{A}}^*_{s_{q'\sigma'}}(\mathbf{r})d^3r=\frac{\hbar}{2\varepsilon\omega_q}\delta_{qq'}\delta\sigma\sigma' \tag{3.5}$$

and in an infinite volume to

$$\int_{-\infty}^{\infty}\tilde{\mathbf{A}}_{s_{q\sigma}}\cdot\tilde{\mathbf{A}}^*_{s_{q'\sigma'}}d^3r=\frac{\hbar}{2\varepsilon\omega_q}\delta(\mathbf{q}-\mathbf{q}')\delta_{\sigma\sigma'}\ , \tag{3.6}$$

where ε is the dielectric constant in the interaction region (in vacuum $\varepsilon=\varepsilon_0$). In some case, when there is no room for confusion, we drop the indices $\mathbf{q}\sigma$ for the sake of clear presentation [$\tilde{\mathbf{A}}_s(\mathbf{r})\equiv\tilde{\mathbf{A}}_{s_{q\sigma}}(\mathbf{r})$].

With this normalization the creation and annihilation operators satisfy the commutation relation

$$[\hat{a}_{q\sigma},\hat{a}^{\dagger}_{q'\sigma'}]=\delta_{\sigma\sigma}\delta_{qq'} \tag{3.7}$$

in a finite volume, and

$$[\hat{a}_{q\sigma},\hat{a}^{\dagger}_{q'\sigma'}]=\delta(\mathbf{q}-\mathbf{q}')\delta_{\sigma\sigma'} \tag{3.8}$$

in an infinite volume.

This model, one may note, is so far completely general, and it covers all the radiation schemes discussed in the previous sections.

The Hamiltonian equation to be solved is the time-dependent Schrödinger equation,

$$i\hbar\frac{\partial}{\partial t}\psi=(H_0+H')\psi\ . \tag{3.9}$$

The eigenstates of the unperturbed Hamiltonian are $|k,\nu\rangle$, where

$$H_0\,|k,\nu\rangle=E_{k\nu}\,|k,\nu\rangle\ . \tag{3.10}$$

The index k stands for all the quantum numbers of the electron state, at least one of which is continuous, and the others may be discrete. The index $\nu_{q\sigma}$ stands for the photon occupation number of mode $\mathbf{q}$ in polarization state σ. The occupation states are discrete. For simplicity we assume that only one radiation mode state is occupied and drop the indices $\mathbf{q}\sigma$, hence $\nu\equiv\nu_{q\sigma}$. The total energy eigenvalues of the noninteracting electron and radiation field system are

$$E_{k\nu}=\mathscr{E}_k+\hbar\omega_{\mathbf{q}}(\nu+\tfrac{1}{2})\ . \tag{3.11}$$

We generalize our discussion slightly and present an analysis of a general quantum-mechanical problem defined by Eqs. (3.9) and (3.10), where k,ν are any kind of a pair of continuous and discrete indices, respectively. We want to calculate the linear growth rate of one discrete state $|\nu'\rangle$ for arbitrary amplitudes of the states $|k\rangle$. Following a standard time perturbation theory, we expand the perturbed wave function in terms of the unperturbed states (Schiff, 1971),

$$|\psi\rangle=\sum_{k,\nu}C_{k\nu}(t)\exp\left[-i\frac{E_{k\nu}}{\hbar}t\right]|k,\nu\rangle\ , \tag{3.12}$$

where the summation sign also implies integration over the continuous indices.

Before going on with the perturbative analysis, a note is in order with regard to the normalization and dimensions of the parameters in Eq. (3.12). We normalize the total wave function ψ to unity,

$$\langle\psi\,|\,\psi\rangle=1\ , \tag{3.13}$$

and, consequently, its dimension is $m^{-3/2}$. The normalization of the basis functions (unperturbed eigenstates) is, in the case of transversely discrete states,

$$\langle k'\nu'\,|\,\nu k\rangle=\delta_{\nu\nu'}\delta_{\mathbf{k}_\perp\mathbf{k}'_\perp}\delta(k_z-k'_z)\ , \tag{3.14}$$

and in the case of transversely continuous states,

$$\langle k'\nu'\,|\,\nu k\rangle=\delta_{\nu\nu'}\delta(\mathbf{k}-\mathbf{k}')\ . \tag{3.15}$$

There is in principle also an intermediate case in which the electron states are discrete in one of the transverse dimensions and continuous in the other. This case is relevant, for example, in the analysis of planar channeling. However, for the sake of brevity we will avoid elaborating on this case, except for noting that the orthonormalization in this case will be performed by means of a single Kronecker delta in the discrete dimension, and by a two-dimensional Dirac delta in the continuous dimensions. The dimension of the expansion coefficient $C_{k\nu}$ in each case can be deduced from Eqs. (3.12)–(3.15), and can be verified to be $m^{1/2}$, $m^{3/2}$, and m for the transversely discrete, transversely continuous, and the intermediate (a single discrete dimension) cases, respectively.

Substitution of (3.12) in (3.9) results in a standard perturbation theory set of equations:

$$i\hbar\dot{C}_{k'\nu'}=\sum_{k\nu}C_{k\nu}\langle k'\nu'\,|\,H'\,|\,\nu k\rangle\exp\left[-i\frac{E_{k\nu}-E_{k'\nu'}}{\hbar}t\right]\ . \tag{3.16}$$

Note that for the case in which H' is the first-order radiative interaction Hamiltonian (3.3), and $|\nu\rangle$ are the quantized field occupation states, most of the terms in the summation over ν in (3.16) vanish, except for the terms $\nu=\nu'+1$ and $\nu=\nu'-1$. Consequently, (3.16) is an infinite set of coupled ordinary differential equations, which couple each photon occupation state to the next higher and lower states, describing the cascade process of multiphoton emission and absorption. In order to investigate the multiphoton emission process, one would reduce (3.16) into the standard form of Raman-Nath

equations.[6] These were analyzed in detail in the general case (Raman and Nath, 1936) and also specifically in reference to the FEL problem (Dattoli and Renieri, 1985). However, as we explained in Sec. II.F, we avoid solving the exact multiphoton emission problem, and, for the purpose of this paper, we confine our analysis to first-order perturbation solution (single photon emission), viz., $\sum_{k'} |C_{k'\nu'\neq\nu}|^2 \ll 1$.

Limiting the analysis to the standard first-order perturbation theory (Schiff, 1971), the coefficients $C^1_{k'\nu'}(t)$ are calculated to first order by substituting on the right-hand side of (3.16) $C^0_{k\nu}=C_{k\nu}(0)=\text{const}$ and integrating over t. We now define the probability that a discrete photon state $|\nu'\rangle$ is occupied independently of the amplitudes of the electron final states,

$$P_{\nu'}=\sum_{k'} |C_{k'\nu'}|^2 ;$$

subsequently, we define the transition rate into this state, $W^e_{\nu'}\equiv P^e_{\nu'}/t$. We extend our analysis to many particles by assuming that the transition rate into state $|\nu'\rangle$ in the presence of N_e identical electrons in the interaction region is simply a factor N_e larger (single electron emission model).[7] This normalization is only a matter of convenience, aimed in order to obtain directly the homogeneous broadening emission rate equation of a finite current electron beam. In a more rigorous formulation the wave function ψ would be normalized to 1 (a single electron) in order to allow the Fermi-Dirac statistics to determine the initial parameter distribution of the entire electron beam. However, assuming $C^0_{k'\nu'}=C_{k'\nu}(0)\delta_{\nu\nu'}$, the integration over time is straightforward, and a transition rate (expected to be constant for a time t short enough to keep $P^e_{\nu'\neq\nu}\ll 1$) is obtained:

$$W_{\nu'}=N_e\frac{t}{\hbar^2}\sum_{k'}\left|\sum_{k,\nu} C^0_{k\nu}\langle k'\nu'|H'|\nu k\rangle \operatorname{sinc}\left(\frac{E_{k\nu}-E_{k'\nu'}}{2\hbar}t\right)\right|^2 . \tag{3.17}$$

[6]To obtain the standard form of Raman-Nath equations (Raman and Nath, 1936; Dattoli and Renieri, 1985), substitute $C_{k\nu}$ in terms of the fast varying amplitude $a_{k\nu}$: $a_{k\nu}\equiv C_{k\nu}\exp(-iE_{k\nu}t/\hbar)$, and eliminate the vanishing terms in the summation over ν. This reduces (3.16) into

$$i\hbar\dot{a}_{k'\nu'}=E_{k'\nu}a_{k'\nu'}+\sum_k (a_{k\nu'+1}\langle k',\nu'|H'|\nu'+1,k\rangle + a_{k\nu'-1}\langle k',\nu'|H'|\nu'-1,k\rangle) .$$

In a one-dimensional model (Dattoli and Renieri, 1985) the electron quantum number k is completely determined by the conservation of energy condition, and the summation over k is omitted. The evaluation of the matrix elements results in the coefficients of the two off-diagonal terms, which relate to each other as $\sqrt{\nu+1}/\sqrt{\nu}$.

[7]For a vacuum electron beam it is unlikely that statistical considerations (Fermi-Dirac statistics) will make an "homogeneous broadening" assumption (same initial states for all electrons) an inappropriate approximation. What is required for an homogeneous broadening assumption is that the initial conditions of different electrons (for example, their axial velocity) are similar to the extent that the spread in their center emission lines is much smaller than their homogeneous line broadening $\Delta\omega_L$ (2.32). This is indeed a quite relaxed condition that allows us to assume that many electrons have almost the same quantum numbers without any need to worry about violating the Pauli exclusion principle. The consideration of radiative transition by an extremely dense electron beam when the Pauli exclusion principle should be taken into account is a matter of scientific curiosity that is irrelevant for all practical radiation devices based on relativistic electrons in a vacuum, with the possible exception of some peculiar solid state carriers radiation schemes. Stimulated transitions by an electron beam with a shifted Fermi sphere distribution was considered in 1976 and 1978 (Gover, 1976; Gover and Yariv, 1978a). One can show (Gover and Friedman, 1986) that for an electron beam with minimal spread in $\mathbf{k}-\mathbf{r}$ phase space (uniform distribution of two opposite spin electrons per quantum state of free-space quantization in a box), a sufficient condition for homogeneous broadening is

$$N_e<\frac{1}{8\pi\beta_z}\frac{\lambda_w\lambda^2}{\lambda^3_{\mathrm{DB}}} .$$

Here N_e is the total number of interacting electrons, and λ_{DB} is the de Broglie wavelength:

$$\lambda_{\mathrm{DB}}=\frac{\hbar}{mc}\frac{1}{\gamma\beta_z}=(2.4\times 10^{-12}m)\frac{1}{\gamma\beta_z} .$$

It can be easily verified that the number on the right-hand side of the equation is very high and hard to exceed with practical electron beam current. Furthermore, in practice inhomogeneous broadening will be set probably at much lower current levels due to thermal energy and angular spread. The inhomogeneous broadening regime is discussed in the next section. It should also be noted that the simple generalization to a many-particle beam invoked by Eq. (3.13) also implies a model of single particle interaction. Interaction between the particles, collective and cooperative effects are not included in the present formulation.

In the particular problem which is of interest in this paper, the discrete index ν is the photon occupation number, and in order to calculate the emission and absorption rates in the single photon emission-absorption limit we need to calculate (3.17) for $\nu'=\nu+1$ and $\nu'=\nu-1$, respectively. On the other hand, the eigenstates of the quasifree-electrons must be taken continuously (at least in the longitudinal dimension). This leads in general to results that are different, or that are a generalization of Fermi's golden rule, as is shown in the next sections. This approach should be contrasted with the approach taken in the standard semiclassical atomic radiation and atomic laser theory, where the Fermi golden rule is derived within a model in which opposite assumptions are used: the electrons occupy discrete states and the radiation modes are continuous (Schiff, 1971; Yariv, 1975). Equation (3.17) would result directly in the standard Fermi golden rule if the initial wave function is a single discrete eigenstate $C_{k\nu}=C_{k_0\nu}\delta_{\mathbf{k}\mathbf{k}_0}$ (as in an atom). However, such a model is not appropriate for deriving the results of this paper, in which the electrons always occupy a continuum of states, and where in some cases the physical situation requires the use of an electron wave packet rather than a single eigenstate.

B. The transition rate calculation for different electron transverse states

In the present stage of our derivation we assume that the interaction takes place in all cases in the longitudinally quantum-mechanical limit. This would usually mean that a single longitudinal eigenfunction infinite in the longitudinal dimension is used to describe the electron initial state. However, in order to keep track of the electron number normalization, we substitute the single state function with a more general narrow spectrum wave packet composed of a single longitudinal initial-state function limited in the longitudinal dimension by a finite width envelope function that is much longer than the interaction length (see Appendix C).

To complete the electron wave-function normalization one should also consider the transverse dimensions. In the case of *transversely discrete states* (1), the single transverse-state function of the electron is transversely finite and can be easily normalized. In the case of transversely continuous states, two different subcases should be distinguished: (2) the *transversely continuous (inherently quantum)* case, and (3) the *transversely continuous transversely classical* case. In the first of the continuous-states cases the electron is described by a single transverse eigenstate function, which is infinite in the transverse dimensions, or in general described by a narrow spectrum transverse-states wave packet that, along the entire interaction length, must have a large width relative to the transverse variation of the radiation wave [see Fig. 6(a) and the discussion in Appendix B]. By contrast, the second case of transverse continuous states corresponds to a well-localized electron, which can keep a narrow width relative to the transverse variation of the radiation wave along the entire interaction length [see Fig. 6(b)], and therefore must contain a wide spectrum of transverse eigenstates.

The three cases—(1) the transversely discrete, (2) the transversely continuous quantum, and (3) the transversely continuous classical—require different analyses and different electron wave-function normalizations. Since in all cases there is a continuum of final states, at least in the longitudinal dimension, the first-order calculation of the transition rates results in—not surprisingly—equations that are formally similar to the standard Fermi golden rule equation. However, there are fine distinctions in the interpretation of the transition rate equation parameters in the different cases. These distinctions are delineated in the following subsections for the three different cases, which summarize the results of the more detailed derivation given in Appendix C.

1. The transversely discrete (quantum) case

In this case, assuming a single transverse state and a single (narrow spectrum wave packet) longitudinal state, the initial-state amplitude is given by

$$C^0_{k\nu}=\delta_{\nu\nu_i}\delta_{nn_i}\delta_{ll_i}\delta(k_z-k_{zi})\sqrt{2\pi/L}\ , \tag{3.18}$$

where $1/L$ is the single electron probability density per unit length.

The substitution of Eq. (3.18) in Eq. (3.17) and the use of (3.11) and (2.12) results in a constant transition rate equation

$$W_{\nu_f}=\frac{(2\pi)^2}{\hbar}n_L\int_{-\infty}^{\infty}dk_{zf}\,|\langle n_f l_f k_{zf}\nu_f\,|\,H'\,|\,\nu_i k_{zi} l_i n_i\rangle\,|^2\delta[\mathcal{E}^0_{k_{zi}}-\mathcal{E}^0_{k_{zf}}-(\nu_f-\nu_i)\hbar\omega_q]\ , \tag{3.19}$$

where $N_L\equiv N_e/L$ is the longitudinal electron density. This reduces directly to the Fermi golden rule form (Schiff, 1971)

$$W_{\nu_f}=\frac{(2\pi)^2}{\hbar}\rho(\mathcal{E}_f)n_L\,|\langle n_f l_f k_{zf}\nu_f\,|\,H'\,|\,\nu_i k_{zi} l_i n_i\rangle\,|^2\ , \tag{3.20}$$

where the density of states ρ refers in our case to the continuous longitudinal states of the electrons:

$$\rho(\mathcal{E}_f)=\left.\frac{dk_{zf}}{d\mathcal{E}_{k_{zf}}}\right|_{\mathcal{E}^0-(\nu_f-\nu_i)\hbar\omega_q}=\frac{1}{\hbar v_{gzf}}\ . \tag{3.21}$$

Note that v_{gzf} is the axial velocity of the electron in its *final* state (k_{zf},n_f,l_f) and may be slightly different from the initial axial velocity, which is defined similarly to Eq. (3.21) but at (k_{zi},n_i,l_i). In many practical cases this

quantum recoil effect is negligible, but as long as we stay in the quantum limit the distinction must be kept. Furthermore, even in the classical limit this distinction may be important when considering stimulated emission, since then the emission and absorption rates are almost equal, and the tiny recoil effects may eventually determine the net gain equation (see Sec. III.F).

2. The transversely continuous (inherently quantum) case

In the case of transversely continuous states both the transverse and axial quantum numbers of the electron eigenstates are continuous. This is a significantly different physical situation from the transversely discrete states when the radiative transition involves transfer of transverse momentum (e.g., in off-axis radiative emission), since in this case the electron may absorb a continuous range of transverse momentum (transverse recoil) the same way in which it does in the longitudinal dimension (longitudinal recoil). As in the previous case we assume an initial electron wave function with a single longitudinal state k_{zi}, but we still need to choose whether to describe the electron by a single *transverse* quantum state or by a wave packet of transverse states. The first choice is the appropriate model to use in the transverse (inherently) quantum-mechanical limit discussed in Sec. II.F (observation 3). We will first analyze this case, which is somewhat simpler. The second case (the transversely classical limit) will be analyzed in the next section.

Since a single initial electron quantum state and a single photon occupation state are assumed, we substitute in Eq. (3.17)

$$C^0_{k\nu}=\sqrt{n_\nu}\,\delta_{\nu\nu_i}\delta(\mathbf{k}-\mathbf{k}_i)\sqrt{(2\pi)^3}/V\ , \tag{3.22}$$

where V is the volume in which the probability of finding the electron is one. The substitution of Eq. (3.22) in (3.17) and the use of Eq. (3.11) results again in a constant transition rate equation,

$$W_{\nu_f}=\frac{2\pi}{\hbar}(2\pi)^3 n_V\int_{-\infty}^{\infty}d^3k_f\,|\langle\nu_f\mathbf{k}_f\,|\,H'\,|\,\mathbf{k}_i\nu_i\rangle\,|^2\delta[\mathscr{E}_{\mathbf{k}_i}-\mathscr{E}_{\mathbf{k}_f}-(\nu_f-\nu_i)\hbar\omega]\ , \tag{3.23}$$

where $n_V\equiv N_e/V$ is the electron number density (per unit volume).

The delta function in Eq. (3.23) leads to integration over a surface in the final electron states space $\mathbf{k}_f$, which ensures satisfaction of the energy conservation condition

$$\mathscr{E}_{\mathbf{k}_f}=\mathscr{E}_{\mathbf{k}_i}-(\nu_f-\nu_i)\hbar\omega_{\mathbf{q}}\ . \tag{3.24}$$

The integration over space in the matrix element calculation may limit further the possible final states. In particular when the interaction volume is large, it results in the additional momentum conservation conditions. Further simplification of (3.23) is thus possible only when the matrix element can be calculated for a particular problem.

For the sake of illustration we examine the common case in which a transverse uniformity of the wiggler (laminated structure) can be assumed (as was done in Sec. II.G). The electron wave function is given in this case by

$$|\,\mathbf{k}\,\rangle=\frac{1}{2\pi}\exp(i\mathbf{k}_\perp\cdot\mathbf{r}_\perp)\phi_{\mathbf{k}_\perp k_z}(z)\ . \tag{3.25}$$

In free space (e.g., in the Čerenkov radiation problem), the longitudinal dimension wave function is a simple harmonic wave $\phi_{\mathbf{k}_\perp k_z}(z)=(2\pi)^{-1/2}\exp(ik_z z)$, and the quantum numbers $\mathbf{k}$ are the free-space electron wave numbers (eigenvalues of the momentum operator). In a configuration of an axially periodic wiggler (e.g., magnetic bremsstrahlung FEL, coherent bremsstrahlung, etc.), the longitudinal-dimension-state function is a Floquet-Bloch mode [compare to Eq. (2.6)] and is given by

$$\phi_{\mathbf{k}_\perp k_z}(z)=\frac{1}{\sqrt{2\pi}}\sum_{m=-\infty}^{\infty}\alpha_{\mathbf{k}_{\perp m}}\exp(ik_{zm}z)\ , \tag{3.26}$$

where $k_{z_m}=k_{z0}+mk_w$. The transverse quantum numbers $\mathbf{k}_\perp$ are in general the eigenvalues of the transverse canonical momentum operator.

Since the wiggler field is assumed transversely uniform, the only dependence of H' on the transverse coordinates $\mathbf{r}_\perp$ is through the radiation field $\mathbf{A}_s(\mathbf{r})$ [see (3.3) and (3.4)]. Assuming that the radiation field is a simple plane wave propagating at an arbitrary direction $\hat{e}_{\mathbf{q}}$ and normalized according to Eq. (3.6) the radiation field operator is

$$\hat{\mathbf{A}}_s=\frac{1}{\sqrt{(2\pi)^3}}\left[\frac{\hbar}{2\varepsilon\omega_{\mathbf{q}}}\right]^{1/2}\hat{e}_{\mathbf{q}\sigma}e^{i\mathbf{q}\cdot\mathbf{r}}\hat{a}_s+\text{H.c.} \tag{3.27}$$

Thus

$$\hat{H}'=\hat{H}'_+(z)e^{i\mathbf{q}_\perp\cdot\mathbf{r}_\perp}+\hat{H}'_-(z)e^{-i\mathbf{q}_\perp\cdot\mathbf{r}_\perp}\ . \tag{3.28}$$

Performing the transverse coordinates integration in the matrix element in Eq. (3.23) with (3.25) and (3.28) results in a delta function for the final transverse wave number,

$$\frac{1}{(2\pi)^2}\int_{-\infty}^{\infty}dr_\perp^2\exp[i(\mathbf{k}_{\perp i}\pm\mathbf{q}_\perp-\mathbf{k}_{\perp f})\cdot\mathbf{r}_\perp]$$
$$=\delta(\mathbf{k}_{\perp f}-\mathbf{k}_{\perp i}\mp\mathbf{q}_\perp)\ .$$

The integration over $\mathbf{k}_{\perp f}$ in (3.23) yields a factor L_xL_y (the transverse cross-section area of the plane wave), since there is a delta function squared in the integrand. This reduces the volume density of the electrons n_V to a longitudinal density n_L. The integration over k_{zf} is carried out, using the substitution $dk_{zf}=\rho(\mathscr{E}_{\mathbf{k}_{\perp f}k_{zf}})d\mathscr{E}_{\mathbf{k}_{\perp f}k_{zf}}$, where

$$\rho(\mathcal{E}_{\mathbf{k}_{\perp f}k_{zf}})=\frac{dk_{zf}}{d\mathcal{E}_{\mathbf{k}_{\perp f}k_{zf}}}=\frac{1}{\hbar v_{gzf}} . \tag{3.29}$$

This results again in a Fermi golden rule relation similar to Eq. (3.20),

$$W_{\nu_f}=\frac{(2\pi)^2}{\hbar}\rho(\mathcal{E}_f)n_L \mid \langle \nu_f k_{zf} \mid H'_{\pm}(z) \mid k_{zi}\nu_i \rangle \mid^2 . \tag{3.30}$$

The electron density of states is defined similarly to Eq. (3.21), except that the final energy is defined by $\mathcal{E}_{\mathbf{k}_f}=\mathcal{E}_{\mathbf{k}_i}-(\nu_f-\nu_i)\hbar\omega_{\mathbf{q}}$, and the final transverse state by $\mathbf{k}_{\perp f}=\mathbf{k}_{\perp i}\pm\mathbf{q}_{\perp}$. The transition rate is then given by

$$W_{\nu_f}=\frac{(2\pi)^2}{\hbar^2 v_{gzf}}n_L \mid \langle \nu_f k_{zf} \mid H'_{\pm}(z) \mid k_{zi}\nu_i \rangle \mid^2 . \tag{3.31}$$

The results for the transversely continuous states (transversely) quantum case are thus similar to those of the transversely discrete case (1). Contrary to case (1), there is no need now for any additional summation over final transverse states. The final transverse state is uniquely defined by the exact transverse momentum conservation (transverse recoil) ($\mathbf{k}_{\perp f}=\mathbf{k}_{\perp i}-\mathbf{q}_{\perp}$) imposed by the assumption of transverse uniformity. The transverse recoil effect, which is included in (3.29) and absent in (3.21), will introduce a substantial difference in the final net gain equations at off-axis radiation conditions in the two different cases (see Sec. III.F). Notice also that contrary to Eq. (3.20), the matrix element calculation in Eq. (3.31) involves only integration over the z dimension.

3. The transversely continuous classical case

While in the previous section we assumed that the initial electron wave function can be described in terms of a single transverse quantum state, we presently consider the case when the conditions of the problem require that we keep a wave packet of transverse states. This is required if the transverse wave-packet dimensions remain small relative to the transverse variation parameters of the radiation wave and the wiggler field along the entire interaction length, so that the electron's interaction can be characterized by the particular classical trajectory drawn by the center of the wave packet [see Fig. 6(b)]. This can be the case in bremsstrahlung FEL radiation schemes when the radiation wave is a high-order transverse mode and the position of the electron trajectory relative to the nodes and *maxima loci* of the radiation mode is important. It is clearly the case in slow-wave radiation schemes where the radiation field decays exponentially away from the slow-wave structure (Gover and Sprangle, 1981), and the classical trajectory of the electron determines the radiation field intensity that it experiences.

In the present case, contrary to that of transversely discrete states, the electron may drift away from the structure axis. In fact, one may generally distinguish three different natural axes of the problem: the structure axis (for a periodic structure—the direction of the periodicity $\mathbf{k}_w$), the electron (average) motion direction, and the radiation direction. The present formulation is applicable for treating the general case in which all of these directions are different. We cannot avoid, thus, some intrication of our notation, which is necessary in order to indicate the coordinates frame of reference (for the derivation step, it is advantageous to use a coordinate system aligned with the electron motion). Before introducing the quantum wave packet and the calculation of the transition rate, we dedicate a couple of paragraphs to clarifying the notation used.

A model illustration of the present transversely classical case is shown in Fig. 7. The electron trajectory $\mathbf{r}_{cl\perp}(z)$ shown can be interpreted, for example, as the classical trajectory of an electron in a magnetic wiggler. This motion consists in general of two components: $\mathbf{r}_{cl\perp}(z)=\bar{\mathbf{r}}_{cl\perp}(z)+\mathbf{r}_{w\perp}(z)$, where $\mathbf{r}_{w\perp}(z)$ is the periodic wiggler motion (of period λ_w), which is superimposed on the slow variation average motion of the center of oscillation $\bar{\mathbf{r}}_{cl\perp}(z)$, which can deviate from a straight line if there is an additional external (focusing) force applied on the electron (e.g., due to "betatron oscillation" rendered by the transverse gradient of the wiggler field). Figure 7 may also describe an electron that propagates in the transversely varying radiation field of a slow-wave structure (e.g., Smith-Purcell radiation), experiencing varying amplitude of the radiation field due to slow transverse excursion of its trajectory relative to the structure axis z (both because of off-axis injection $\Theta_e\neq 0$ and a possible external focusing force applied throughout the interaction length). In this latter case, of course, $\mathbf{r}_{w\perp}(z)=0$ and the short period ripple shown in the figure is eliminated.

A rigorous quantum representation of a classical electron trajectory consists of a wave packet of quantum-mechanical eigenfunctions centered around the classical trajectory of the electron. Since in the longitudinal dimension we still want to stay in the quantum regime, we

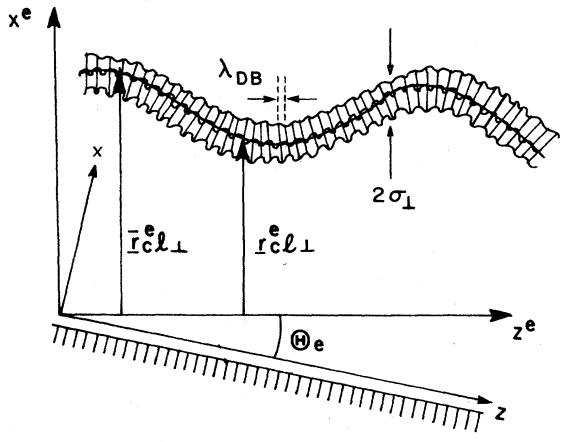

FIG. 7. Description of the electron transverse wave-packet trajectories relative to the structure axis (z) and the electron average motion axis (z^e).

compose the wave packet only of eigenmodes of different transverse-state numbers $\mathbf{k}_{\perp i}$ and of the same single longitudinal wave number k_{zi}. The notions of transverse and longitudinal dimensions become somewhat ill defined when the average classical trajectory is curved. A possible way to circumvent this difficulty is to use curvilinear coordinates with varying axes, aligned with the electron trajectory. We will use here a simpler model, defining a fixed longitudinal (z^e) axis as the long-range average direction of the classical trajectory. We will assume that the angular deviation of the trajectory off its average direction is always small (paraxial approximation), and we will denote the "average electron coordinates" in the frame aligned with the average motion axis z^e by $\mathbf{r}^e$ (see Fig. 7).

Based on the above model and assumptions, we take for the initial electron wave function in the transversely classical limit (written in the average coordinates)

$$\psi(\mathbf{r}^e,0)=(2\pi)^{3/2}/L^{1/2}\phi_{\mathbf{k}^e_{\perp 0}k^e_{zi}}(\mathbf{r}^e)f_\perp[\mathbf{r}^e_\perp-\bar{\mathbf{r}}^e_{c\perp\perp}(z)]\ , \qquad (3.32)$$

where $\phi_{\mathbf{k}^e_{\perp 0}k^e_{zi}}(\mathbf{r}^e)$ is a single eigenstate function in an external field structure (e.g., a wiggler), which is assumed to be transversely uniform at least around the average trajectories. In the case of a periodic field structure the eigenstate function is a Floquet mode, which can be described by [compare Eqs. (2.6), (3.25), and (3.26)][8]

$$\psi_{\mathbf{k}^e}(\mathbf{r}^e)=\frac{1}{(2\pi)^{3/2}}\sum_{m=-\infty}^{\infty}\phi_{\mathbf{k}^e m}e^{i\mathbf{k}^e_\perp\cdot\mathbf{r}^e_\perp}e^{i(k^e_z+mk^e_w)z^e}\ . \qquad (3.33)$$

The envelope function $f_\perp(\mathbf{r}_\perp)$ is a narrow function of typical width $\sigma_\perp$ (see Fig. 7) and can be taken to be, for example, the Gaussian function of Eqs. (B11) and (B12). Note that our specific choice of coordinates implies $\mathbf{k}^e_\perp=\mathbf{k}^e_{\perp 0}=0$. Consequently, Eq. (3.33) is independent of $\mathbf{r}^e_\perp$.

The exact form of the wave-packet envelope function $f_\perp(\mathbf{r}^e_\perp-\mathbf{r}^e_{c\perp\perp})$ is immaterial, since in the transverse classical limit we will be able to neglect its finite width and will only need to know the position of its center locus $\mathbf{r}^e_{c\perp\perp}(z)$. This is correct as long as $\sigma_\perp$ is much smaller than the characteristic dimensions of the transverse variation of the wiggler fields or the radiation mode fields. On the other hand, we must assume that $\sigma_\perp$ is still large enough so that, throughout the electron transit time, the transverse expansion (diffraction) of the wave packet is negligible. These are exactly the conditions of the transversely classical limit as explained in Sec. II.C and Appendix B, and as illustrated in Fig. 6(b).[9]

In order to see the temporal evolution of the wave packet, it is necessary to decompose the initial wave packet [see Eq. (3.32)] into its transverse-state functions and propagate each state $\mathbf{k}_i$ in time according to its dispersed energy $\mathcal{E}_{\mathbf{k}_i}$. This is formally done in Appendix C, but the result can also be derived from simple considerations as follows. Because of the choice of coordinates, the transverse derivative of the energy (namely, the transverse velocity) is null $\nabla\mathcal{E}_{\mathbf{k}^e_\perp=\mathbf{k}^e_{\perp 0}=0}=0$. Furthermore, in the transversely classical limit, the higher-order dispersion of the energy as a function of $\mathbf{k}^e_\perp$ is assumed to be too small to cause substantial expansion in the wave-packet envelope during the transit time. Consequently, to a good approximation, all eigenstates in the wave packet propagate in time with the same center state energy $\mathcal{E}_{\mathbf{k}^e_{\perp 0}k^e_{zi}}$, and the time evolution of the wave packet [see Eq. (3.32)] is simply

$$\psi(\mathbf{r}^e,t)=(2\pi)^{3/2}/L^{1/2}\phi_{\mathbf{k}^e_{\perp 0}k^e_{zi}}(\mathbf{r}^e)f_\perp[\mathbf{r}^e_\perp-\bar{\mathbf{r}}^e_{c\perp\perp}(z)]\times e^{-i(\mathcal{E}_{\mathbf{k}^e_{\perp 0}k^e_{zi}})t/\hbar}\ . \qquad (3.34)$$

The picture of the time evolution of the longitudinally quantum transversely classical approximate wave function (3.34) is illustrated in Fig. 7. The winding envelope function remains frozen in width and shape, at least throughout the electron transit time period. A "carrier" Floquet mode plane wave propagates axially inside the envelope with the electron de Broglie wave number and wavelength λ_{DB}, and the phase fronts are approximately perpendicular to the average motion axis z^e.

Our goal is to find the transition rate. Since the initial electron wave function is a superposition of eigenstates, we need to go back to Eq. (3.17) and substitute in it the amplitudes of the individual transverse eigenstates C^0_{kv}. This formal eigenstates decomposition is used in Appendix C in the same way used there to derive (3.34). Again a simpler, but less rigorous, derivation of the same results may be obtained by employing the assumption that the

[8]In the transversely classical limit, contrary to the other two quantum limits (Secs. III.B.1 and III.B.2), the average electron coordinates system is preferable over the structure coordinates for describing the electron wave function. This choice of coordinates will simplify the derivation of the matrix element for this case, but the final (classical) results should be independent of the choice of coordinates.

[9]The physical meaning of (3.33) with $\mathbf{k}^e_\perp=0$ is of a wave packet that propagates in the z^e direction sensing the periodicity of the structure in the z^e dimension only ($k^e_w=k_w\cos\Theta_e$). In the classical limit the transverse extent of the wave packet is assumed to be so small that the periodicity in the transverse dimensions (x^e) is not sensed. For most classical devices (e.g., magnetic bremsstrahlung FEL), this transverse periodicity ($\lambda_w/\sin\Theta_e$) is immense when measured in an electron wave-number scale. Effects such as coherent bremsstrahlung in a crystal, for which this assumption may not hold at large angle Θ_e, need to be solved in a transverse quantum formulation (case 2).

spatial dimension of $f_\perp[\mathbf{r}_\perp^e-\bar{\mathbf{r}}_{c\perp}^e(z)]$ is small in all dimensions relative to the spatial variation of the wiggler and radiation fields, but large relative to the de Broglie wavelength. Consequently, after comparing Eqs. (3.34) and (3.12), we may express the initial eigenstate amplitude as

$$C^0_{\mathbf{k}^e\nu}=(2\pi)^{3/2}/L^{1/2}\delta(k_z^e-k_{zi}^e)\delta(\mathbf{k}_\perp^e)f_\perp[\mathbf{r}_\perp^e-\bar{\mathbf{r}}_{c\perp}(z)]\delta_{\nu\nu_i} . \tag{3.35}$$

Within the spatial range of negligible fields variation, $C^0_{\mathbf{k}^e\nu}$ can be considered spatially constant despite the envelope function $f[\mathbf{r}_\perp^e-\bar{\mathbf{r}}_{c\perp}^e(z)]$.

Substituting (3.35) or the more rigorous Eq. (C11) in (3.17), and now taking advantage of the narrowness of the envelope function $f_\perp$ relative to the fields (or more specifically, relative to the spatial variation of the interaction Hamiltonian H'), one arrives again (see Appendix C) at the simple equation

$$W_{\nu_f}=\frac{(2\pi)^2}{\hbar}\rho(\mathscr{E}_f)n_L|\langle k_{zf}^e\nu_f\,|\,H'[\bar{\mathbf{r}}_{c\perp}^e(z^e),z^e]\,|\,\nu_i k_{zi}^e\rangle|^2 , \tag{3.36}$$

where $\rho(\mathscr{E}_f)$ is given by Eq. (3.29).

Equation (3.36) expresses the intuitively expected result that, in calculating the transition rate of a transversely classical electron, what is important is the value of the interaction Hamiltonian only along the trajectory of the electron.

A simple example that illustrates the implication of Eq. (3.36) is that of radiation by an electron interacting with a transversely evanescent surface wave. This takes place in slow-wave radiation schemes like Smith-Purcell radiation (Smith and Purcell, 1953; Salisbury, 1970; Bachheimer, 1972; Burdette and Hughes, 1976; and Gover *et al.*, 1984) and Čerenkov FEL's based on a dielectric waveguide (Von Laven *et al.*, 1982). Assume, for example, a planar surface slow-wave structure that lies on the plane $x=0$. The radiation field operator can then be written in general in terms of the structure coordinates $\mathbf{r}$ as

$$\hat{\mathbf{A}}_s=\hat{a}_{\mathbf{q}}\sum_{m=-\infty}^{\infty}\mathbf{A}_m e^{-\alpha_m x+iq_y y+iq_{zm}z}+\text{H.c.} , \tag{3.37}$$

where $\alpha_m=[q_y^2+q_{zm}^2-(\omega/c)^2]^{1/2}$. In a periodic slow-wave structure (grating) $q_{zm}=q_{z0}+mk_w$, the fundamental space harmonic is radiating ($\alpha_0=-iq_{x0}$, where q_{x0} is real). In a Čerenkov FEL based on a dielectric waveguide, Eq. (3.37) reduces into a single transversely decaying slow wave. We recall that in the derivation of (3.36), the coordinate z^e was assumed to be the average electron motion direction. Consequently, if we assume in the present example that an electron propagates in the plane $y=0$ at an average angle Θ_e relative to the slow-wave structure plane (see Fig. 7), then the field operator (3.37) needs to be transformed into the electron coordinates using the rotation transformation ($z=z^e\cos\Theta_e-x^e\sin\Theta_e$, $x=z^e\sin\Theta_e+x^e\cos\Theta_e$):

$$\hat{\mathbf{A}}_s^e=\hat{a}_q\sum_m\mathbf{A}_m^e e^{-\alpha_m x^e\cos\Theta_e-\alpha_m z^e\sin\Theta_e+i\mathbf{q}_\perp^e\cdot\mathbf{r}_\perp^e+iq_z^e z^e}+\text{H.c.} \tag{3.38}$$

In both slow-wave structure examples (a Smith-Purcell grating or a Čerenkov dielectric slab) we can single out at least one synchronous term in the sum (3.39) and write the perturbation Hamiltonian as an exponentially decaying function times an oscillatory function of $\mathbf{r}$:

$$H'=e^{-\alpha_m x^e\cos\Theta_e-\alpha_m z^e\sin\Theta_e}H_{\text{osc}}(\mathbf{r}_\perp^e,z^e) . \tag{3.39}$$

Substitution of (3.39) in (3.36)[10] results in a general equation for interaction in a planar slow-wave structure:

$$W_{\nu_f}=\frac{(2\pi)^2}{\hbar}n_L\rho(\mathscr{E}_f)\times|\langle k_{zf}^e\nu_f\,|\,e^{-\alpha_m\bar{x}^e(z^e)\cos\Theta_e-\alpha_m z^e\sin\Theta_e}\times H_{\text{osc}}[\bar{\mathbf{r}}_{c\perp}^e(z^e),z^e]\,|\,\nu_i k_{zi}^e\rangle|^2 . \tag{3.40}$$

This is a general equation for the emission rate from planar slow-wave structures, which permits transverse excursion of the classical trajectory of the electron in the $\mathbf{x}$ dimension due either to initial angular deviation or to continuous focusing along the interaction region (as shown in Fig. 7). The significance of the conclusion, that the Hamiltonian must be evaluated along the classical trajectory of the electron in the computation of the matrix element, is well demonstrated here when one examines the simple example of straight-line propagation parallel to the slow-wave surface [$\bar{x}(z)=x_0$, $\bar{y}(z)=0$, $\Theta_e=0$]. Equation (3.40) indicates an attenuation by a factor $e^{-2\alpha_m x_0}$ relative to an electron propagating right next to the surface. In the more general case of propagation in an angle $\Theta_e\neq0$, the line-shape function will not only be characterized by the finite interaction length, but will also be dependent on the propagation angle Θ_e and on α_m (as we will present in Sec. III.D).

C. The relativistic regime

Most radiation schemes considered in this paper operate with relativistic electrons. Hence we need to extend the previous treatment, which is based on the Schrödinger equation, to the relativistic regime. The most general approach would rely on the Dirac equation to describe the electrons. However, since spin effects are usually negligible (Bosco *et al.*, 1983; Kurizki and

[10]The transverse classical limit condition, which made this substantial simplification, is in this case the requirement that the transverse dimensions of the electron wave packet are much less than the electromagnetic decay length $1/\alpha$.

McIver, 1984), considerable simplification of the formulation is gained by using the Klein-Gordon equation:

$$\left[i\hbar\frac{\partial}{\partial t}+eV\right]^2\psi=c^2(-i\hbar\nabla+e\,\mathbf{A})^2\psi+m^2c^4\psi\ . \tag{3.41}$$

Unfortunately Eq. (3.41) is a second-order differential equation in time and cannot be combined with the quantized radiation field equation for use with the perturbation procedure presented in Sec. III.A, since that procedure was based on a first-order (in time derivatives) Schrödinger equation [see Eq. (3.9)]. However, if the charged particle is relativistic only in one dimension (the average particle motion direction), which is the case for $a_w\equiv eA_w/mc\ll 1$, then it can still be approximated by a Schrödinger-type equation, which is first order in the time derivative. There are a number of ways to obtain such a quasirelativistic effective Schrödinger equation by approximating the Klein-Gordon or Dirac equation (Fujiwara, 1961; Beloshitskii and Kumakhov, 1978). A formal reduction of the relativistic equations into a first-order equation can be obtained by second-order quantization of the particle wave-function field, as demonstrated in Appendix D. In this section we sketch a simpler derivation of the Schrödinger-type relativistic equation by an iterative approximation of the Klein-Gordon equation (3.41) around a center energy E_0, which is about the particle energy in the wiggler in the absence of radiation fields. The approximation is based on the assumption that the solution of (3.41) is a single quasiharmonic positive energy wave (for an electron):

$$\psi=u(\mathbf{r},t)\exp(-iE_0t/\hbar)\ , \tag{3.42}$$

where $u(\mathbf{r},t)$ is a slowly varying function of t, and the negative-energy (positron) wave solution is not excited. This assumption is well justified in practical cases for which the radiative perturbation energy is much smaller than the relativistic electron energy γmc^2.

Substitution of Eq. (3.42) in (3.41) results in

$$i\hbar\frac{\partial}{\partial t}u=\frac{1}{2(E_0+eV)}\left\{c^2(-i\hbar\nabla+e\,\mathbf{A})^2+(mc^2)^2-(E_0+eV)^2-i\hbar e\frac{\partial}{\partial t}V\right\}u+\hbar^2\frac{\partial^2}{\partial t^2}u\ .$$

Successive iterative substitution of this equation into its right-hand side, neglecting third-order derivatives in time and space ($\hbar^3$ terms), and neglecting the time derivatives of the electromagnetic fields ($\hbar\omega\ll E_0$) results in the effective quasirelativistic Schrödinger equation

$$i\hbar\frac{\partial}{\partial t}\psi=H\psi\ , \tag{3.43}$$

where[11]

$$H=E_0+\frac{1}{2}\frac{c^2(-i\hbar\nabla+e\,\mathbf{A})^2+(mc^2)^2-(E_0+eV)^2}{E_0+eV}-\frac{1}{8}\frac{[c^2(-i\hbar\nabla+e\,\mathbf{A})^2+(mc^2)^2-(E_0+eV)^2]^2}{(E_0+eV)^3}\ . \tag{3.44}$$

The Hamiltonian (3.44) can be split into an electronic unperturbed part and a radiative perturbation part: $H=H_{0\mathrm{el}}+H_R'$, where

$$H_{0\mathrm{el}}=E_0+\frac{1}{2}\frac{c^2(-i\hbar\nabla+e\,\mathbf{A}_w)^2+(mc^2)^2-(E_0+eV_w)^2}{E_0+eV_w}-\frac{1}{8}\frac{[c^2(-i\hbar\nabla+e\,\mathbf{A}_w)^2+(mc^2)^2-(E_0+eV_w)^2]^2}{(E_0+eV_w)^3}\ , \tag{3.45}$$

$$H_R'=e\frac{\frac{1}{2}[\mathbf{A}_s\cdot(-i\hbar\nabla+eA_w)+(-i\hbar\nabla+eA_w)\cdot\mathbf{A}_s]-eV_s(E_0+eV_w)}{E_0+eV_w}\ . \tag{3.46}$$

Here we assumed electron energies in the range $E\approx E_0$. Since, by definition,

$$[c^2(-i\hbar\nabla+e\,\mathbf{A}_w)^2+(mc^2)^2-(E_0+eV_w)^2]\psi_{E_0}=0\ ,$$

Eq. (3.46) is the correct first-order radiative interaction Hamiltonian (in terms of the radiative field $\mathbf{A}_s, V_s$) and $H_{0\mathrm{el}}$ is the unperturbed Hamiltonian, correct to second order in the wiggler fields $\mathbf{A}_w, V_w$.

We note that for the mere purpose of computing the first-order radiative perturbation Hamiltonian, the series expansion of Eq. (3.44) could have been stopped after the second term. However, the third term is non-negligible in the calculation of the unperturbed problem of the electron in the wiggler, and in the case of a uniformly periodic wiggler it is needed in order to obtain the anisotropy of the effective-mass tensor (2.90). In many cases, however, the solution of the unperturbed Hamiltonian wave functions (which are needed eventually for the computation of the perturbation matrix element) can be found by solving directly the Klein-Gordon equation instead of the

[11]Equation (3.44) can be formally derived by a second-order Taylor expansion of the square root in the classical identity $E-E_0=(E_0+eV)\{1-[1+(c^2(\mathbf{p}_c+e\,\mathbf{A})^2+(mc^2)^2-(E_0+eV)^2)/(E_0+eV)^2]^{1/2}\}$ and by the substitution $\mathbf{p}_c\rightarrow-i\hbar\nabla$. The conditions for the validity of this symbolic operator expansion are apparently the ones indicated in the paragraph before Eqs. (3.43) and (3.44).

effective Schrödinger equation (3.43) with (3.45).

In all practical applications, $eV_w=0$ or is negligible relative to $E_0=\gamma_0 mc^2$ in the denominator of Eq. (3.46). Taking a transverse radiation gauge for the radiation fields $\nabla\cdot\mathbf{A}_s=0$, $V_s=0$ [in analogy to the derivation of (3.3)], the relativistic perturbation Hamiltonian may be written in the compact form

$$[H'_R]=\frac{e}{m\gamma_0}\mathbf{A}_s\cdot(-i\hbar\nabla+e\,\mathbf{A}_w)=\frac{1}{\gamma_0}[H'_{\rm NR}]\ , \tag{3.47}$$

where $[H']_{\rm NR}$ is the nonrelativistic perturbation Hamiltonian given by (3.3).

When combined with the unperturbed quantized radiation field Hamiltonian, Eq. (3.45) replaces the unperturbed electronic Hamiltonian part (first two terms on the right-hand side) of Eq. (3.2). The first-order perturbation formulation that we developed in the previous section can therefore be applied with only a minor modification, which requires that we divide the nonrelativistic perturbation Hamiltonian $[H']_{\rm NR}$ [Eq. (3.3)] by γ_0. However, the electron eigenstate functions that should be used to calculate the matrix element in the final equations are the solutions of the unperturbed relativistic equations (3.43) and (3.45) or the Klein-Gordon equation (3.41) with the wiggler potentials $\mathbf{A}_w, V_w$.

There is some uncertainty about the value of the dividing factor γ_0 in Eq. (3.47), since the electron energy is changing in an unknown way through the interaction region due to photon emission. The proper choice for γ_0, which takes into account the radiation process, must lie between γ_i and γ_f, the initial and final electron energies before and after the interaction region (where $V_w=0=\mathbf{A}_s$). The standard procedure of Feynman diagram perturbative calculation (Bjorken and Drell, 1965) suggests that the appropriate value of γ_0 to be used is the geometric average between the initial and final values:

$$\gamma=\sqrt{\gamma_i\gamma_f}\ . \tag{3.48}$$

In Appendix D we derived this specific result together with the equation for the relativistic perturbation Hamiltonian (3.47) in a more rigorous procedure based on second quantization of the Klein-Gordon equation.

D. Calculation of the matrix element and homogeneous broadening line-shape function for various radiation schemes

In order to evaluate the transition rate, it is always necessary to calculate first the transition matrix element. It is preferable to execute first the photon-state matrix calculation, which can always be done explicitly and straightforwardly. Substituting Eq. (3.4) in (3.47), one obtains

$$\begin{aligned}M_{\nu_f}&=\langle k_f\nu_f\,|\,H'\,|\,\nu_i k_i\rangle\\&=\langle k_f\,|\,H'_{\rm ab}\,|\,k_i\rangle\sqrt{\nu_i}\,\delta_{\nu_f,\nu_{i-1}}\\&\quad+\langle k_f\,|\,H'_{\rm em}\,|\,k_i\rangle\sqrt{\nu_i+1}\,\delta_{\nu_f,\nu_{i+1}}\ ,\end{aligned} \tag{3.49}$$

where

$$H'_{\rm ab}=e\,\tilde{\mathbf{A}}_s(\mathbf{r})\cdot\frac{-i\hbar\nabla+e\,\mathbf{A}_w}{\gamma m}\ , \tag{3.50}$$

$$H'_{em}=e\,\tilde{\mathbf{A}}^*_s(\mathbf{r})\cdot\frac{-i\hbar\nabla+e\,\mathbf{A}_w}{\gamma m}\ . \tag{3.51}$$

For the case in which the quantization modes are traveling plane waves, the normalized mode vector potential field is the coefficient of the operator $\hat{a}_s$ in Eq. (3.27):

$$\tilde{\mathbf{A}}_s=\{\hbar/[(2\pi)^3 2\varepsilon\omega]\}^{1/2}\hat{e}_{q\sigma}e^{i\mathbf{q}\cdot\mathbf{r}}\ .$$

What is left to calculate in any particular radiation scheme are only the electronic-states matrix elements. The detailed calculation of these elements for any radiation scheme lies outside the scope of this paper. We will show, however, the exact procedure necessary for calculating each radiation scheme and will dwell upon the common characteristics. The common feature of all the radiation schemes we will consider is the extended interaction between the electron and radiation waves along the axial (z) dimension. This results in similar emission line-shape functions for all radiation schemes, which stems from the axial coordinate overlap integral in the electronic matrix elements in Eq. (3.49). The transverse overlap integration leads merely to a numerical factor, and we discussed its computation in Sec. III.B for three specific cases.

The electronic matrix element measures the spatial overlap between the initial and final electron states and the electromagnetic fields. This determines the strength of the interaction and various exclusion rules of the transition; in particular, conservation of momentum conditions. For demonstration purposes we now focus discussion on the emission matrix element $M_{\nu_f=\nu_i+1}=\langle k_f\,|\,H'_{em}\,|\,k_i\rangle\sqrt{\nu_i+1}$. It is clear that the calculation of the absorption matrix element is completely analogous. We start with the simplest example of a free-space electron state and a plane electromagnetic wave propagating in a uniform interaction region of finite dimensions:

$$|\,k\,\rangle=\frac{1}{\sqrt{(2\pi)^3}}e^{i\mathbf{k}\cdot\mathbf{r}}\ , \tag{3.52}$$

$$\tilde{\mathbf{A}}_{q\sigma}(\mathbf{r})=\mathbf{A}_{q\sigma}e^{i\mathbf{q}\cdot\mathbf{r}}\ , \tag{3.53}$$

where σ is the helicity or polarization-state index of the radiation wave. We choose here to describe the electron in a fully quantum-mechanical model (both longitudinally and transversely).

The calculation of the emission matrix element with Eqs. (3.52) and (3.53) results in

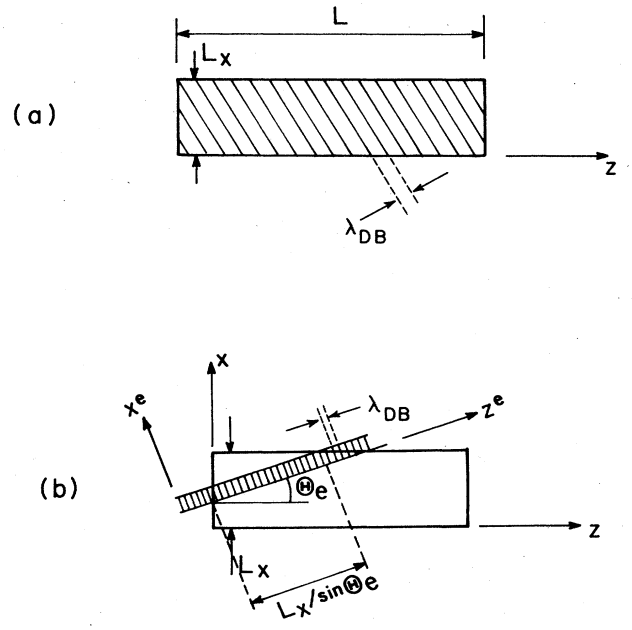

FIG. 8. Finite interaction length broadening the Čerenkov in a dielectric slab geometry.

$$|M_{\nu_f=\nu_i+1}|^2 \propto \mathrm{sinc}^2\left[\frac{(k_{xi}-k_{xf}-q_x)L_x}{2}\right] \times \mathrm{sinc}^2\left[\frac{(k_{yi}-k_{yf}-q_y)L_y}{2}\right] \times \mathrm{sinc}^2\left[\frac{(k_{zi}-k_{zf}-q_z)L}{2}\right], \quad (3.54)$$

where (L_x,L_y) and L are the transverse and longitudinal dimensions of the interaction region [see Fig. 8(a)].

In the limit of large interaction region dimensions $(L_x,L_y,L\to\infty)$ the line-shape functions of (3.54) vanish unless $\mathbf{k}_i-\mathbf{k}_f=\mathbf{q}$, vividly recovering the familiar momentum conservation condition in uniform space [see Eq. (2.2)]. As is well known, this condition cannot be satisfied in free space simultaneously with the energy conservation condition, and therefore Fig. 8(a) and Eqs. (3.52) and (3.53) correspond to a realizable radiation scheme only if the interaction region contains a dielectric medium (e.g., gas), thus representing the Čerenkov effect in a quantum model. In this case the radiation wave vector (2.20) is modified by the index of refraction, $\mathbf{q}=\hat{e}_q n\omega/c$, and the matrix element line-shape functions (3.54) can simultaneously attain their maxima on the condition that the *total vectorial* momentum conservation equation (2.2) is satisfied.

It is noted that Eq. (3.54) includes three line-shape functions, corresponding to the three spatial dimensions. In practice one of these functions is dominant. In the transversely classical limit, usually the transverse line-shape functions are eliminated by the process described in Sec. III.B.3 (illustrated by Fig. 7). This case is shown again in Fig. 8(b) for the present example of Čerenkov emission in a "dielectric slab," depicting a narrow wave-packet electron wave function propagating at a straight line at an angle Θ relative to the axis of a dielectric block with dimensions (L_x,L_y,L). We note that in the electron coordinate system (x^e,y^e,z^e) the dominant (narrowest) line-shape function that remains after the evaluation of the matrix element is $\mathrm{sinc}^2[(k^e_{zi}-k^e_{zf}-q^e_z)L^e/2]$. It is thus the effective interaction length of the electron L^e that determines the emission and absorption line-shape functions. This length is usually determined by the longitudinal dimension of the structure (the dielectric slab in the present example): $L^e=L/\cos\Theta_e$. However, at large angles, as depicted in Fig. 8(b), the transverse dimensions of the structure may be the ones that determine the effective electron interaction length ($L^e=L_x/\sin\Theta_e$) and the interaction line-shape function.

The free-electron interaction configurations of most interest in the present review are ones that are characterized by a periodic structure in the axial (z) dimension. We confine our analysis to the cases discussed in Sec. III.B, in which the matrix element calculation involves only z integration, or in which the longitudinal line-shape function is dominant. If the periodic structure affects the radiation field, the radiation modes satisfy the Floquet theorem (2.5). If the periodic structure affects the electron, the electron eigenstate functions are also Floquet (Bloch) waves [Eq. (2.6)]. In some problems, such as when an electron is channeled through the crystal lattice, both the electrons and the radiation field are affected by the periodicity. It is instructive then to examine the combined contributions of both effects to the matrix element.

Keeping in Eqs. (2.56) and (2.57) only the terms that will produce axial phase matching (momentum conservation) via first-order harmonics, the emission matrix element can be written

$$M_{\nu_f=\nu_i+1}=\sqrt{\nu_i+1}\left\langle\psi_f^{(0)}+\psi_f^{(1)}\left|\frac{e}{\gamma m}(\tilde{\mathbf{A}}_s^{(0)}+\tilde{\mathbf{A}}_s^{(1)})\cdot(\mathbf{p}_c+e\,\mathbf{A}_w^{(1)})\right|\psi_i^{(0)}+\psi_i^{(-1)}\right\rangle, \quad (3.55)$$

where

$$\tilde{\mathbf{A}}_s^{(m)}=\tilde{\mathbf{A}}_m(\mathbf{r}_\perp)\exp[i(q_{z0}+mk_w)z], \quad (3.56)$$

$$\psi^{(m)}=\psi_m(\mathbf{r}_\perp)\exp[i(k_{z0}+mk_w)z], \quad (3.57)$$

are the m-order space harmonics of the radiation and

electron waves, respectively, and $\mathbf{A}_w^{(1)}$ is the first-order Fourier component of the periodic wiggler.[12]

We focus our attention now on the axial overlap integral, assuming that the transverse overlap integral is nonvanishing. It is clear that after integration over the z coordinate all "first-order" products of the various terms in (3.55) produce the same detuning function:

$$|M_{\nu_f=\nu_i+1}|^2 \propto (\nu_i+1)\,\mathrm{sinc}^2[(k_{zi}-k_{zf}-q_z-k_w)L/2]\ . \tag{3.58}$$

This fully justifies the axial conservation momentum condition (2.14), which was hypothesized in Sec. II for an infinite interaction length. It also fits well with the axial momentum uncertainty assumption of (2.26). In a similar way one can also show that

$$|M_{\nu_f=\nu_i-1}|^2 \propto \nu_i\,\mathrm{sinc}^2[(k_{zf}-k_{zi}-q_z-k_w)L/2]\ . \tag{3.59}$$

It is worth drawing attention to the fact that the different first-order terms in Eq. (3.55) add up in a phase-coherent way. It is thus very important, when a number of radiation mechanisms exist, to determine the phase of the various terms as well as the amplitude, in order to find out if their contributions to the proportionality coefficient of (3.58) add up constructively or destructively.

It is quite instructive to relate the contributions of the various terms in (3.55) to a number of well-known radiation schemes. We do it with the aid of a series of Feynman diagrams (Fig. 9), which illustrate the various interaction terms. It should be noted that although in Feynman diagrams each junction usually represents an order of perturbation in the fields, in the presently discussed problems the unperturbed electron and radiation fields (before they interact with each other) can often be solved exactly in terms of the wiggler field or the periodic electromagnetic structure. The first-order components in (3.55) may represent therefore exact *first-order Floquet space harmonic* calculation and not a *first-order perturbation* calculation. However, the interaction of the electron with the radiation wave is indeed a first-order calculation. The Feynman diagrams should be regarded here

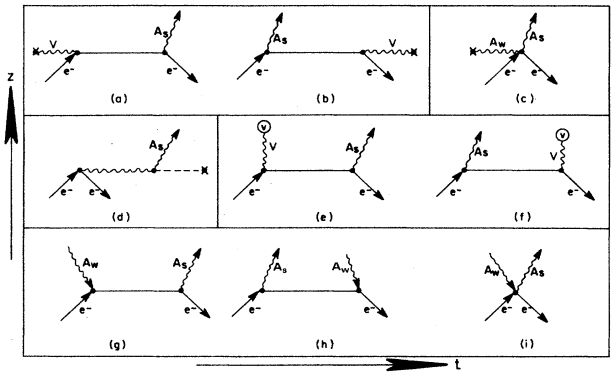

FIG. 9. Feynman diagram representation of different free-electron radiative emission schemes.

only as a symbolic means for classifying and illustrating the basic physical processes in the various radiation schemes. Figure 9 classifies the various interaction schemes reviewed in this article into five classes of elementary processes.

(1) The leading process in coherent bremsstrahlung radiation (Uberal, 1956; Walker *et al.*, 1975) and in electrostatic bremsstrahlung FEL (Gover, 1980a), and one of the contributing terms in off-axis undulator radiation (Motz, 1951; Kincaid, 1977), is the basic bremsstrahlung process for which $\mathbf{A}_s^{(1)}=\mathbf{A}_w^{(1)}=0$. The matrix element is composed of two terms,

$$M_{\nu_f=\nu_i+1}=\sqrt{\nu_i+1}\left[\left\langle\psi_f^{(0)}\left|\frac{e}{\gamma m}\mathbf{A}_s^{(0)*}\cdot\mathbf{p}_c\right|\psi_i^{(-1)}\right\rangle+\left\langle\psi_f^{(1)}\left|\frac{e}{\gamma m}\mathbf{A}_s^{(0)*}\cdot\mathbf{p}\right|\psi_i^{(0)}\right\rangle\right]. \tag{3.60}$$

These terms are represented by the Feynman diagrams of Figs. 9(a) and 9(b), respectively.

(2) The leading process in the most familiar radiation effect of magnetic bremsstrahlung FEL (Elias *et al.*, 1976; Deacon *et al.*, 1977) or undulator synchrotron radiation (Motz, 1951; Kincaid, 1977) is based (assuming on-axis radiation and zero transverse electron canonical momentum) only on the term

$$M_{\nu_f=\nu_i+1}=\sqrt{\nu_i+1}\left\langle\psi_f^{(0)}\left|\frac{e^2}{\gamma m}\mathbf{A}_s^{(0)}\cdot\mathbf{A}_w^{(1)}\right|\psi_i^{(0)}\right\rangle\ . \tag{3.61}$$

This term is represented by the degenerate diagram of Fig. 9(c). The conventional bremsstrahlung process diagrams [Figs. 9(a) and 9(b); Eq. (3.60)] contribute to the FEL radiation scheme only when off-axis radiation or nonvanishing transverse canonical electron momentum are considered. It should be pointed out that diagram 9(c) is unique to the Schrödinger and Klein-Gordon equations representation, since they both are second order in the vector potential. In a Dirac equation formulation, which is first order in the vector potential, the mag-

[12]For the transversely classical case (Sec. III.B.3), contrary to the other cases, the electron Floquet wave-function harmonics were assumed to have the form (3.57) in the average electron coordinates $\mathbf{r}^e$ and not in the structure coordinates $\mathbf{r}$. For the purpose of clarity in the general discussion of different free-electron interaction schemes, we keep using the structure coordinates, but it should be kept in mind that in the transversely classical regime, the longitudinal coordinate parameters really correspond to the average electron coordinates. Of course there is no distinction between the different regimes in the specific simple case of electron propagation on axis ($\Theta_e=0$).

netic bremsstrahlung FEL scheme would also be represented by the conventional bremsstrahlung diagrams 9(a) and 9(b), but diagram 9(c) would not exist.

(3) In the Smith-Purcell radiation effect and other effects based on a periodic electromagnetic structure, $\psi_i^{(-1)}=\psi_f^{(1)}=\mathbf{A}_w^{(1)}=0$, and the only contributing term is

$$M_{\nu_f=\nu_i+1}=\sqrt{\nu_i+1}\left\langle\psi_f^{(0)}\left|\frac{e}{\gamma m}\mathbf{A}_s^{(1)}\cdot\mathbf{p}\right|\psi_i^{(0)}\right\rangle . \tag{3.62}$$

This process is presented symbolically by diagram 9(d), which is a "generalized" Feynman diagram (Gover and Yariv, 1978a). Here the first interaction junction represents generation of a subluminous radiation wave by the electron, and the second interaction junction on the photon wave symbol represents elastic scattering by the optical grating. This scattering can be described as a process in which the grating endows the subluminous electrostatic (Coulomb) wake field of the electron with a negative crystal momentum that turns it into a luminous radiation wave.

It should be noted that also in the conventional Smith-Purcell radiation effect there is some transverse electrostatic force that is applied to the electron by its image charge in the grating (Smith and Purcell, 1953). Hence there is some contribution (presumably small) to this radiation effect also due to electrostatic bremsstrahlung terms [see Eq. (3.60) and Figs. 9(a) and 9(b)].

(4) In addition to the three radiation processes, which are possible in an axially periodic structure, we discussed in previous sections radiation effects in a transversely confining force, such as the cyclotron resonance maser and channeling radiation. In these radiation schemes $\mathbf{A}_w=\mathbf{A}_s^{(1)}=\psi_i^{(-1)}=\psi_f^{(1)}=0$. The axial coordinate overlap integral in the matrix element produces in this case a line-shape function similar to (3.58), but with $k_w=0$. This corresponds to the axial momentum conservation condition (2.50) in interbranch transitions (Sec. II.D). In this case the transition is made possible between initial and final states that correspond to two different transverse energy branches, and the energy conservation condition can be satisfied simultaneously with the momentum conservation condition due to the excess intrabranch (transverse) energy exchange involved in the transition [see Eq. (2.49)].

Using a general point of view the different transverse energy states of the transverse confinement interaction schemes can be regarded as timelike electron scattering processes presented by Figs. 9(e) and 9(f). The central force field generates in the $\mathcal{E}-k_z$ plane perturbed energy branches above the free-electron energy diagram [Fig. 1(c)]. This is contrary to the spacelike perturbation by the bremsstrahlung process that produces branches, spaced horizontally from each other, in the $\mathcal{E}-k_z$ plane [Brillouin zones—see Fig. 1(b)]. While the spacelike process is represented by horizontal lines in Figs. 9(a) and 9(b) the timelike process is represented by vertical lines [Figs. 9(e) and 9(f)].

(5) For the sake of completeness we also show in Figs. 9(g)–9(i) the Feynman diagrams of the Compton scattering radiation scheme (electromagnetic wiggler FEL). Both the electromagnetic pump (wiggler) and the emitted radiation are represented by slanted lines of slope c. For the sake of simple formulation the Compton scattering radiation effect was not included in the analysis of this paper. However, most of the common features that we identified in the other radiation schemes are found in this radiation scheme as well (Gover, 1981, 1984), and the extension of the formulation to this scheme is quite straightforward.

The actual quantitative calculation of the matrix elements for specific electron radiation schemes is outside the scope of this paper. We limit ourselves to showing, that up to a proportionality constant a large number of radiation schemes in various operation regimes display the same emission and absorption line-shape functions, which are given by (3.58) and (3.59). These "homogeneous broadening" line-shape functions are the result of a finite interaction length and are common to all radiation schemes where the interaction between the electron wave functions and the radiation wave is extended over a long interaction length.

In concluding this section we discuss an alternative longitudinal homogeneous broadening mechanism, which takes place in some radiation schemes. This mechanism is one in which the interaction Hamiltonian or the electron wave functions decay exponentially as a function of z. The line broadening may then be limited by the exponential decay length instead of the interaction length L. The line-shape function is derived in these cases from the z integration implied in the matrix element (3.55), where the inclusion of an exponential factor $\exp(-\kappa z)$ in the integrand modifies (3.58) and (3.59) to read

$$|M_{\nu_f=\nu_i+1}|^2\propto(\nu_i+1)2e^{-\kappa L}\frac{\cosh(\kappa L)-\cos(k_{zi}-k_{zf}-q_z-k_w)L}{[\kappa^2+(k_{zi}-k_{zf}-q_z-k_w)^2]L^2} , \tag{3.63}$$

$$|M_{\nu_f=\nu_i-1}|^2\propto\nu_i 2e^{-\kappa L}\frac{\cosh(\kappa L)-\cos(k_{zf}-k_{zi}-q_z-k_w)L}{[\kappa^2+(k_{zf}-k_{zi}-q_z-k_w)^2]L^2} . \tag{3.64}$$

This result reduces to the sinc^2 line-shape functions (3.58) and (3.59) in the limit $\kappa L\ll 1$, and to a Lorentzian line-shape function

$$|M_{\nu_f=\nu_i\mp 1}|^2\propto(\kappa L)^{-2}[1+(k_{zi}-k_{zf}\pm q_z\pm k_w)^2/\kappa^2]^{-1} \tag{3.65}$$

in the opposite limit. In the latter case the wave-number mismatch width of the line-shape function is κ and is independent of the interaction length L. Hence, when considering the frequency linewidth for this case, κ would replace π/L in (2.26) and (2.27).

Some examples in which line-shape functions as (3.63)

and (3.64) or Lorentzian line shapes [see (3.65)] are obtained are those where the radiation wave decays exponentially due to losses, or when the electron wave function decays. A typical case is that of channeling radiation, when the initial-state wave function decays into other transverse electronic states due to inelastic collisions (scattering by phonons and electronic excitations; see Kurizki and McIver, 1985). This can be described approximately by an exponential decay factor accounting for the finite coherence length of the electron wave function when subjected to these scattering mechanisms.[13] In this case any of the homogeneous line-shape functions [(3.63),(3.64),(3.65)] may be used where $\kappa=\kappa_i+\kappa_f$ and κ_i,κ_f are the exponential decay constants of the channeled electron initial- and final-state functions, respectively (Andersen and McIver, 1981).

The inhomogeneous line-shape functions [(3.63), (3.64),(3.65)] also describe the line broadening of electron emission when interacting with an evanescent electromagnetic wave (such as Smith-Purcell radiation and Čerenkov interaction with a radiation mode of a dielectric slab). The matrix element for this case was derived at the end of Sec. III.B.3 for a transversely classical electron propagating at an angle Θ_e relative to the structure surface (Fig. 7). Assuming straight-line propagation of the electron $\bar{x}^{e}(z^{e})=\bar{x}^{e}_{0}=\text{const}$, the axial integration implied in Eq. (3.40) results in the matrix element calculation (3.62), the same exponential decay homogeneous broadening line-shape functions (3.63)–(3.65) with $\kappa=\alpha\sin\Theta_e$ and $(k_z,q_z,k_w,L)\rightarrow(k_z^e,q_z^e,k_w^e,L^e)$.

E. The transition rate calculation

We have found that for the various electron models (transversely discrete states, transversely continuous quantum, transversely continuous classical) and the various radiation schemes listed and described in the previous section, the single photon emission and absorption transition rates involve similar transition matrix elements [Eqs. (3.20), (3.31), and (3.36)]. The squared absolute value of these emission and absorption matrix elements are proportional in turn to homogeneous broadening detuning functions given by (3.58) and (3.59) or (3.63) and (3.64). The initial and final axial wave numbers k_{zi},k_{zf} that appear in the detuning functions are restricted by the total energy conservation condition, which is dictated, for instance, for the case of transversely discrete states, by the delta function in Eq. (3.19). The delta function argument nulls and manifests the energy conservation conditions for emission $\mathcal{E}^0_{k_{zi}}-\mathcal{E}^0_{k_{ze}}=\hbar\omega$ and absorption $\mathcal{E}^0_{k_{za}}-\mathcal{E}^0_{k_{zi}}=\hbar\omega$ for the two nonvanishing photon-state matrix elements $\nu_f=\nu_i+1$ and $\nu_f=\nu_i-1$, respectively.

It is important to note that contrary to the conservation of energy conditions, (2.13) and (2.15), written specifically for the center line frequencies $\omega=\omega_e$ and $\omega=\omega_a$, respectively, we now require the energy conservation condition to be satisfied exactly for a given arbitrary frequency ω. Consequently, the axial momentum conservation conditions (2.14) and (2.16) are not necessarily satisfied. For a fixed transverse state in the case of transversely discrete states and for an assumption of exact transverse momentum conservation in the case of transversely continuous states, the initial wave number k_{zi} and the radiation frequency ω determine completely the final state k_{zf} and the corresponding momentum conservation mismatch $k_{zf}-k_{zi}-q_z-k_w(k_{zi}-k_{zf}-q_z-k_w)$ that need to be inserted in the detuning curves (3.58), (3.59), (3.63), and (3.64).

The emission and absorption transition rates are proportional to their corresponding detuning functions [(3.58),(3.59),(3.63),(3.64)] with the same proportionality coefficient, except for the factor $1/v_{zf}$ that appears in Eqs. (3.20), (3.31), and (3.36) and the factor $1/\gamma_f$ that emerged from the relativistic generalization of Sec. III.C [see Eq. (3.48)]. This makes it possible to write the net photon emission rate into a given radiation mode $\mathbf{q}\sigma$ at frequency ω in the form

$$\begin{aligned}\frac{d\nu_{\mathbf{q}\sigma}}{dt}&=W_{\nu_f=\nu_i+1}-W_{\nu_f=\nu_i-1}\\&=\Gamma_{\mathrm{sp}}\gamma_i v_{zi}\left[(\nu_{\mathbf{q}\sigma}+1)\frac{1}{\gamma_e v_{ze}}F(\bar{\theta}_e)\right.\\&\quad\left.-\nu_{q\sigma}\frac{1}{\gamma_a v_{za}}F(\bar{\theta}_a)\right],\end{aligned}\tag{3.66}$$

where

$$F(\bar{\theta})=\mathrm{sinc}^2\left[\frac{\bar{\theta}}{2}\right]\tag{3.67}$$

for the case of interaction-length-limited line-shape function [(3.58),(3.59)], and

$$F(\bar{\theta})=\frac{(\kappa L)^2}{\cosh(\kappa L)-1}\frac{\cosh(\kappa L)-\cos\bar{\theta}}{(\kappa L)^2+\bar{\theta}^2}\tag{3.68}$$

for the exponential decay case [(3.63),(3.64)]. The emission and absorption detuning parameters $\bar{\theta}_e,\bar{\theta}_a$ are the phase mismatches between the electron, radiation, and wiggler waves accumulated along the length L due to the corresponding initial longitudinal momentum (wave number) mismatch,

$$\bar{\theta}_e=\theta_e L,\quad \theta_e\equiv k_{zi}-k_{ze}(\omega,k_{zi})-q_z(\omega)-k_w\ ,\tag{3.69}$$

$$\bar{\theta}_a=\theta_a L,\quad \theta_a\equiv k_{za}(\omega,k_{zi})-k_{zi}-q_z(\omega)-k_w\ .\tag{3.70}$$

The common coefficient Γ^0_{sp} is the spontaneous emission transition rate at the emission line center, and can be cal-

[13] A more accurate model should consider also the "refeeding effect," i.e., the scattering of the electron back into the original state (Andersen and McIver, 1981).

culated for a given radiation scheme and electron model according to the procedure outlined in the previous section. Both detuning functions were normalized to satisfy $F(0)=1$.

We note that the dependence of $\bar{\theta}_e, \bar{\theta}_a$ on k_{zi}, ω is implicit in the conservation of energy conditions that are assumed to be satisfied exactly for a given frequency ω: $\mathcal{E}_{k_{zi}} - \mathcal{E}_{k_{ze}} = \hbar\omega$, $\mathcal{E}_{k_{za}} - \mathcal{E}_{k_{zi}} = \hbar\omega$ [(2.13) and (2.15) with $\omega_e = \omega_a = \omega$]. The dependence on ω, k_{zi} can be made explicitly by expanding $\mathcal{E}_{k_{ze}}$ and $\mathcal{E}_{k_{za}}$ to a second order in $\hbar$ in the same way that was used to derive (2.17) and (2.42). For an electron and electromagnetic wave propagating on axis with the wiggler, or in general in the absence of transverse recoil, this results in

$$\bar{\theta}_e = \bar{\theta} + \frac{\varepsilon}{2} , \tag{3.71}$$

$$\bar{\theta}_a = \bar{\theta} - \frac{\varepsilon}{2} , \tag{3.72}$$

where

$$\bar{\theta} = \frac{\bar{\theta}_e + \bar{\theta}_a}{2} = \left[\frac{\omega}{v_z(k_{zi})} - q_z(\omega) - k_w \right] L , \tag{3.73}$$

$$\varepsilon = (\bar{\theta}_e - \bar{\theta}_a) = \frac{\hbar}{m_{\parallel}^* \bar{v}_z} \left[\frac{\omega}{\bar{v}_z} \right]^2 L . \tag{3.74}$$

The latter parameter is the longitudinal quantum recoil parameter. Comparing it to (2.42) we find that it relates to the emission and absorption line-centers spacing $\delta\omega = \omega_a - \omega_e$ and to the finite-length broadening linewidth $\Delta\omega_L$ by the simple equality

$$\varepsilon = 2\pi \frac{\omega_a - \omega_e}{\Delta\omega_L} . \tag{3.75}$$

Clearly the condition $\varepsilon \ll 2\pi$ is equivalent to the classical limit condition $\Delta\omega_L \gg |\delta\omega|$ [see (2.35)], and therefore the recoil parameter ε is also the longitudinal classical limit indicator.

The other parameters in Eq. (3.66) that contain quantum terms are $\gamma_e v_{ze} = \hbar k_{ze}/m$ and $\gamma_a v_{za} = \hbar k_{za}/m$. Using the definitions (3.69), (3.70), and (3.73), we can rewrite these terms (to first order in $\hbar$) as

$$\gamma_e v_{ze} = \gamma_i v_{zi}(1 - \eta/2) , \tag{3.76}$$

$$\gamma_a v_{za} = \gamma_i v_{zi}(1 + \eta/2) , \tag{3.77}$$

where

$$\eta = \frac{2\hbar}{p_{zi}} \frac{\omega}{v_z} . \tag{3.78}$$

Clearly also $\eta \ll 1$ is a classical limit condition. However, for all practical cases $\varepsilon \gg \eta$ [$\varepsilon = (1/2\gamma_z^2)(\omega/v_z)L\eta \approx 2\pi N_w \eta$, where the second equality applies to periodic structure FEL's with $\gamma_z \gg 1$]. Consequently, the condition $\varepsilon \ll 1$ is a sufficient classical limit condition. Because η is so much smaller than ε for most practical cases, we will mostly use in this paper a simplified version of Eq. (3.66) with $\eta = 0$, assuming (as is usually done) that the main quantum recoil effect is inside the detuning function:

$$\frac{d\nu_{q\sigma}}{dt} = \Gamma_{sp}[(\nu_{q\sigma} + 1)F(\bar{\theta}_e) - \nu_{q\sigma}F(\bar{\theta}_a)] . \tag{3.79}$$

Equations (3.73), (3.74), and (3.78) are applicable to a general electromagnetic mode (e.g., a waveguide mode or a free-space Gaussian mode within a Rayleigh length) as long as the electron propagates perpendicular to the wave phase fronts (forward radiative emission). For off-axis radiative emission in the case of transversely continuous states, transverse quantum recoil must be taken into account in the series expansion of the conservation of energy and momentum condition, which needs to be carried out in order to obtain an explicit $(\omega, \mathbf{k}_i)$ dependence of the detuning parameters. Following the same method used to derive $\delta\omega/\Delta\omega$ [Eq. (2.89)] in Sec. II, we specify the derivation to plane-wave radiation modes. The analysis is still quite general, since the radiation direction and the electron average motion direction are both allowed to be arbitrary. Equations (3.71), (3.72), (3.75)–(3.77) are valid for this case as well, but the recoil parameter ε and the classical detuning parameter $\bar{\theta}$ are given by (see Appendix E)

$$\varepsilon = \frac{\hbar L}{v_z} \sum_{i,j=1}^{3} (\mathbf{q} + \mathbf{k}_w)_i \left[\frac{1}{m^*} \right]_{ij} (\mathbf{q} + \mathbf{k}_w)_j , \tag{3.80}$$

$$\bar{\theta} = [\omega - (\mathbf{q} + \mathbf{k}_w) \cdot \mathbf{v}_g] L_z / v_z . \tag{3.81}$$

As was predicted in Sec. III.B, the equation for the classical detuning parameter $\bar{\theta}$ [Eq. (3.81)] is independent of the choice of the coordinates system and is only dependent on the projection of $\mathbf{q} + \mathbf{k}_w$ on the electron propagation direction and the transit time $t_{tr} = L_z/v_z = L^e/\bar{v}$. The recoil parameter definition also is independent of the choice of coordinates. In Appendix F we explore the symmetry properties of the mass tensor. We show there that for a uniform (on the average) wiggler structure [for which the mass tensor terms are given by Eq. (2.90)], the mass tensor diagonalizes in a coordinate system that is aligned with the electron average motion direction. This system is therefore the principal system of the mass tensor. The recoil parameter is shown there to be given by

$$\varepsilon = \frac{\hbar L}{\bar{v}} \frac{1}{m\gamma} \left[\frac{1}{\bar{\gamma}^2} [(\mathbf{q} + \mathbf{k}_w) \cdot \hat{e}_e]^2 + [(\mathbf{q} + \mathbf{k}_w) \times \hat{e}_e]^2 \right]$$

$$= \hbar t_{tr} \frac{1}{m\gamma} \left[\frac{1}{\bar{\gamma}^2} (q_z^e + k_{wz}^e)^2 + (\mathbf{q}_\perp^e + \mathbf{k}_{w\perp}^e)^2 \right] . \tag{3.82}$$

This indicates that the recoil parameter depends only on two parameters: the longitudinal and transverse components of the vector $(\mathbf{q} + \mathbf{k}_w)$ relative to the axis defined by the electron average motion.

We cite from Appendix F two more forms for the important recoil parameter. Expressing the various parameters in (3.82) in terms of the electron rest-frame parame-

ters[14] reveals an illuminating physical interpretation of the recoil parameter:

$$\varepsilon=\frac{\hbar t'_{\rm tr}}{m\gamma'}(\mathbf{q}'+\mathbf{k}'_w)^2=\delta\omega t'_{\rm tr} \ , \tag{3.83}$$

where

$$\delta\omega'/2=\omega'_0-\omega'_0=\mathcal{E}'_f/\hbar=\hbar k'^2_f/(2m\gamma')$$
$$=\hbar(\mathbf{q}'+\mathbf{k}'_w)^2/(2m\gamma')$$

is the well-known Compton recoil frequency shift of a photon scattered by an electron at rest (with effective mass $m\gamma'$), and $t'_{\rm tr}=L^e_z/(\bar{v}\,\bar{\gamma})$ is the wiggler transit time in the electron rest frame. The second part of Eq. (3.83) can also be derived directly from (3.75) when applied in the electron (average motion) rest frame. This is permissible because, as we show in Appendix F, Eq. (3.75) is a covariant equation—form invariant under general Lorentz transformations. Equation (3.83) provides a tie between general free-electron radiation and the conventional Compton scattering effect. Indeed, starting at the electron rest frame with the known Compton recoil Eq. (3.83) and then transforming back to the laboratory frame is an alternative way for deriving the quantum and classical regime equations (Gover, 1984). Also the original paper by Madey (1971) on the FEL was based on modeling the device as a stimulated Compton scattering effect.

Another form for the recoil parameter, expressed in terms of the laboratory parameters, can be derived from Eq. (3.82) (Appendix E):

$$\varepsilon=\frac{\hbar L\omega_0^2}{m\gamma\bar{v}^3}\left[\frac{1}{\bar{\gamma}^2}+\tan^2\Theta_{\rm rec}(\omega_0)\right] \ , \tag{3.84}$$

where $\Theta_{\rm rec}$ is the angle between the recoil momentum vector[15] $\hbar(\mathbf{q}+\mathbf{k}_w)$ and the electron motion direction,

$$\cos\Theta_{\rm rec}=\hat{e}_{\mathbf{q}+\mathbf{k}_w}\cdot\hat{e}_e=\hat{e}_e\cdot(\mathbf{q}_0+\mathbf{k}_w)/|\,\mathbf{q}_0+\mathbf{k}_w\,| \ , \tag{3.85}$$

and ω_0 is the synchronism frequency $[\bar{\theta}(\omega_0)=0]$. The detuning parameter may then be expressed in a compact way in terms of $\Theta^e_{\rm rec}$:

$$\bar{\theta}=\left[\frac{\omega}{\bar{v}}-|\,\mathbf{q}(\omega)+\mathbf{k}_w\,|\cos\Theta_{\rm rec}(\omega)\right]L^e \ . \tag{3.86}$$

For practical applications, it is useful to express the recoil angle $\Theta_{\rm rec}$ in terms of the angles between the mutually misaligned electron motion axis, wiggler axis, and radiation direction:

$$\cos\Theta^e_q=\hat{e}_{\rm q}\cdot\hat{e}_e, \quad \cos\Theta^e_w=\hat{e}_w\cdot\hat{e}_e, \quad \cos\Theta^q_w=\hat{e}_w\cdot\hat{e}_{\rm q} \ ,$$

where $\hat{e}_{\rm q},\hat{e}_e,\hat{e}_w$ are unit vectors in the radiation, electron motion, and wiggler directions, respectively. Equation (3.85) can then be written, in general, as

$$\cos\Theta_{\rm rec}=\frac{\dfrac{\omega}{k_w c}\cos\Theta^e_q+\cos\Theta^e_w}{\left[1+\left[\dfrac{\omega}{k_w c}\right]^2+2\dfrac{\omega}{k_w c}\cos\Theta^w_q\right]^{1/2}} \ . \tag{3.87}$$

In addition, the detuning parameter (3.81) can be expressed in terms of the recoil angle

$$\bar{\theta}=\left[\frac{\omega}{\bar{v}}-\frac{\omega}{c}\cos\Theta^e_q+k_w\cos\Theta^e_w\right]L^e \ . \tag{3.88}$$

The recoil parameter (3.84) expressed in terms of the mutual angles (3.87) and the detuning parameter expression (3.88) can now be used in Eqs. (3.66) and (3.71)–(3.94) to provide a very general equation for free electron spontaneous and stimulated emission at arbitrary electron, wiggler, and radiation wave directions.

We note that most of the analyses previous carried out for free-electron lasers are applicable only to the limit $\Theta^e_q=\Theta^e_w=\Theta^w_q=0$ (on-axis propagation and emission). Some of them (Krinsky *et al.*, 1982; Kroll, 1982) apply in the more general case $\Theta^w_q=0$, $\Theta^e_q=\Theta^e_w\neq 0$ (radiative emission on the wiggler axis by an electron that may propagate off axis). In this latter case $\bar{\theta}=[\omega/\bar{v}-(\omega/c+k_w)\cos\Theta^e_w]L^e$, and $\Theta_{\rm rec}=\Theta^e_w$, which also makes Eq. (3.84) for the recoil parameter a simple explicit equation given in terms of the electron propagation angle Θ^e_w. In the most general case of arbitrary radiative emission and electron propagation direction, which we derived here, two angle parameters (Θ^e_q,Θ^e_w) need to be known.

Explicit representation of the frequency dependence of the line-shape functions can be obtained by first-order expansion of the detuning parameter around the emission and absorption line centers. For both the models of longitudinal recoil [Eqs. (3.71)–(3.75)] and arbitrary recoil arbitrary plane-wave emission angle [Eqs. (3.80) and (3.81)], this results in (Appendix F)

$$\bar{\theta}_e=2\pi\frac{\omega-\omega_e}{\Delta\omega_L} \ , \tag{3.89}$$

$$\bar{\theta}_a=2\pi\frac{\omega-\omega_a}{\Delta\omega_L} \ , \tag{3.90}$$

which also permits us to write the classical detuning pa-

[14]Recall that the barred parameters $\bar{\gamma},\bar{v}$ refer to the group velocity of the electron which in the classical limit is the average (over wiggler period) velocity of an electron quivering in a general wiggler. In addition, $\gamma=\bar{\gamma}\gamma_T$, $\gamma_T=\sqrt{1+\bar{a}^2_w}=\gamma'$, where γ' is the relativistic mass factor in the electron average rest frame, and $\bar{a}_w\equiv e\bar{A}_w/mc$.

[15]The wiggler wave number was defined to have negative momentum (to indicate primary motion opposite to the signal wave direction), hence $\hbar[\mathbf{q}-(-\mathbf{k}_w)]$ indicates the transfer of momentum to the electron in a process in which one (virtual) wiggler photon of momentum $-\hbar\mathbf{k}_W$ is absorbed, and one photon of momentum $\hbar\mathbf{q}$ is emitted.

TABLE I. The finite-length homogeneous line-broadening parameters for periodic structure schemes.

Parameter	Wave-number domain	Frequency domain
Emission detuning parameter	$\bar{\theta}_e=(k_{zi}-k_{ze}-q_z-k_w)L$	$2\pi\frac{\omega-\omega_e}{\Delta\omega_L}$
Absorption detuning parameter	$\bar{\theta}_a=(k_{za}-k_{zi}-q_z-k_w)L$	$2\pi\frac{\omega-\omega_a}{\Delta\omega_L}$
Classical detuning parameter:	$\bar{\theta}=\frac{\bar{\theta}_e+\bar{\theta}_a}{2}$	$2\pi\frac{\omega-\omega_0}{\Delta\omega_L}$
(1) Longitudinal recoil	(1) $\left[=\left[\frac{\omega}{v_z}-q_z-k_w\right]L\right]$	
(2) Arbitrary angle plane wave	(2) $\{=[\omega-(\mathbf{q}+\mathbf{k}_w)\cdot\bar{\mathbf{v}}]L_z/v_z\}$	
Quantum recoil parameter	$\varepsilon=(\bar{\theta}_e-\bar{\theta}_a)$	$2\pi\frac{\delta\omega}{\Delta\omega_L}$

rameter (3.73) as

$$\bar{\theta}=2\pi\frac{\omega-\omega_0}{\Delta\omega_L}\ , \tag{3.91}$$

where $\Delta\omega_L$ is the finite-length homogeneous broadening linewidth (2.31) or (2.84). There is a slight difference between the emission and absorption linewidths, but in all practical cases it is negligible (as explained in Appendix F).

The frequency dependence of the finite-length homogeneous broadening net emission line-shape function [(3.79),(3.67)] is illustrated as a function of ω by the upper curve of Fig. 2(a) for the quantum limit $\varepsilon\gg 2\pi(\omega_a-\omega_e\gg\Delta\omega_L)$. The upper curve of Fig. 2(b) illustrates the Lorentzian homogeneous broadening line-shape function (3.65) in the same limit. The linewidth of this line-shape function is wider than the finite-length broadening width: $\Delta\omega_h=\Delta\omega_L\kappa L/\pi$. We note that the linewidth parameter is in this case independent of L as expected.

Table I summarizes the homogeneous line-broadening parameters according to the two different notations used for describing the lines detuning in the wave number domain and in the frequency domain. The second column expresses the detuning parameters $\bar{\theta}_e,\bar{\theta}_a$ as the wave number (momentum) mismatches for emissive and absorptive transitions, respectively, normalized to the interaction length. It presents (implicitly) the dependence of the emission and absorption lines on both ω and $\mathcal{E}_{k_i}$. The third column expresses the detuning parameters explicitly in terms of the frequency parameters of the emission and absorption lines: the signal frequency ω, the line centers ω_e,ω_a, and the frequency linewidth $\Delta\omega_L$. The latter representation is manifestly similar to the representation of atomic transition lines. The dependence on the electron energy and wiggler parameter is implicit in the line-center frequency parameters (ω_e,ω_a) and the bandwidth parameter $\Delta\omega_L$. Table I helps to draw the connection between the results of the dynamical analysis of this section and those of the kinematic analysis in the previous section.

The transition rate equations (3.66)–(3.70) apply without change for the Čerenkov radiation and the transverse binding interbranch transition radiation schemes with the substitution $k_w=0$. However, since the energy conservation condition [(2.49), (2.51)] of the transverse binding radiation schemes are different, Eqs. (3.71)–(3.74), (3.80), and (3.81) should be modified. Following the analysis in Sec. II.D, we redefine for the case of nondegenerate spacing of the energy branches (e.g., in electron channeling radiation),

$$\bar{\theta}_e=\bar{\theta}_d+\frac{\varepsilon_e}{2}\ , \tag{3.92}$$

$$\bar{\theta}_a=\bar{\theta}_u-\frac{\varepsilon_a}{2}\ , \tag{3.93}$$

$$\bar{\theta}_d\equiv\left[\frac{\omega-\omega_d}{v_z}-q_z\right]L\ , \tag{3.94}$$

$$\bar{\theta}_u\equiv\left[\frac{\omega-\omega_u}{v_z}-q_z\right]L\ . \tag{3.95}$$

Equations (3.89) and (3.90) are still valid, except that ω_e and ω_a are given by (2.55) and (2.56), and the emission and absorption recoil parameters are [as in the derivation of (2.65)]

$$\varepsilon_{e,a}=2\pi\frac{\delta\omega_{e,a}}{\Delta\omega_L}=\frac{\hbar}{m_{\parallel}^*}\frac{L}{v_z}\frac{\omega_{e0,a0}^2}{c^2}\cos^2\Theta_q\ . \tag{3.96}$$

The detuning parameters of the transverse binding force interbranch transitions are summarized in Table II in terms of both phase (wave number) mismatch and frequency tuning parameters. Note that in the transverse binding interbranch transition case, there are two independent classical limits: (1) the negligible longitudinal recoil limit $\varepsilon_{e,a}\ll 2\pi$; (2) the degenerate spacing of the transverse-states limit. In the first case the longitudinal recoil is negligible [vertical transitions in the diagram of Fig. 1(c)], but the problem can still be quantum because

TABLE II. The finite-length homogeneous line-broadening parameters for transverse binding force schemes.

Parameter	Wave-number domain	Frequency domain
Emission detuning parameter	$\bar{\theta}_e=(k_{zi}-k_{ze}-q_z)L$	$2\pi\frac{\omega-\omega_e}{\Delta\omega_L}$
Absorption detuning parameter	$\bar{\theta}_a=(k_{za}-k_{zi}-q_z)L$	$2\pi\frac{\omega-\omega_a}{\Delta\omega_L}$
Longitudinal classical emission detuning parameter	$\bar{\theta}_d$	$2\pi\frac{\omega-\omega_{e0}}{\Delta\omega_L}$
(1) On-axis emission	(1) $\left[=\left[\frac{\omega-\omega_d}{v_z}-q_z\right]L\right]$	
(2) Arbitrary angle plane wave	(2) $[=(\omega-\omega_d-\mathbf{q}\cdot\bar{\mathbf{v}})L_z/v_z]$	
Longitudinal classical absorption detuning parameter	$\bar{\theta}_u$	$2\pi\frac{\omega-\omega_{a0}}{\Delta\omega_L}$
(1) On axis	(1) $\left[=\left[\frac{\omega-\omega_u)}{v_x}-q_z\right]L\right]$	
(2) Arbitrary angle plane wave	(2) $[=(\omega-\omega_u-\mathbf{q}\cdot\bar{\mathbf{v}})L_z/v_z]$	
Quantum recoil parameter	$\varepsilon_e=2(\bar{\theta}_e-\bar{\theta}_d)$ $\varepsilon_a=2(\bar{\theta}_u-\bar{\theta}_a)$	

of unequal spacing between the transverse-states branches ($|\omega_{e_0}-\omega_{a_0}|>\Delta\omega_L$). The opposite can happen in the second case. In Table II we assume only the first limit and expand only the longitudinal recoil quantum parameter to first order in $\hbar$ (the transverse energy parameters $\bar{\theta}_d,\bar{\theta}_u,\omega_d,\omega_u$ may remain fully quantum). This is a reasonable model for problems such as electron channeling radiation, where the electron system is inherently quantum mechanical in the transverse dimensions. In other problems, such as the cyclotron resonance maser and positron channeling radiation, it may be necessary to expand the transverse quantum parameters to first order in $\hbar$, as we did in (2.66) and (2.67). This will be discussed in the next section.

F. The longitudinal classical limit

Until now we considered cases in which the electron is described either quantum mechanically or classically in the transverse dimensions. In all cases, however, it was described *quantum mechanically* in the longitudinal dimension. In this section we derive for all cases the practical limit of "negligible quantum recoil" (the longitudinal classical limit). In taking this limit one should bear in mind the observations made in Sec. II.F regarding this limit.

As indicated in the previous section, a sufficient condition for the longitudinal classical limit is $\varepsilon=2\pi\delta\omega/\Delta\omega_L\ll 2\pi$, which is also identical with the classical limit condition (2.35) derived earlier from kinematic considerations. Necessarily, when this condition is satisfied, $\eta\ll 1$ is also satisfied (since $\eta\ll\varepsilon$). Thus the expansion of the transition rate, Eq. (3.66), to first order in $\hbar$ in the classical limit can be carried out straightforwardly by expansion in terms of ε and η using Eqs. (3.71), (3.72), (3.76), and (3.77). Since $\eta\ll\varepsilon$, we will neglect in the present discussion the resulting terms that are proportional to η[16] and will use in effect Eq. (3.79) instead of (3.66). Taking the differential of (3.79) in the $\varepsilon\ll 2\pi$ limit, we find

$$\frac{d\nu_{q\sigma}}{dt}=\Gamma_{sp}\left[F(\bar{\theta})+\frac{1}{2}\varepsilon\frac{d}{d\bar{\theta}}F(\bar{\theta})+\nu_{q\sigma}\varepsilon\frac{d}{d\bar{\theta}}F(\bar{\theta})\right]. \tag{3.97}$$

For finite-length homogeneous broadening this result reduces to the well-known spontaneous and stimulated emission classical line-shape functions

$$\mathrm{sinc}^2(\bar{\theta}/2) \quad \text{and} \quad (d/d\bar{\theta})\,\mathrm{sinc}^2(\bar{\theta}/2)\,,$$

previously derived for various kinds of FEL's (Madey, 1971; Gover and Livni, 1978; Sprangle and Smith, 1980;

[16]The ratio ε/η scales as L (in the limit $\gamma_z\gg 1$ or periodic structure FEL's $\varepsilon/\eta=2\pi N_w$). Consequently the terms proportional to η may make a non-negligible contribution only for a very short wiggler. Similar terms with quadratic scaling of the classical gain in terms of the interaction length L (instead of cubic) were identified in the FEL gain equation from direct classical formulation (Sprangle and Smith, 1980). They were found to be negligible for practical FEL's with $N_w\gg 1$.

Gover and Sprangle, 1981; Piestrup and Finman, 1983). We note that the second term in (3.97) is a spontaneous emission term, though it has the same line-shape function as the stimulated emission (third term). This term is the only quantum-electrodynamical contribution left after taking the electron classical limit $\varepsilon \ll 2\pi$. However, in this limit this term is always negligible relative to the classical spontaneous emission (first term).

Equations similar to (3.97) were derived before from a quantum model of magnetic bremsstrahlung FEL's by a number of authors (Soln, 1981; Becker and McIver, 1982; Dattoli and Renieri, 1983, 1985; Gover, 1984). This equation states that the classical spontaneous and stimulated photon emission rate functions are related to each other by a simple relation of a derivative. Such a relation can also be derived using a classical model as was shown by Madey (1979) for the magnetic bremsstrahlung FEL. Our derivation extends the theorem derived by Madey to a large number of additional quasifree-electron radiation schemes and operating regimes that were discussed earlier in this paper. Furthermore, it extends it, when the more general equations for the recoil parameter (3.80) and (3.84) are used, to the general case of arbitrary electron propagation and radiative emission directions.

An exception to the generality of (3.97) is the case of transverse binding radiation schemes. Only when the vertical spacing between the branches of the transverse quantum states is degenerate ($\omega_d = \omega_a$) are the detuning parameters (3.94) and (3.95) identical, $\theta_d = \theta_u = \theta$, and (3.97) holds. In other cases (as in electron channeling radiation) $\omega_d \neq \omega_u$, and then the emission and absorption lines do not overlap even in the longitudinal classical limit $\varepsilon \ll 2\pi$. In this case (3.66) does not reduce into (3.97) as long as the condition $|\omega_u - \omega_d| L/v_z > 2\pi$, or the equivalent condition $|\omega_{e0} - \omega_{a0}| < \Delta\omega_L$, is satisfied.

If the deviation from degeneracy (the difference between the spacings) of the transverse-states energies $\hbar(\omega_u - \omega_d)$ is a second-order quantum parameter ($|\omega_u - \omega_d|$ is proportional to $\hbar$), one can expand $\bar{\theta}_e, \bar{\theta}_a$ [Eqs. (3.92) and (3.93)] to first order in $\varepsilon_e, \varepsilon_a$ and $(\omega_u - \omega_d)$. One can then obtain, similarly to (3.97), expressions for the spontaneous and stimulated emission rate, which are classical in both the longitudinal and transverse parameters. Such an expansion was carried out in Appendix A for the special case of the cyclotron resonance maser, in which the vertical spacings between the transverse-states branches are nearly degenerate. The transverse "recoil" effect is manifested in this case by transitions to lower or higher transverse states (Landau levels). Considering emission into a particular harmonic $\Delta n = n_i - n_f$, we find that the electron will radiate at central frequency

$$\omega_0^{(\Delta n)} = \Delta n \frac{\omega_{c0}/\gamma}{1 - \beta_z \cos\Theta_q} , \tag{3.98}$$

where $\Delta n = 1, 2, \ldots$. There is no overlap between the emission line functions of different radiation harmonics, emitted at the same angle Θ_q, as long as the emission linewidth (2.31) is narrower than the fundamental cyclotron frequency $\Delta\omega_L < \omega_0^{(1)}$.

The "total" recoil parameter (both longitudinal and transverse with respect to the magnetic axis) $\varepsilon = 2\pi\delta\omega/\Delta\omega_L$ of a cyclotron resonance maser operating at arbitrary cyclotron harmonic Δn can then be found directly from (2.67) by substituting $\omega_{c0} \rightarrow \Delta n \omega_{c0}$:

$$\varepsilon^{(\Delta n)} = -(\Delta n)^2 \frac{\sin^2\Theta_q}{1 - \beta_z \cos\Theta_q} \frac{\hbar\omega_{c0}}{\gamma^3 mc^2} \frac{\omega_{c0} L}{v_{gz}} . \tag{3.99}$$

This can be used directly in Eq. (3.97), which is valid also for the degenerate spacings transverse binding FEL with an appropriately defined general recoil parameter ε. The resulting equation is a general formula for spontaneous and stimulated emission of cyclotron resonance radiation in an arbitrary direction, and contains therefore both the effects of relativistic mass instability (gyrotron effect; see Hirshfield *et al.*, 1965; and Chu and Hirshfield, 1978), which is dominant for $\Theta_q \approx \pi/2$, and the "Weibel instability" (Weibel, 1959), which is dominant for $\Theta_q \approx 0$ [see the discussion in Sec. II.D in reference to Eq. (2.67)].

We can now appreciate the generality of both the quantum Eq. (3.66) and the electron classical (or negligible recoil) Eq. (3.97), which together with (3.67) or (3.68) and Tables I and II define the spontaneous and stimulated emission rates in the homogeneous broadening regimes for the wide class of quasifree-electron radiation schemes introduced in the first section. The emission rate functions of all of these radiation schemes are characterized by only four parameters, Γ_{sp}, ω_0, $\Delta\omega$, and ε (or $\delta\omega$); for interbranch transitions in the case of transversely discrete states, there may be two separate values for each of these parameters, corresponding to up and down transverse-states transitions. For complete determination of the emission rate, the spontaneous emission parameter Γ_{sp} has to be either calculated from the matrix element of the transition or experimentally measured. For the other three parameters, we derived explicit equations, which are listed in Table III for the general cases of (1) transversely continuous states, (2) transversely discrete intrabranch transitions, and (3) transversely discrete interbranch transitions, and for the special case of (4) the cyclotron resonance maser. This table applies to a free-space plane-wave radiation model, and the radiation direction relative to the structure (wiggler) axis [in case (1), including the electron propagation direction] is arbitrary.

Finally we note that Eq. (3.97) is not yet a fully classical equation, since we only took the electron classical limit and left the radiation field quantization. Equation (3.97) is still written in terms of photon occupation number transition rates. In the next section we reverse the order of taking limits. We will start by taking the radiation classical limit of Eq. (3.66) and will then examine the electron classical and quantum-mechanical limits.

TABLE III. The main radiation parameters of various schemes for plane-wave emission.

	ω_0	$\Delta\omega_L$	$\varepsilon=2\pi\dfrac{\delta\omega}{\Delta\omega_L}$
Transversely continuous	$\dfrac{k_w v_z}{1-\bar{\beta}\cos\Theta_q^e}$	$\dfrac{v_z}{1-\bar{\beta}\cos\Theta_q^e}\dfrac{2\pi}{L}$	$\dfrac{\hbar L}{v}\dfrac{\omega_0^2}{\bar{v}^2}\dfrac{1}{m\gamma}\left[\dfrac{1}{\bar{\gamma}^2}+\tan^2\Theta_{\rm rec}\right]$
Transversely discrete intrabranch transition	$\dfrac{k_w v_z}{1-\beta_z\cos\Theta_q}$	$\dfrac{v_z}{1-\beta_z\cos\Theta_q}\dfrac{2\pi}{L}$	$\dfrac{\hbar L\omega_0^2}{m_{\parallel}^* v_z^3}$
Transversely discrete interbranch transition	$\dfrac{\omega_{u,d}}{1-\beta_z\cos\Theta_q}$	$\dfrac{v_z}{1-\beta_z\cos\Theta_q}\dfrac{2\pi}{L}$	$\dfrac{\hbar\omega_{e0,a0}^2\cos^2\Theta_q}{m_{\parallel}^* c^2}\dfrac{L}{v_z}$
CRM	$\dfrac{\Delta n\,\omega_{c0}/\gamma}{1-\beta_z\cos\Theta_q}$	$\dfrac{v_z}{1-\beta_z\cos\Theta_q}\dfrac{2\pi}{L}$	$(\Delta n)^2\dfrac{\sin^2\Theta_q}{1-\beta_z\cos\Theta_q}\dfrac{\hbar\omega_{c0}}{\gamma^3 mc^2}\dfrac{\omega_{c0}L}{v_z}$

IV. SPONTANEOUS AND STIMULATED EMISSION

In the previous section we used a quantum-electrodynamical model, in which we expressed the spontaneous and stimulated emission in terms of photon growth rates. We now take the radiation classical limit and express the spontaneous and stimulated radiation emission in terms of more practical laboratory (radiometric) parameters as radiant intensity and gain. The radiation classical limit can be taken independently of the electron classical limit ($\varepsilon \ll 2\pi$). Contrary to Sec. III.F, we take the radiation classical limit first, and then examine the spontaneous and stimulated emission parameters and the relations between them in both electron classical and electron quantum-mechanical limits. In Sec. IV.C we extend these results to inhomogeneous line broadening. In the longitudinally quantum-mechanical limit we will relate our equations to the well-known Einstein coefficients relations (Einstein, 1917; Yariv, 1975). In the longitudinal classical limit new practical relations extending Madey's relations (Madey, 1971, 1979; Kroll *et al.*, 1981; Krinsky *et al.*, 1982; Kroll, 1982) are derived.

A. Radiant intensity and gain

Although most of the analysis in this paper applies to general radiation modes, we have reduced the discussion in many cases to the simple and most useful example of plane traveling waves in free space. In this case it is most practical to describe the spontaneous radiation emission in terms of radiometric parameters like the spectral radiant intensity. This parameter can be related to the quantum parameter of photon growth rate of mode $\mathbf{q}$ in polarization state σ by the relation

$$\left[\frac{d^2P_\sigma}{d\Omega\,d\omega}\right]_{\rm sp}=\hbar\omega\frac{d^2N_{{\rm mode},\sigma}}{d\Omega\,d\omega}\left[\frac{d\nu_{\mathbf{q},\sigma}}{dt}\right]_{\rm sp}, \tag{4.1}$$

where $(d\nu_{q,\sigma}/dt)_{\rm sp}$ is the spontaneous emission rate of N_e electrons into the mode $\mathbf{q}\sigma$, and $N_e=(I_0/e)(L/v_z)$ is the instantaneous number of electrons inside the interaction region. It was assumed that all the electrons enter with the same initial conditions (homogeneous broadening case). The number of modes per unit solid angle and unit radian frequency for each polarization (helicity) state is given for plane waves quantized in a box of volume V by

$$\frac{d^2N_{{\rm mode},\sigma}}{d\Omega\,d\omega}=\frac{\omega^2V}{8\pi^3c^3}\,. \tag{4.2}$$

The total spectral radiant intensity $(d^2P/d\Omega\,d\omega)_{\rm sp}$ is the summation of Eq. (4.1) over the two polarization states σ. Since the density of states (4.2) is independent of σ, the polarization-states summation is actually carried out only over the radiation-states photon growth rates $(d\nu_{q,\sigma}/dt)_{\rm sp}$.

The power carried by mode $(\mathbf{q},\sigma)$ is related to the number of photons in the same mode by

$$P_{\mathbf{q},\sigma}=\left[\frac{E_{\mathbf{q},\sigma}}{V}A_{{\rm em},\mathbf{q}}\right]c=\frac{\hbar\omega\nu_{\mathbf{q}\sigma}}{V}A_{{\rm em},\mathbf{q}}c\,. \tag{4.3}$$

Here $E_{\mathbf{q},\sigma}/V$ is the stored energy density in the mode, and $A_{{\rm em},\mathbf{q}}$ is the effective cross-section area of the radiation mode perpendicular to its direction of propagation.[17] The stimulated power generated in mode $\mathbf{q},\sigma$ is related to the stimulated photon-state growth rate by

$$(\Delta P_{\mathbf{q}\sigma})_{\rm st}=\hbar\omega\left[\frac{d\nu_{\mathbf{q},\sigma}}{dt}\right]_{\rm st}. \tag{4.4}$$

This can be interpreted as either the energy growth rate in an oscillator cavity or the single path power increment in an amplifier configuration.

[17] In the more general case of arbitrary radiation modes, e.g., in a waveguide or in a dielectric material (Čerenkov radiation), the speed of light c in (4.3) should be replaced by the mode energy velocity v_E. For the Čerenkov radiation example: $v_E=c/(n+\omega\,dn/d\omega)$.

The substitution of Eq. (3.79) in Eqs. (4.1)–(4.4) results in the equations for the spontaneous emission spectral radiant intensity and the stimulated emission gain in the longitudinally (electronic) quantum-mechanical limit:

$$\left[\frac{d^2P_{\mathbf{q},\sigma}}{d\Omega\, d\omega}\right]_{\rm sp}=R_\sigma F(\bar{\theta}_e)\ , \tag{4.5}$$

$$R_\sigma\equiv\frac{1}{\lambda^3}(\hbar V\Gamma_{\rm sp})\ , \tag{4.6}$$

$$G_{\mathbf{q},\sigma}=\frac{(\Delta P_{\mathbf{q},\sigma})_{\rm st}}{P_{\mathbf{q},\sigma}}=M_\sigma[F(\bar{\theta}_e)-F(\bar{\theta}_a)]\ , \tag{4.7}$$

$$M_\sigma\equiv\frac{\Gamma_{\rm sp}V}{A_{{\rm em},q}c}\ . \tag{4.8}$$

In the finite-length homogeneous broadening case, $F(\bar{\theta})\equiv{\rm sinc}^2(\bar{\theta}/2)$. For this case the gain curve (4.7) is drawn in the upper curve of Fig. 2(a). We note that the parameter $\Gamma_{\rm sp}$ would turn out to be inversely proportional to $\hbar$ and to V, and consequently the coefficient R_σ (4.6) is a classical equation, independent of $\hbar$ and V. On the other hand M_σ, the coefficient of the gain function (4.7), is independent of V but dependent on $\hbar$. The equation is explicitly quantum mechanical as long as the emission and absorption lines are well separated [upper curve of Fig. 2(a)], which for the finite-length homogeneous broadening case requires $\varepsilon\gg 2\pi$.

The explicit calculation of $\Gamma_{\rm sp}$ for specific electron radiation schemes is outside the scope of this paper. However, the proportionality to $\Gamma_{\rm sp}$ of both the spectral radiant intensity parameter [Eqs. (4.5) and (4.6)] and the gain parameter [Eqs. (4.7) and (4.8)] allows us to reveal universal relations that hold for all the radiation schemes discussed before. The ratio between the coefficients [Eqs. (4.8) and (4.6)] is

$$\frac{M_\sigma}{R_\sigma}=2\pi\frac{\lambda^2}{A_{\rm em}}\frac{1}{\hbar\omega}=\frac{\lambda^3}{A_{\rm em}\hbar c}\ . \tag{4.9}$$

Consequently, for frequencies within the emission line, assuming the absorption line is well separated from the emission line, the gain is related to the spectral radiant intensity by a universal relation:

$$G(\omega)=\frac{\Delta P_{\mathbf{q}\sigma}(\omega)_{\rm st}}{P_{\mathbf{q}\sigma}(\omega)}=2\pi\frac{\lambda^2}{A_{\rm em}}\frac{1}{\hbar\omega}\left[\frac{d^2P_{\mathbf{q}\sigma}(\omega)}{d\Omega\, d\omega}\right]_{\rm sp}\ . \tag{4.10}$$

Based on this equation, a measurement of the spectral radiant intensity at direction $\mathbf{q}$ through a polarizer, which admits only polarization state σ, makes possible an estimate of the stimulated emission gain $G(\omega)$ of a radiation mode propagating in the same direction with the same polarization. The line-shape functions of the gain and the spontaneous spectral radiant intensity are identical.

In many practical examples the experimentally measured parameter is the spontaneous emission radiant intensity (spectral radiant intensity integrated over the entire frequency linewidth). This parameter is given by $dP_\sigma/d\Omega=\Delta\omega_h d^2P_\sigma(\omega_e)/d\Omega\, d\omega$, where $\Delta\omega_h$ is the homogeneous broadening linewidth and ω_e the emission line peak frequency. The relation (4.10) can be thus written in the alternative useful form

$$G(\omega)=\frac{\lambda^3}{A_{\rm em}\hbar c}\frac{1}{\Delta\omega_h}\left[\frac{dP_{\mathbf{q}\sigma}}{d\Omega}\right]\ . \tag{4.11}$$

For finite-length homogeneous broadening, the linewidth parameter is $\Delta\omega_h=\Delta\omega_L$, where the equations for $\Delta\omega_L$ are listed in the third column of Table III for different interaction schemes. In the exponential decay Lorentzian line-shape limit $-\kappa L\gg 1$ (3.65), one uses $\Delta\omega_h=\kappa L\Delta\omega_L$. For all the cases of emission from a periodic structure, the finite-length linewidth can be written as $\Delta\omega_L=\omega_0/N_w$ [see Eq. (2.32)], and the equation for the gain curve in terms of the total spontaneous emission radiant intensity can be written in a very explicit way:

$$G(\omega)=\frac{\lambda^4N_w}{2\pi A_{\rm em}\hbar c^2}\left[\frac{dP_{\mathbf{q}\sigma}}{d\Omega}\right]_{\rm sp}{\rm sinc}^2(\bar{\theta}_e)\ . \tag{4.12}$$

The general relations between the quantum-mechanical limit gain parameter and spontaneous emission parameters are summarized in the second row of Table IV. The

TABLE IV. The general relations between the gain and spontaneous emission radiometric parameters for a given line-shape function.

	$\dfrac{G_\sigma(\omega)}{[d^2P_\sigma(\omega_0)/d\Omega\, d\omega]_{\rm sp}}$	$\dfrac{G_\sigma(\omega)}{[dP_\sigma(\omega_0)/d\Omega]_{\rm sp}}$
Quantum $2\pi\dfrac{\delta\omega}{\Delta\omega}\gg 1$	$\dfrac{\lambda^3}{A_{\rm em}\hbar c}$	$\dfrac{\lambda^3}{A_{\rm em}\hbar c}\dfrac{1}{\Delta\omega}$
Classical $2\pi\dfrac{\delta\omega}{\Delta\omega}\ll 1$	$\dfrac{\lambda^3}{A_{\rm em}\hbar c}2\pi\dfrac{\delta\omega}{\Delta\omega}\dfrac{g\left[2\pi\dfrac{\omega-\omega_0}{\Delta\omega}\right]}{g(0)}$	$\dfrac{\lambda^3}{A_{\rm em}\hbar c}2\pi\dfrac{\delta\omega}{(\Delta\omega)^2}\dfrac{g'\left[2\pi\dfrac{\omega-\omega_0}{\Delta\omega}\right]}{g(0)}$

same relations, specified for the particular case of periodic structure devices with finite-length homogeneous broadening, are summarized in the second row of Table V. These equations and Eqs. (4.10) and (4.12) are written in a form that is useful for straightforward comparison of measurable spontaneous and stimulated emission parameters.

An alternative and more physically suggestive representation of the relation between spontaneous and stimulated emission is revealed when one expresses the spectral radiant intensity in terms of the spontaneous emission power $[\Delta P_{q\sigma}(\omega)]_{sp}$ measured in an infinitesimal solid angle $\Delta\Omega$ and an infinitesimal frequency band $\Delta\omega=2\pi\Delta f$ within the frequency bandwidth of the *emission* line. Equation (4.10) then reads

$$\frac{(\Delta P_{q\sigma})_{st}}{P_{q\sigma}}=\frac{(\Delta P_{q\sigma})_{sp}}{P_{QN}}\ , \tag{4.13}$$

where

$$P_{QN}\equiv\hbar\omega\Delta f\frac{A_{em}\Delta\Omega}{\lambda^2}\ . \tag{4.14}$$

Since the phase-space areas ratio $A_{en}\Delta\Omega/\lambda^2$ is the number of transverse radiation modes intercepted in the spontaneous emission measurement, and $\hbar\omega\Delta f$ is the fundamental quantum noise power (zero temperature quantum vibration) in a single mode, P_{QN} can be interpreted as the quantum noise "input" power that "generates" the spontaneous emission. The gain of a radiation scheme can thus always be calculated from the ratio between the measured spontaneous emission power $(\Delta P_{q\sigma})_{sp}$ and the quantum noise "input power" P_{QN}. In the particular case in which $(\Delta P_{q\sigma})_{sp}$ is the spontaneous emission power measured into a single radiation mode, the relation $A_{em}\Delta\Omega=\lambda^2$ holds. Equation (4.13) then holds with $P_{QN}=\hbar\omega\Delta f$. In fact, such a relation would be expected to be valid not only with free-space plane-wave modes, as presently assumed, but with any kind of radiation mode.

An interesting extension of the discussion up until now is the inclusion of radiation photon-states occupation due to the finite temperature T in the cavity. The mode occupation number is given by the Bose-Einstein statistics (Reif, 1965): $[\exp(\hbar\omega/kT)-1]^{-1}$, where T is the background temperature (the mirrors temperature in the case of a resonator). Following the work of Gover (1984), we extend our previous analysis by simply substituting in (3.79) $\nu_{q\sigma}=\nu_s+[\exp(\hbar\omega/kT)-1]^{-1}$, where ν_s is the number of photons in the traveling signal (input) wave (or in the case of an oscillator, the number of photons in the circulating coherent power), and the second term is the "thermal noise" contribution. Equation (3.79) is then modified to

$$\frac{d\nu_{q\sigma}}{dt}=\Gamma_{sp}\{[\nu_s+(e^{\hbar\omega/kT}-1)^{-1}+1]F(\bar{\theta}_e) -[\nu_s+(e^{\hbar\omega/kT}-1)^{-1}]F(\bar{\theta}_a)\}\ . \tag{4.15}$$

With this extension the spectral radiant intensity of spontaneous emission [see Eq. (4.5)] may be replaced by an

TABLE V. The relations between the maximum gain and maximum spontaneous emission radiometric parameters for some particular schemes in the finite-length homogeneous broadening regime.

	$\dfrac{G_\sigma(\omega_m)}{[d^2P_\sigma(\omega_0)/d\Omega\,d\omega]_{sp}}$	$\dfrac{G_\sigma(\omega_m)}{[dP_\sigma(\omega_0)/d\Omega]_{sp}}$
Quantum ($\varepsilon\gg1$)		
A periodic structure	$\dfrac{\lambda^3}{A_{em}\hbar c}$	$\dfrac{\lambda^4N_w}{2\pi A_{em}\hbar c^2}$
Negligible recoil ($\varepsilon\ll1$)		
Transversely continuous	$0.27(2\pi)^2\dfrac{\lambda L}{A_{em}\bar{\beta}^3\gamma mc^2}\times\left[\dfrac{1}{\bar{\gamma}^2}+\tan^2\Theta_{rec}(\omega_0)\right]$	$0.27(2\pi)\dfrac{\lambda^2LN_w}{A_{em}\bar{\beta}^3\gamma mc^3}\times\left[\dfrac{1}{\bar{\gamma}^2}+\tan^2\Theta_{rec}(\omega_0)\right]$
Transversely discrete intrabranch	$0.27(2\pi)^2\dfrac{\lambda L}{A_{em}\beta_z^3m_\parallel^*c^2}$	$0.27(2\pi)\dfrac{\lambda^2LN_w}{A_{em}\beta_z^3m_\parallel^*c^3}$
CRM	$-0.27(2\pi)^2\dfrac{(\Delta n)^2\lambda L}{A_{em}\beta_z\gamma mc^2}\times(1-\beta_z\cos\Theta_q)^{-1}\sin^2\Theta_q$	$-0.27\dfrac{(\Delta n)^2\lambda^2L^2\omega_{c0}}{A_{em}\beta_z^2\gamma^2mc^4}\times(1-\beta_z\cos\Theta_q)^{-1}\sin^2\Theta_q$

equation for the total noise emission spectral radiant intensity:

$$\left[\frac{d^2P_{q\sigma}}{d\Omega\, d\omega}\right]_{\text{noise}} = R_\sigma[1+(e^{\hbar\omega/kT}-1)^{-1}]F(\bar{\theta}_e)\ . \tag{4.16}$$

The differential power relations [Eq. (4.13)], within the gain and spontaneous emission bandwidth, may also then be extended to

$$\frac{(\Delta P_{q\sigma})_{\text{st}}}{P_{q\sigma}} = \frac{(\Delta P_{q\sigma})_{\text{sp}}}{P_{\text{QN}}} = \frac{\Delta P_{\text{noise}}}{P_{\text{noise}}} = \frac{\Gamma_{\text{sp}}V}{A_{\text{em}}c}F(\bar{\theta}_e)\ , \tag{4.17}$$

where we define the effective input noise power as

$$P_{\text{noise}} \equiv \hbar\omega\Delta f[1+(e^{\hbar\omega/kT}-1)^{-1}]A_{\text{em}}\frac{\Delta\Omega}{\lambda^2}\ , \tag{4.18}$$

which is the finite-temperature input noise power including both the quantum zero vibration contribution (4.14) and the thermal noise contribution. We defined ΔP_{noise} as the differential noise emission power measured at finite temperature with no deliberate signal power in ($P_{q\sigma}=0$). This noise power is larger than the zero temperature spontaneous emission $(\Delta P)_{\text{sp}}$ by a factor $1+[\exp(\hbar\omega/kT)-1]^{-1}$. We note, though, that only for frequencies $\omega < kT/\hbar$ ($\lambda > 50$ μm at room temperature) does the Bose-Einstein factor become larger than unity. For shorter wavelengths the finite-temperature extension is usually (and rightfully) neglected.

B. The longitudinal classical limit in the homogeneous broadening regime

The electron quantum-mechanical gain regime that was discussed in the previous section is interesting because of its clear physical interpretation. The FEL (in the wide sense the stimulated emission device of any of the quasifree-electron radiation schemes discussed before) behaves in this regime according to the general characteristics of any two-level quantum system, and most of the equations derived above are not unique to FEL's. However, the case of practical interest in almost all FEL devices is the electron classical (or negligible recoil) limit. In this limit the emission and absorption lines are no longer isolated [see lower curve of Fig. 2(a)], and the special features of the particular quasifree-electron radiation schemes appear. Consequently, the electron radiation source no longer behaves as a simple two-level quantum system. The previous results for the relations between spontaneous and stimulated emission should then be modified correspondingly.

Taking the negligible (recoil) classical limit $\varepsilon \ll 2\pi$ of the photon emission rate (4.15) with $\nu_s=0$ [or alternatively (3.97) with $\nu_{q\sigma}=(e^{\hbar\omega/kT}-1)^{-1}$], and substituting in Eqs. (4.1) and (4.2), we obtain a general equation for the total noise emission spectral radiant intensity at finite temperature

$$\left[\frac{d^2P_{q\sigma}}{d\Omega\, d\omega}\right]_{\text{noise}} = R_\sigma F(\bar{\theta}) + \varepsilon R_\sigma[\tfrac{1}{2}+(e^{\hbar\omega/kT}-1)^{-1}]\frac{d}{d\bar{\theta}}F(\bar{\theta})\ , \tag{4.19}$$

where $\bar{\theta}$ is given for a general radiative emission direction by (3.81) and R_σ by (4.6). For $\hbar\omega \gg kT$ ($\lambda \ll 50$ μm at room temperature), the Bose-Einstein statistical term is negligible, and since $\varepsilon \ll 2\pi$ the entire second term on the right-hand side of Eq. (4.19) is negligible. It is interesting to note that in the opposite limit $\hbar\omega \ll kT$, the second term in (4.19) turns out to be completely classical. The coefficient of the detuning function $dF(\bar{\theta})/d\bar{\theta}$ is then $R_\sigma(\varepsilon/\hbar)(kT/\omega)$, which is $\hbar$ independent. Nevertheless, for most practical cases[18] this coefficient is still significantly smaller than R_σ. Consequently, in all practical cases of high-energy electron radiators at any frequency regime, it is usually safe to neglect the second term of (4.19) altogether and to assume that the classical noise power emission at finite temperature is equal to the zero-temperature noise, namely, the spontaneous emission:

$$\left[\frac{dP_{q\sigma}}{d\Omega\, d\omega}\right]_{\text{noise}} \approx \left[\frac{d^2P_{q\sigma}}{d\Omega\, d\omega}\right]_{\text{sp}} = R_\sigma F(\bar{\theta})\ . \tag{4.20}$$

The classical limit equation of the stimulated emission gain is derived directly from (4.7) using (3.71) and (3.72),

$$G = \bar{Q}\frac{d}{d\bar{\theta}}F(\bar{\theta})\ , \tag{4.21}$$

where

$$\bar{Q} = \frac{\Gamma_{\text{sp}}V}{A_{\text{em}}c}\varepsilon\ . \tag{4.22}$$

We note that Γ_{sp} is dependent on $\hbar$ and V in an inverse proportional way while ε is proportional to $\hbar$, and, consequently, $\bar{Q}$ is an entirely classical equation. In the finite-length homogeneous broadening limit $F(\bar{\theta})=\text{sinc}^2(\bar{\theta}/2)$, and then (4.21) is the well-known FEL gain formula in the low gain cold tenuous beam regime (Deacon *et al.*, 1977; Gover and Sprangle, 1981). It is drawn as the lower curve in Fig. 2(a). The corresponding gain detuning function for the case of exponential decay homogene-

[18]Some solid state carriers radiation schemes may be an exception. Using the forward emission equation for ε (3.74), the thermal noise contribution to the spectral radiant intensity [second term of (4.19)] can be written as $R_\sigma(\omega L/v_z)(kT/m_\parallel^* v_z^2)F'(\bar{\theta})$. With low-energy electrons, this parameter may conceivably be larger than the spontaneous emission contribution $R_\sigma F(\bar{\theta})$.

ous broadening ($\kappa L \gg 1$) is drawn in Fig. 2(b).

In analogy to Eqs. (4.10) and (4.11) the classical relation between the net stimulated emission gain (4.21) and the spontaneous emission spectral radiant intensity or total radiant intensity can be expressed in the proportionality forms,

$$G(\omega)=\frac{\bar{Q}_\sigma}{R_\sigma}\left[\frac{\partial^2 P_{q\sigma}(\omega_0)}{\partial\Omega\,\partial\omega}\right]_{sp}\frac{1}{F(\bar{\theta})}\frac{d}{d\bar{\theta}}F(\bar{\theta})$$
$$=\frac{\bar{Q}_\sigma}{R_\sigma}\frac{1}{\Delta\omega_h}\left[\frac{dP_{q\sigma}}{d\Omega}\right]_{sp}\frac{1}{F(\bar{\theta})}\frac{d}{d\bar{\theta}}F(\bar{\theta})\ , \quad (4.23)$$

where

$$\frac{\bar{Q}_\sigma}{R_\sigma}=\frac{\lambda^3\varepsilon}{A_{em}\hbar c} \quad (4.24)$$

is an entirely classical coefficient.

Both of these general proportionality relations are summarized in the third row in Table IV. In Table IV the proportionality relations are written in terms of general linewidth functions g. In the case of homogeneous broadening, g can be expressed in terms of the line-shape function F by the simple substitution $F(\bar{\theta})=g[2\pi(\omega-\omega_0)/\Delta\omega]$ and $\Delta\omega=\Delta\omega_h$. Note that Table I relates to the ratio between the gain at arbitrary frequency ω and the spontaneous emission parameters at the *maximum* point of the spontaneous line-shape function $\omega=\omega_0$ ($\bar{\theta}=0$), which is different now from the maximum point of the net stimulated emission line-shape function $F'(\bar{\theta})$ We also note that the normalization of the homogeneous line-shape functions permits the substitution $g(0)=F(0)=1$ in Table IV.

Because of the overlap of the stimulated emission and absorption line-shape functions, the elegant universal form of the quantum limit relations (second row in Tables IV and V) is lost, and the radiation parameters ratios are unavoidably dependent on the line-shape functions, and through them on the parameters of the specific radiation schemes. To obtain explicit scaling law dependencies on the operating parameters (wavelength, beam energy, etc.), the parameters of the specific radiation schemes should be used. Table V summarizes these scaling laws for the particular practical case of finite-length homogeneous line broadening for which $F(\bar{\theta})$ is given by Eq. (3.67). The linewidth parameters $\Delta\omega_L$, used to construct this table, were listed before in Table III for the general schemes of transversely continuous and transversely discrete intrabranch transitions and the special scheme of the cyclotron resonance maser. The proportionality coefficients of these schemes are given in rows 4–6 in Table V for arbitrary emission direction. The gain parameter G is assumed to be measured at the maximum gain frequency $\omega=\omega_m$, which corresponds to $\bar{\theta}=-2.6$ and $F'(\bar{\theta})=0.27$. The spontaneous emission parameters are assumed to be measured (as in Table IV) at $\omega=\omega_0$ ($\bar{\theta}=0$) for which $F(0)=1$.

One should note that the classical limit relation (4.23) and the explicit relations of Table V, rows 4–6, predict quite different parameter scaling laws (e.g., dependence on λ, L) than the corresponding quantum relations (4.10) and (4.11), which are universal relations specifically applicable only to two quantum level systems. This is an important observation, since these scaling laws are often used in estimating the performance of various radiation effects in new operation regimes (especially in attempts to predict feasibility of new x-ray laser schemes).

Similarly to Eqs. (4.13) and (4.17), an alternative representation of the relation between spontaneous and stimulated emission powers is given in the classical limit by the differential relations

$$\frac{(\Delta P_{q\sigma})_{st}}{P_{q\sigma}}=\frac{[\Delta P_{q\sigma}(\omega_0)]_{sp}}{P_{QN}}\varepsilon\frac{d}{d\bar{\theta}}F(\bar{\theta})=\frac{\Gamma_{sp}V}{A_{em}c}\varepsilon\frac{d}{d\bar{\theta}}F(\bar{\theta})\ . \quad (4.25)$$

There is no need for an equality analogous to the third part of Eq. (4.17), since in the classical limit $\Delta P_{noise}\approx(\Delta P)_{sp}$. Considering that the classical detuning curve $F'(\bar{\theta})$ is of the order of one (near its maximum), the comparison of (4.25) to (4.17) leads to the general conclusion that the ratio $(\Delta P_{q\sigma})_{st}/(\Delta P_{q\sigma})_{sp}$ is reduced by roughly a factor of $\varepsilon \ll 2\pi$ in the classical-limit case as compared with the quantum-limit case. This reduction factor can be traced to the overlap between the emission and absorption lines in the classical limit, which reduces the net stimulated emission.

C. Inhomogeneous broadening and Einstein relations

While in the previous section we assumed that all electrons enter with the same initial conditions, in general different electrons may experience different perturbation Hamiltonian because of differences in their interaction parameters. These differences may stem from different reasons, such as a spread in the longitudinal and transverse canonical momenta, different initial transverse coordinates, or different interaction lengths. Discussion of the inhomogeneous and homogeneous broadening limits and the transition between them was already given by Madey (1971) in his first paper on FEL. In the present discussion we generalize our homogeneous broadening relations to the inhomogeneous broadening regime, preserving their general validity for the extensive class of quasifree electron radiation schemes, which was detailed in Sec. I. We also bring out the connection of our formulation to the well-known Einstein coefficients relation between spontaneous and stimulated emission.

In the case of electrons that enter the interaction region with different initial conditions, the previously derived equations for the photon transition rates of an homogeneous electron beam [Eqs. (3.66) and (4.15)] should be averaged over all the electrons in the interaction region:

$$\frac{d\nu_{q\sigma}}{dt}=\sum_{j=1}^{N_e}\left[\frac{d\nu^e_{q\sigma}}{dt}\right]_{\text{homog},j}=\int dk_{zi}d^2k_{\perp i}d^2r_{\perp 0i}dL\,f(k_{zi})f(\mathbf{k}_{\perp i})f(\mathbf{r}_{\perp 0i})f(L)\left[\frac{d\nu_{q\sigma}}{dt}\right]_{\text{homog}}, \tag{4.26}$$

where $(d\nu^e_{q\sigma}/dt)_j$ is the photon emission rate of a single electron j, and $(d\nu_{q\sigma}/dt)_{\text{homog}}$ is the photon emission rate of N_e identical electrons. Normalized distribution functions of the electrons are $f(k_{zi})$, $f(\mathbf{k}_{\perp i})$, $f(\mathbf{r}_{\perp 0i})$, and $f(L)$ in axial and transverse wave-number spaces, transverse initial coordinates, and interaction lengths, respectively. Here the inhomogeneous distribution functions were normalized to unity, since the homogeneous transition rate was defined to correspond to the total number of electrons N_e.

The axial wave-number (momentum) spread is usually due to the electron beam total energy spread or due to angular spread (finite emittance). This axial momentum spread is usually the most significant inhomogeneous broadening mechanism in FEL's and the other free-electron radiation schemes discussed in this paper, since in all of these schemes the axial momentum conservation (or synchronism) condition determines the homogeneous broadening linewidth. The transverse wave-number (canonical momentum) spread and transverse initial-coordinates spread are a result of the finite emittance of the beam. If the perturbation Hamiltonian is independent of transverse coordinates, or depends on them weakly (as is the case, for example with the conventional magnetic bremsstrahlung FEL at on-axis emission conditions), then the transverse coordinate and momentum spreads do not introduce significant inhomogeneous line broadening [through the function $f(k_{\perp i})$]. However, finite emittance of the beam will introduce in many practical cases inhomogeneous broadening indirectly [through the function of $f(k_{zi})$] because it will result in an axial velocity spread.

A spread in interaction lengths may be a consequence of strong electron collisions, which scatter the electrons out of the interaction region or change their momentum to such a degree that they cannot continue to interact with the radiation field. An example for this spread is the collision broadening of channeling radiation due to latter imperfection scattering [note, though, that soft collisions, which only gradually couple the electron wave function into other transverse states, are responsible for *homogeneous* broadening, which was described by (3.63) and (3.64)]. Another example for interaction lengths spread is in Smith-Purcell FEL's (Gover *et al.*, 1984) and dielectric waveguide Čerenkov FEL's (Felch *et al.*, 1981) where the interaction lengths of the individual electrons are the lengths traversed by them, before impinging on the gratings or the slow-wave structure surface, or before drifting away from the surface outside of the interaction region. In this last example the broadening effects due to the spreads in the transverse momentum, transverse initial coordinates, and interaction lengths are all coupled together. The entrance angle and initial coordinates of the electron also determine its interaction length.

In many cases the integrations in (4.26) reduce to convolution integrals of the distribution functions with the homogeneous line-shape functions $F(\bar{\theta})$ of (3.66) or (4.15). If the homogeneous line-shape functions are much wider than the inhomogeneous broadening (electron distribution) functions, and Γ_{sp} can be considered approximately constant, then the inhomogeneous broadening functions behave as delta functions and the homogeneous broadening emission rate equations (3.66) or (4.15) are restored. In other cases the widest inhomogeneous broadening function dominates the convolution in (4.26) and determines the total line-shape function.

For simplicity we focus in this paper only on the longitudinal momentum spread inhomogeneous broadening, neglecting all the other inhomogeneous broadening functions in (4.26). In the limit where the width of the function $f(k_{zi})$ is much larger than the widths of $F(\bar{\theta})$ in the k_{zi} dimension, (4.15) substituted in (4.26) results in

$$\frac{d\nu_{q\sigma}}{dt}=\Gamma_{sp}\Delta k_{zh}\{[\nu_s+(e^{\hbar\omega/kT}-1)^{-1}+1]f(k_{zu})-[\nu_s+(e^{\hbar\omega/kT}-1)^{-1}]f(k_{zd})\}, \tag{4.27}$$

where

$$\Delta k_{zh}\equiv\int_{-\infty}^{\infty}F(\bar{\theta}_e)dk_{zi}=m\gamma\bar{\gamma}^2\frac{\bar{v}^2}{\hbar\omega}\Delta\theta_h . \tag{4.28}$$

Δk_{zh} is the width of the initial and final electron wave-numbers regions around the central upper state wave number k_{zu} and the central lower state wave number k_{zd}, between which regions radiative transitions are allowed due to the homogeneous broadening [see Fig. 10(a)]. The width of this region Δk_{zh} is determined by the homogeneous broadening allowed wave number mismatch $\Delta\theta_h=\Delta\bar{\theta}/L$ [where $\Delta\bar{\theta}_h$ is the width of the homogeneous line-shape function $F(\bar{\theta})$ in terms of the detuning parameter $\bar{\theta}$]. The value of Δk_{zh} is derived in Appendix G. For the finite-length homogeneous broadening, Eq. (4.28) becomes explicit by substituting in it $\Delta\theta_h=2\pi/L$. For the Lorentzian (decay length limited) homogeneous broadening, $\Delta\theta_h=2\pi\kappa$.

We note that k_{zu} and k_{zd} have in (4.27) the original meaning of k_{zi} and k_{ze} in (2.14), which is different from their meaning in the detuning parameter Eq. (3.69). In the latter equations, $k_{ze}(k_{zi},\omega)$ was the exact solution of the energy conservation condition for given k_{zi},ω. The momentum conservation condition there did not have to be satisfied exactly, but only up to a wave number mismatch θ_e given by (3.69). On the other hand, in the present inhomogeneous broadening case, integration over k_{zi} was already carried out and k_{zu},k_{zd} are selected by the narrow homogeneous broadening linewidths at values corresponding to $\theta_a=\theta_e=0$. In other words, k_{zu},k_{zd} are

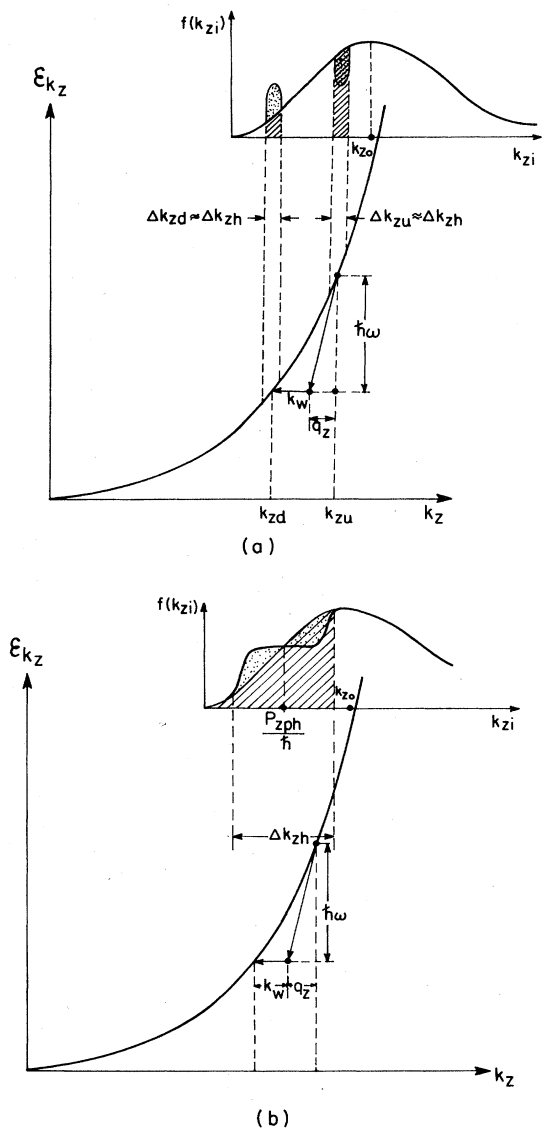

FIG. 10. Interacting electron regions and saturation mechanisms in the inhomogeneous broadening regime.

the "exact" solutions of the energy and momentum conservation conditions, which in the intrabranch transitions case are given by Eqs. (2.13) and (2.14), with $\omega_e=\omega$,

$$\mathcal{E}_{k_{zu}}-\mathcal{E}_{k_{zd}}=\hbar\omega,\quad k_{zu}-k_{zd}=q_z(\omega)+k_w\ . \tag{4.29}$$

In the general case of continuous transverse states, they are defined by Eqs. (2.76) and (2.77), with $\omega_e=\omega$,

$$\mathcal{E}_{\mathbf{k}_u}-\mathcal{E}_{\mathbf{k}_d}=\hbar\omega,\quad \mathbf{k}_u-\mathbf{k}_d=\mathbf{q}+\mathbf{k}_w\ . \tag{4.30}$$

For a given ω, the wave number parameters k_{zu},k_{zd} are solutions of a well-defined set of equations [(4.29) or (4.30)]. Consequently $k_{zu}(\omega),k_{zd}(\omega)$ are functions of ω implicitly defined by these equations, and therefore Eq. (4.27) describes the emission and absorption frequency-dependent line functions.

Equation (4.27) can be compared to the transition rate probability in conventional atomic lasers. The spontaneous emission rate parameter $\Gamma_{\rm sp}$ is proportional to N_e, the number of electrons in the interaction region. Taking in (4.27) $T=O$ and rearranging terms, we can split the photon emission rate into two main terms: (a) a term proportional to $N_e f(k_{zu})\Delta k_{zh}$—the number of electrons in the upper quantum levels (the spontaneous emission term); plus (b) a term proportional to $v_s[N_e f(k_{zu})-N_e f(k_{zd})]\Delta k_{zh}$—the number of photons times the population inversion between the upper and lower levels (the stimulated emission-absorption term). The electrons that participate in the transitions are represented by the shaded sections in Fig. 10(a). The situation is completely analogous to the transition rate probability in an atomic two-quantum-level system. The only difference is that in the present case the upper and lower energy levels are dependent on the radiation frequency and emission direction $\hat{e}_{\mathbf{q}}$, or in general determined by the mode dispersion relation, while in atomic lasers these levels are properties of the material only. In Appendix G we discuss in more detail the ramifications of our observations in identifying the classes of electrons that participate in the radiative transitions in the inhomogeneous regime. The width in initial wave numbers of these classes of interacting electrons Δk_{zh} is calculated there. However, it only appears in the coefficient of the transition rate, Eq. (4.27), and therefore does not affect at all the ratio between spontaneous and stimulated emission. The more detailed examination of the inhomogeneous emission process, which is presented in Appendix G, enables one to make some illuminating observations on the relations between the present free-electron radiation formulation and the conventional atomic laser approach. It also helps to predict the saturation process of quasifree-electron lasers in the inhomogeneous broadening regime. These are the processes of "hole burning" and "pile heaping" in the quantum limit, and of "plateau formation" in the classical limit [see Figs. 10(a) and 10(b), respectively; see also Gover, 1980b].

Another interesting observation can be made by inspecting Eq. (4.27) and comparing the coefficients of the spontaneous emission, stimulated emission, and stimulated absorption to the corresponding equations for atomic radiators and lasers (Yariv, 1975). For atomic radiators, the relation between these coefficients was found by Einstein in a classical paper published in 1917 (Einstein, 1917). The correspondence between the free-electron radiation coefficients and Einstein's A,B coefficients must be done with some care, taking into account the differences, which still exist, between atomic and free-electron radiators, even in the quantum two-level limit. This correspondence is studied in some detail in Appendix H.

Because of the anisotropy of the radiation pattern of free-electron radiators, which emit at angle-dependent frequencies, the stimulated and spontaneous transition

rates must be defined in a differential way [Eqs. (H8),(H9),(H13)], defining emission rates into prescribed frequency segment $\Delta\omega$ and solid angle segment $\Delta\Omega$, which are determined by the emission line-shape function at a specified emission direction. With this differential definition, explicit equations for the Einstein A,B coefficients can be derived straightforwardly for a free-electron radiator (Appendix H), and the Einstein coefficients relations result in, as a direct consequence of the basic QED principles on which Eqs. (4.15) and (4.27) are based,

$$B_{21}=B_{12}=\frac{\Gamma_{\rm sp}^0}{\hbar\omega}\frac{\Delta\Omega}{4\pi}\Delta\omega\ , \tag{4.31}$$

$$A_{21}=\Gamma_{\rm sp}^0\rho(\omega)\frac{\Delta\Omega}{4\pi}\Delta\omega=\hbar\omega\rho(\omega)B_{21}\ , \tag{4.32}$$

where $\Gamma_{\rm sp}^0\equiv\Gamma_{\rm sp}/N_e$ is the spontaneous emission rate per electron into a single radiation mode, and $\rho(\omega)=\omega^2V/(\pi^2c^3)$ is the total mode density in both polarization states per unit frequency.

D. Relations between spontaneous and stimulated emission in the inhomogeneous broadening regime

We now proceed with the study of the relations between spontaneous and stimulated emission in the inhomogeneous broadening regime. For the purpose of simplifying the final equations, it is desirable to present the electron distribution function in terms of a normalized function (Gover and Sprangle, 1981),

$$f(k_{zi})=\frac{1}{k_{\rm th}}g\left[\frac{k_{zi}-k_{z0}}{k_{\rm th}}\right]\ , \tag{4.33}$$

where $\hbar k_{z0}=p_{z0}$ is the average longitudinal momentum of the electron beam and $\hbar k_{\rm th}=p_{\rm th}$ is the beam longitudinal momentum spread. Because of the unity normalization of $f(k_{zi})$, $g(x)$ also is normalized according to $\int_{-\infty}^{\infty}g(x)dx=1$. For the common model of a shifted Maxwellian distribution, the normalized function $g(x)$ is

$$g(x)=\frac{1}{\sqrt{\pi}}e^{-x^2}\ . \tag{4.34}$$

We now represent the electron distribution function in terms of the detuning parameter $\bar\theta(\omega,k_{zi})$ (3.73). Defining

$$\bar\theta_0\equiv\bar\theta(\omega,k_{z0}) \tag{4.35}$$

(the detuning parameter corresponding to the average momentum of the beam), we may substitute in (4.33) a linear variable transformation:

$$k_{zi}-k_{z0}=\left[\frac{\partial\bar\theta}{\partial k_{zi}}\right]^{-1}(\bar\theta-\bar\theta_0)\ , \tag{4.36}$$

where we assume that the coefficient $(\partial\bar\theta/\partial k_{zi})_\omega$ is nearly constant within the inhomogeneous broadening linewidth. This coefficient was calculated in Appendix G for both intrabranch transition (longitudinal recoil) and general schemes of transverse continuous states. It is given for both cases by

$$\left.\frac{\partial\bar\theta}{\partial k_{zi}}\right|_{v_{k_{zi}}=\bar v_{\rm ph}}=\frac{\hbar\omega}{\gamma_{\rm ph}\bar\gamma_{\rm ph}^2\bar v_{\rm ph}^2m}L\ , \tag{4.37}$$

leading to an equation for the inhomogeneous spread in the detuning parameter $\bar\theta$,

$$\bar\theta_{\rm th}=\frac{\partial\bar\theta}{\partial k_{zi}}k_{\rm th}=\frac{\omega L}{\gamma_{\rm ph}\bar\gamma_{\rm ph}^2\bar v_{\rm ph}^2m}p_{\rm th}\ . \tag{4.38}$$

The synchronism velocity $\bar v_{\rm ph}$ in Eqs. (4.37) and (4.38) is defined by $\bar v_{\rm ph}=v_{z_{\rm ph}}=\omega/(q_z+k_w)$ in the zero transverse recoil case (k_w is the periodicity in the periodic structure axis direction), and by $\bar v_{\rm ph}=v_{z_{\rm ph}}^e=\omega/(q_z^e+k_w^e)$ in the general recoil case (q_z^e and k_w^e are the projections of $\mathbf{q}$ and $\mathbf{k}_w$ on the electron propagation direction). In both cases $\bar\gamma_{\rm ph}\equiv(1-\bar\beta_{\rm ph}^2)^{-1/2}$, and $\gamma_{\rm ph}=(1-\beta^2)^{-1/2}$ is the relativistic mass factor, which is defined with β being the total mean-square velocity of the electron (including wiggling motion), when the electron axial velocity (v_z or $\bar v$) is assumed synchronous with $\bar v_{\rm ph}$. In most practical cases one operates with an electron distribution function of relatively narrow spread and near synchronism with the e-beam average velocity $\bar v_{\rm ph}\approx v_{z0}$. Consequently, for most cases one may substitute in Eqs. (4.37) and (4.38) $\bar\beta_{\rm ph}=\beta_{z0}\bar\gamma_{\rm ph}=\gamma_{z0}$ and $\gamma_{\rm ph}=\gamma_0$.

We may express the longitudinal momentum spread homogeneous broadening integral (4.26) as a convolution between the homogeneous and inhomogeneous line-shape functions in the detuning parameter coordinate:

$$\frac{d\nu_{q\sigma}}{dt}=\frac{\Gamma_{\rm sp}}{\bar\theta_{\rm th}}\int d\bar\theta[(\nu_{q\sigma}+1)F(\bar\theta_e)-\nu_{q\sigma}F(\bar\theta_a)]g\left[\frac{\bar\theta_0-\bar\theta}{\bar\theta_{\rm th}}\right]\ . \tag{4.39}$$

A FEL, or any free-electron radiation scheme, operates in the homogeneous or inhomogeneous broadening regime, depending on which of the line-broadening functions is wider. If $\Delta\bar\theta_h$ is the detuning parameters width of the homogeneous broadening line-shape function (for finite-length homogeneous broadening $\Delta\bar\theta_h=2\pi$, and for decay-length-limited homogeneous broadening $\Delta\bar\theta_h=2\pi\kappa L$), then the condition for inhomogeneous broadening is

$$\bar\theta_{\rm th}\gg\bar\Delta\bar\theta_h\ , \tag{4.40}$$

for which case (4.39) reduces to

$$\frac{d\nu_{q\sigma}}{dt}=\frac{\Delta\bar\theta_h}{\bar\theta_{\rm th}}\Gamma_{\rm sp}\left[(\nu_{q\sigma}+1)g\left[\frac{\bar\theta_{u0}}{\bar\theta_{\rm th}}\right]-\nu_{q\sigma}g\left[\frac{\bar\theta_{d0}}{\bar\theta_{\rm th}}\right]\right]\ , \tag{4.41}$$

where [using (3.71) and (3.72)]

$$\bar{\theta}_{u0}\equiv\bar{\theta}_e(\omega,k_{z0})=\bar{\theta}_0+\frac{\varepsilon}{2}\ ,$$

$$\bar{\theta}_{d0}\equiv\bar{\theta}_a(\omega,k_{z0})=\bar{\theta}_0-\frac{\varepsilon}{2}\ .$$

Equation (4.41) is the photon emission rate (4.27) written in a normalized form. Together with Eqs. (3.71)–(3.74) and (4.35) in the longitudinal recoil case, and (3.88) in the general case of transverse continuous states, it gives the full explicit dependence of the spontaneous and stimulated emission rates on the operating parameters ($\omega,\gamma,$v, etc.). This is valid for the inhomogeneous broadening regime of general quasifree radiation schemes. The normalized presentation reveals the fact that both the spontaneous and stimulated emission rates are reduced in the inhomogeneous broadening regime relative to the corresponding emissions in the homogeneous broadening regime by a factor roughly equal to the ratio between the homogeneous and inhomogeneous linewidths (for a finite-length homogeneously broadened line, further broadened by inhomogeneous broadening, this factor is $\Delta\bar{\theta}/\bar{\theta}_{\rm th}=2\pi/\bar{\theta}_{\rm th}$).

An alternative presentation of the general linewidth, Eq. (4.39), could be made by substituting Eqs. (3.89) and (3.90) for the detuning parameters $\bar{\theta}_e,\bar{\theta}_a$ in the homogeneous broadening line function, thus expressing explicitly the frequency (ω) tuning dependence [but the energy (γ) tuning dependence is then implicit in the center emission and absorption frequencies ω_e,ω_a]. Then instead of Eq. (4.36), one transforms the inhomogeneous variable k_{zi}, expressing it in terms of the line-center frequency variables ω_e, ω_a, or ω_0 [$\omega_e=\omega_0(k_{zi})-\delta\omega/2$, $\omega_e=\omega_0(k_{zi})+\delta\omega/2$]. This would result in, instead of (4.39), a convolution integral over the inhomogeneously varying line centers of the individual electrons $\omega_0(k_{zi})$, in a complete analogy to Doppler inhomogeneous broadening in atomic radiation systems (Yariv, 1975). In the inhomogeneous broadening limit we can obtain straightforwardly the explicit frequency presentation by substituting in (4.41) $\bar{\theta}_{u0}/\bar{\theta}_{\rm th}=2\pi(\omega-\omega_{u0})/\omega_{\rm th}$, $\bar{\theta}_{d0}=2\pi(\omega-\omega_{a0})/\omega_{\rm th}$, where $\omega_{u0}=\omega_e\mid_{\beta_z=\beta_{z0}}$, $\omega_{d0}=\omega_a\mid_{\beta_z=\beta_{z0}}$, $\omega_e=\omega_0-\delta\omega/2$, $\omega_a=\omega_0+\delta\omega/2$ [(2.36) and (2.37)], and $\delta\omega$ can be determined for specific radiation schemes using Table III. The axial velocity spread inhomogeneous broadening linewidth $\omega_{\rm th}$ is found to be [using Eqs. (4.38), (3.89), and (3.90)]

$$\omega_{\rm th}=\Delta\omega_L\bar{\theta}_{\rm th}=\frac{\omega^2\lambda_w p_{\rm th}}{\gamma_{\rm ph}\bar{\gamma}_{\rm ph}^{\,2}\bar{v}_{\rm ph}^{\,2}m}\ . \tag{4.42}$$

The second part of (4.42) was written for the specific case of free-electron radiation schemes based on periodic structures [using (2.32)]. Near synchronism the phase velocity parameter $\gamma_{\rm ph}\bar{\gamma}_{\rm ph}\bar{v}_{\rm ph}$ may be replaced by the average beam parameters $\gamma_{\rm ph}=\gamma_0\bar{\gamma}_{\rm ph}=\gamma_{z0}\bar{v}_{\rm ph}=v_{z0}$. In terms of these parameters, Eq. (4.41) is expressed as

$$\frac{d\nu_{q\sigma}}{dt}=\frac{\Delta\omega_h}{\omega_{\rm th}}\Gamma_{\rm sp}\left[(\nu_{q\sigma}+1)g\left[2\pi\frac{\omega-\omega_{u0}}{\omega_{\rm th}}\right]-\nu_{q\sigma}g\left[2\pi\frac{\omega-\omega_{d0}}{\omega_{\rm th}}\right]\right]\ . \tag{4.43}$$

The stimulated emission-absorption line-shape function part of Eq. (4.43) is drawn in the upper curve of Fig. 2(c) for the case of Maxwellian electron momentum distribution [Gover and Livni, 1978; see also Eq. (4.34)].

We note that in the extreme opposite of (4.40), the homogeneous broadening limit, the convolution in (4.39) reduces this equation back into the homogeneous broadening one of Eq. (3.79). This result is obtained using the normalization condition $\int g(x)dx=1$ and the fact that in this limit $g(\bar{\theta}/\bar{\theta}_{\rm th})$ is a narrow function relative to $F(\bar{\theta})$ and behaves as a delta function.

We now can generalize all the results for spontaneous and stimulated emission that were derived in the previous section for homogeneous broadening and apply them to the case of inhomogeneous broadening, taking advantage of the apparent formal similarity between (3.79) and (4.41). This can be done by substituting in all equations $(\Delta\bar{\theta}_h/\bar{\theta}_{\rm th})g(\bar{\theta}/\bar{\theta}_{\rm th})$ instead of the homogeneous line-broadening function $F(\bar{\theta})$.

We first consider the quantum-limit case in which the emission and absorption lines are well spaced:

$$\varepsilon\gg\bar{\theta}_{\rm th}\gg\Delta\bar{\theta}\ . \tag{4.44}$$

Instead of Eqs. (4.5) and (4.7), the spectral radiant intensity and gain will be given by

$$\left[\frac{d^2P_{q\sigma}}{d\Omega\,d\omega}\right]_{\rm sp}=\frac{\Delta\bar{\theta}_h}{\bar{\theta}_{\rm th}}R_\sigma g\left[\frac{\bar{\theta}_{u0}}{\bar{\theta}_{\rm th}}\right]\ , \tag{4.45}$$

$$G=\frac{\Delta\bar{\theta}}{\bar{\theta}_{\rm th}}M_\sigma\left[g\left[\frac{\bar{\theta}_{u0}}{\bar{\theta}_{\rm th}}\right]-g\left[\frac{\bar{\theta}_{d0}}{\bar{\theta}_{\rm th}}\right]\right]\ , \tag{4.46}$$

where M_σ is defined by (4.8).

The homogeneous broadening relation between the stimulated emission gain and the spontaneous spectral radiant intensity [Eq. (4.10)] applies without any change also in the inhomogeneous broadening regime, but the relation to the total spontaneous radiant intensity [Eq. (4.11)] changes because the emission linewidth (in frequency domain) is now $\omega_{\rm th}$ instead of $\Delta\omega_L$. Instead of (4.11) we have

$$G(\omega)=\frac{\lambda^3}{A_{\rm em}\hbar c}\frac{1}{\omega_{\rm th}}\left[\frac{dP_{q\sigma}}{d\Omega}\right]_{\rm sp}\frac{g(\bar{\theta}_{u0})}{g(0)}\ . \tag{4.47}$$

The universal relations between the stimulated and spontaneous emission power differentials (4.13) and (4.17) remain without change except for the last equality of (4.17), which is substituted by the first (stimulated emission) term of (4.46).

The longitudinal classical limit of the inhomogeneous broadening regime is found by taking the limit $\varepsilon\ll\bar{\theta}_{\rm th}$ in Eqs. (4.45) and (4.46). This results in

$$\left[\frac{d^2P_{q\sigma}}{d\Omega\, d\omega}\right]_{sp}=\frac{\Delta\bar{\theta}_h}{\bar{\theta}_{th}}R_\sigma g\left[\frac{\bar{\theta}_0}{\bar{\theta}_{th}}\right], \tag{4.48}$$

$$G=\frac{\Delta\bar{\theta}_h}{\bar{\theta}_{th}^2}\bar{Q}g'\left[\frac{\bar{\theta}_0}{\bar{\theta}_{th}}\right], \tag{4.49}$$

in analogy with (4.20) and (4.21). Here, too, we avoid keeping the small quantum field correction to the spontaneous emission equation corresponding to the second term in (4.19). For the finite-length homogeneous broadening line-shape function, one has $\Delta\bar{\theta}_h=2\pi$, and (4.48) and (4.49) are identical with the conventional classical spontaneous and stimulated emission equations derived previously for many kinds of FEL's and other radiation effects (Gover and Yariv, 1975; Gover and Livni, 1978; Gover and Sprangle, 1981). The stimulated emission line-shape function is shown in the lower curve of Fig. 2(c) for a Gaussian distribution function. The dependence of the gain on the derivative of the electron distribution is reminiscent of many plasma instability effects, and indeed in this operating regime the free-electron radiation amplifier can be regarded as an inverse Landau damping effect (Gover and Yariv, 1975).

The relation between stimulated emission gain and spontaneous emission spectral radiant intensity and total radiant intensity in the classical inhomogeneous broadening regime is found from Eqs. (4.48) and (4.49),

$$\begin{aligned}G(\omega)&=\frac{1}{\bar{\theta}_{th}}\frac{\bar{Q}_\sigma}{R_\sigma}\left[\frac{d^2P_{q\sigma}(\omega_0)}{d\Omega\, d\omega}\right]_{sp}\frac{1}{g(0)}g'\left[\frac{\bar{\theta}}{\bar{\theta}_{th}}\right]\\&=\frac{1}{\bar{\theta}_{th}^2}\frac{\bar{Q}_\sigma}{R_\sigma}\frac{1}{\Delta\omega_L}\left[\frac{dP_{q\sigma}}{d\Omega}\right]_{sp}\frac{1}{g(0)}g'\left[\frac{\bar{\theta}}{\bar{\theta}_{th}}\right],\end{aligned} \tag{4.50}$$

which are analogous to Eq. (4.23). An alternative presentation of these relations in terms of the spontaneous and stimulated power differentials is

$$\frac{(\Delta P_{q\sigma})_{st}}{P_{q\sigma}}=\frac{(\Delta P_{q\sigma})_{sp}}{P_{QN}}\frac{\varepsilon}{\bar{\theta}_{th}^2}\frac{1}{g(0)}g'\left[\frac{\bar{\theta}}{\bar{\theta}_{th}}\right], \tag{4.51}$$

which is analogous to the first part of (4.25).

We conclude that only the quantum-mechanical relations between the gain and spontaneous emission spectral radiant intensity (4.10) and the relations (4.13) and (4.17) remain unaltered in the inhomogeneous regime. The other proportionality relations between stimulated and spontaneous emission change and exhibit different scaling laws as a function of wavelength, beam energy, and other parameters. The inhomogeneous broadening proportionality factor of the quantum-mechanical-limit relation between gain and total radiant intensity (4.47) is reduced roughly by a factor $\omega_{th}/\Delta\omega_h>1$ relative to the homogeneous case (4.11). The proportionality factor of the classical-limit gain relation to spectral radiant intensity and total radiant intensity (4.50) is reduced relative to the homogeneous broadening equations (4.23) roughly by factors $\bar{\theta}_{th}$ and $\bar{\theta}_{th}\omega_{th}/\Delta\omega_h=\bar{\theta}_{th}^2\Delta\omega_L/\Delta\omega_h$, respectively.

We may speculate that similar reductions in the spontaneous and stimulated emission powers and in the proportionality factors occur also with other kinds of inhomogeneous line broadening if their predominant effect is to create spread in the emission and absorption homogeneous line centers of the different electrons. In these cases the appropriate detuning parameter linewidth $\Delta\bar{\theta}$ of the corresponding inhomogeneous broadening line-shape function takes the place of $\bar{\theta}_{th}$ in the equations obtained above. In fact, we may extend in such cases our two alternative equations for the inhomogeneous transition rate [Eqs. (4.41) and (4.43)] and write them in the general form

$$\begin{aligned}\frac{d\nu_{q\sigma}}{dt}&=\frac{\Delta\bar{\theta}_h}{\Delta\bar{\theta}}\Gamma_{sp}\left[(\nu_{q\sigma}+1)g\left[\frac{\bar{\theta}_{u0}}{\Delta\bar{\theta}}\right]-\nu_{q\sigma}g\left[\frac{\bar{\theta}_{d0}}{\Delta\bar{\theta}}\right]\right]\\&=\frac{\Delta\omega_h}{\Delta\omega}\Gamma_{sp}\left[(\nu_{q\sigma}+1)g\left[2\pi\frac{\omega-\omega_{u0}}{\Delta\omega}\right]\right.\\&\qquad\left.-\nu_{q\sigma}g\left[2\pi\frac{\omega-\omega_{d0}}{\Delta\omega}\right]\right],\end{aligned} \tag{4.52}$$

where $\Delta\omega\geq\Delta\omega_h$, $\Delta\bar{\theta}\geq\Delta\bar{\theta}_h$ are the inhomogeneous linewidths in the frequency and detuning parameter domains, respectively. These equations are in fact completely general and valid for the inhomogeneous as well as the homogeneous broadening regimes. In the latter case, one should use the substitutions $\Delta\bar{\theta}=\Delta\bar{\theta}_h$, $\Delta\omega=\Delta\omega_h$, $g(\bar{\theta}/\Delta\bar{\theta})=F(\bar{\theta})=F(2\pi\omega-\omega_0/\Delta\omega_h)$.

The relations between the radiometric stimulated and spontaneous emission parameters in both the longitudinal-quantum and classical regimes are summarized in Table IV for arbitrary homogeneous or inhomogeneous distribution function g of frequency linewidth $\Delta\omega$. The ratios and explicit scaling laws listed in Table V for particular interaction schemes were calculated specifically for the case of finite-length homogeneous broadening.

Table V may be generalized to give the corresponding explicit scaling laws in the inhomogeneous regime. To do this one should multiply the equations in this table by the corresponding inhomogeneous broadening reduction factors identified earlier in this section (and summarized in terms of $\Delta\omega$ in Table IV). For the case of axial momentum spread inhomogeneous broadening, the explicit equations for the spread parameters $\Delta\bar{\theta}=\bar{\theta}_{th}$, $\Delta\omega=\omega_{th}$ are given by (4.38) and (4.42). In addition, the numerical value of the homogeneous broadening gain curve peak 0.27 should be replaced in Table V by the appropriate peak value of the normalized inhomogeneous broadening gain curve $g'(x)/g(0)$, which is of the order of unity because of the normalization. For the normalized Maxwellian inhomogeneous distribution function (4.34), the peak of the gain curve $g'(\bar{\theta}_m/\bar{\theta}_{th})/g(0)$ is equal to $\sqrt{2/e}=0.86$, and it is attained at an argument value $\bar{\theta}_m=-1/\sqrt{2}$.

We conclude that the general relations found between

the spontaneous and stimulated emission parameter can be made explicit for a large variety of radiation schemes as well as different operating regimes (classical or quantum, homogeneous or inhomogeneous broadening). The explicit equations make it possible to predict the values and the scaling laws of the gain for various free-electron laser schemes when the spontaneous emission parameters of the same devices are measured first or calculated.

V. CONCLUSION AND EXAMPLES

In this paper we exposed the common features of radiation emission from various quasifree-electron radiation effects and devices and particularly free-electron lasers. The common features are a result of the extended interaction between the electron and the radiation wave along the electron propagation direction. This extended interaction feature, which distinguishes these devices from conventional atomic lasers, results in a requirement of axial momentum (wave number) conservation, which needs to be satisfied in addition to the energy conservation condition.

We have distinguished between cases of discrete and continuous transverse states and, in the latter case, identified transverse quantum-mechanical and classical regimes in addition to the analogous corresponding distinction between quantum-mechanical and classical regimes in the longitudinal dimension. Most free-electron radiation devices and effects (and, in particular, the magnetic bremsstrahlung FEL) fall in the category of the transverse continuous states, operating in their practical mode of operation in the transverse (as well as longitudinal) classical regime. Some well-known radiation effects, such as channeling radiation, may fall into the category of the quantum regime of transversely discrete states. An important physical distinction between the radiation processes in these two cases is the direction of the electron quantum recoil. While in the first case it is arbitrary, in the second case the recoil is purely longitudinal. We define recoil here to mean a direct transfer of linear momentum to the electron (in a wider sense, a transition between *different* transverse states may also be considered to involve transverse recoil due to transverse energy change).

The distinction between processes involving a general recoil and processes constrained to recoil only in the longitudinal dimension is valid also in entirely classical devices (e.g., magnetic bremsstrahlung FEL and CRM, which belong to the first and second categories, respectively). This distinction becomes apparent only when one considers emission processes in which the total recoil momentum $\mathbf{q}+\mathbf{k}_w$, which is composed of the radiation field momentum $\mathbf{q}$ and the wiggler "crystal momentum" $\mathbf{k}_w$, has components perpendicular to the electron average motion. In practice this is mostly relevant to the case of "off-axis" emission by electrons. The distinction is important only when stimulated emission is being considered, because then (in the classical limit) the gain equation is affected through the average motion mass tensor $(1/m^*)_{ij}$, which in the longitudinally constrained recoil case reduces into a single scalar parameter $(1/m^*)_{\|}$. Despite this difference, our formulation allowed the common description of devices and effects operating with these two different emission processes. This unified representation provides, for example, a way for comparing between two different devices, such as a helical wiggler FEL and a cyclotron resonance maser (which belong to the first and second categories, respectively). While both devices have the same spontaneous emission characteristics, their stimulated emission gain is different. This comparison is carried out in detail in Sec. V.C.

In analyzing the dynamics of the radiation process of quasifree electrons we developed a general first-order perturbation theory (in terms of the radiation field) in a framework of a quantum-electrodynamical model. This model leads to general expressions for the spontaneous and stimulated emission photon growth rates. Various fundamental interaction processes (Fig. 9) were identified as possible sources for free-electron radiation, spanning the validity of the formulation over a wide range of free-electron radiation effects and devices. When a number of processes contribute to the radiation synergistically, their matrix element amplitudes and phases add up coherently, and the unified formulation enables correct consideration of the interference between the different contributions. The calculation of the matrix elements for specific radiation effects was not included in the scope of this paper, but the prescription for this calculation was outlined in great detail.

We have derived explicit expressions for the finite-length and exponential decay homogeneous broadening line-shape functions. These expressions are applicable to all radiation effects. We also analyzed inhomogeneous broadening, considering in detail the particular case of longitudinal velocity spread line broadening, which is of most practical relevance. The longitudinal classical regime line-shape functions were derived by taking the negligible recoil limit of the quantum-mechanical expressions in both homogeneous and inhomogeneous broadening cases, and are in both cases the derivatives of the quantum-mechanical (large recoil) line-shape functions.

Expressions useful for experimental characterization of free-electron radiators are derived when one takes the radiation classical limit and expresses the spontaneous and stimulated emission photon growth rates in terms of common laboratory (radiometric) parameters such as radiant intensity and gain. We revealed universal relations between these radiometric parameters in both the electron quantum-mechanical and classical regimes. These relations are common to all the radiation effects and interaction schemes considered, and thus are a generalization to different devices and different radiative emission direction, extending theorems derived previously by Madey (1979) specifically for the magnetic bremsstrahlung FEL at on-axis emission conditions. In the longitudinal quantum limit, where the emission and absorption

lines are well separated, the expressions we derived are universal quantum-electrodynamical relations between spontaneous and stimulated emission in a general two-level system, and are not different from similar relations in atomic lasers. They are then related to the well-known Einstein relations. Only in the longitudinal classical limit, when the emission and absorption lines overlap, are the relations specific to quasifree-electron radiation schemes and depend on the line-shape function's form and, especially, width.

A particularly important feature of the universal relations derived in this paper is in their independence of the kind of effect and interaction scheme involved. Even if a number of the interaction schemes shown in Fig. 9 take place synergistically, as is the case in many radiation effects [for example, both processes of Figs. 9(a), 9(b), and 9(d) take place synergistically in the coherent bremsstrahlung effect], the relations still hold. These relations can thus be used to estimate the stimulated emission gain of lasers that are based on radiation effects for which the spontaneous emission radiant intensity was measured. When simple models for the radiation effect are not available for calculating the gain analytically, and experimental data on radiant intensity is available, such relations are very useful and have the additional advantage of universal applicability (or model independence).

To demonstrate the application of the equations derived before, we will implement them in Secs. V.A and V.B for estimating the laser gain in two specific examples of the Smith-Purcell FEL and the channeling radiation laser, based upon experimentally available data on the spontaneous emission characteristics of these effects.

In addition we will use these relations in Sec. V.C in order to derive general equations for the stimulated emission gain at arbitrary emission direction of two devices of considerable interest: the magnetic bremsstrahlung FEL and the CRM. The gain equations will be found in those cases based on well-known classically derived equations for the spontaneous emission of these devices, and on the general equations we derived for the ratios between stimulated and spontaneous emission parameters.

A. Estimating a Smith-Purcell free-electron laser gain

A reliable quantitative estimate of a Smith-Purcell FEL gain is hard to make, mostly because of the difficulty in solving exactly the electromagnetic problem of the radiation field with the boundary conditions of a metallic grating (Van den Berg, 1973). As in the general optical grating diffraction problem, the amplitudes of the space harmonics (diffraction orders) depend strongly on the grating ruling shapes and, in certain wavelength regimes (especially IR), on the dielectric properties of the grating material. Analytical estimates of these amplitudes usually have limited validity, and, in general, intensive numerical computation techniques must be applied. Here we will base our estimate of FEL gain on measured values of radiant intensity reported earlier (Gover *et al.*, 1984) and the relation given in the third column, fourth row, in Table V. We assume an open resonator Smith-Purcell FEL as shown in Fig. 11. The effective radiation beam cross section is taken to be $A_{\rm em}=W_e L\sin\Theta_q$, where, for maximizing the gain, the radiation beamwidth is taken equal to the e-beam width W_e. The length of the radiation beam spot on the grating is taken equal to the grating length. We also substitute in the relation in Table V $\bar{\beta}=\beta_z=\beta$, since the wiggling motion of the electron is negligible.

To calculate the angle $\Theta_{\rm rec}$ we assume that the electron trajectory and the "wiggler" (grating) wave number $\mathbf{k}_w$ are coaligned. The electromagnetic mode space harmonic, which synchronizes with the electron beam, is purely evanescent perpendicularly to the grating plane. Hence its radiation wave vector $\mathbf{q}_m$ has no real component in the x direction (normal to the grating surface). It may have, though, a component in the lateral y direction, which is defined as the direction in the grating plane perpendicular to the electron trajectory. Using the synchronism condition $q_{mz}\equiv q_z+mk_w=\omega/v$ and the definition of the recoil angle (3.85), $\cos\Theta_{\rm rec}=(q_z+mk_w)/[(q_z+mk_w)^2+q_y^2]^{1/2}$. Defining the lateral angle of the radiation mode Θ_{qy} by $q_y\equiv(\omega/c)\cos\Theta_{qy}$, we can write the recoil angle equation in the relation given in Table V in the form $\tan^2\Theta_{\rm rec}=\beta^2\cos^2\Theta_{qy}$. Consequently the Smith-Purcell FEL gain at the maximum gain detuning point $\bar{\theta}=-2.6$ (assuming finite-length homogeneous broadening) is

$$G_{\max}=0.54\pi\frac{m\lambda^2 L}{mc^3 W_e\lambda_w}\frac{1}{\gamma^3\beta^3\sin\Theta_q}(1+\gamma^2\beta^2\cos^2\Theta_{qy})\times\left[\frac{dP_{q\sigma}}{d\Omega}\right]_{\rm sp}. \tag{5.1}$$

There are a few reports of experiments in which spontaneous Smith-Purcell radiation was measured. However, not many of them include quantitative data on the emission power levels. We use here the measured values for radiant intensity reported by Gover *et al.* (1984). We substitute in (5.1) the reported experiment parameters: $\beta=0.548$ ($V_0=100$ kV), $W_e=0.1$ mm, $\lambda_w=0.556$ μm,

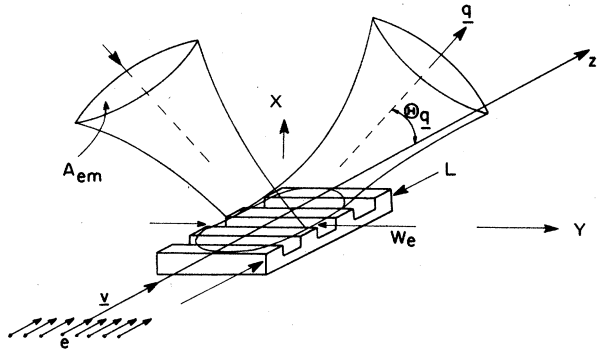

FIG. 11. Smith-Purcell radiation scheme.

$m=2$, $L=25$ mm, $\Theta_q=160°$, $\Theta_{qy}=137°$, $(dP/d\Omega)_{sp}=0.58$ nW/ster, and $\lambda=5835$ Å [computed from the radiation condition (2.23)]. This results in $G_{max}=5.6\times10^{-8}$, which is, of course, a very low gain, indicating that under the same conditions in which the spontaneous emission experiment was carried out, FEL oscillator construction would be impractical.

Enhancement of the Smith-Purcell gain would be possible in a waveguide structure (Gover and Yariv, 1978b), in which case (assuming a planar waveguide) the FEL gain is increased by a factor equal to the number of "zigzag bounces" of the optical rays in the waveguide along the interaction length. However, such approach certainly will not work as long as the FEL gain per bounce is much lower than any conceivable values of reflection loss per bounce. An obvious way to increase the gain is by increasing the electron current in the interaction region. In the experiment conducted by Gover *et al.* (1984), the *e*-beam current was 0.22 μA. It is certainly possible to increase this current by many orders of magnitude, but because of resultant emittance growth (Lawson, 1977; Gover and Sprangle, 1981), this will increase the axial momentum spread of the beam and the collisions rate (with the grating). The emission line would then be likely to be dominated by inhomogeneous broadening due to velocity spread or collisions. From Eq. (4.49) one would expect a strong reduction in gain due to this spread in inverse proportion to the broadened linewidth squared. These considerations do not lead to optimistic predictions with regard to realization of nonrelativistic beam Smith-Purcell FEL's in the visible wavelength. Certainly considerable improvements in the experimental conditions (perhaps optimization of the grating rulings shape for maximal coupling into the interacting slow space harmonic) would be required to change this conclusion.

B. Estimating a channeling radiation free-electron laser gain

Another example we offer for the application of the equations derived in Sec. IV is the estimate of the gain to be expected in a stimulated channeling experiment. We use here spontaneous emission values that were measured by Andersen *et al.* (1981). In that experiment the electrons channeled through the lattice plane {110} of a silicon crystal. In this particular plane there are only two transverse quantum levels in which the electron wave function stays bound to the planar channel. Hence we must use the quantum-mechanical relation between spontaneous and stimulated emission (third column, second row, in Table IV) in order to estimate the expected gain under the same experimental conditions.

We substitute

$$\frac{dP_q}{d\Omega}=\hbar\omega\frac{\Delta\nu_q^e}{\Delta\Omega}\frac{I}{e} \tag{5.2}$$

in the quantum relation in Table IV. $\Delta\nu_q^e$ is the number of photons emitted into the solid angle $\Delta\Omega$ by a single electron traversing the crystal. Assuming $A_{em}=A_e$, A_e is the electron beam cross section, and $\Delta\omega=\Delta\omega_L$, where $\Delta\omega_L$ is the finite-length homogeneous broadening linewidth (2.31), we obtain a simple equation for the gain:

$$G=\frac{\lambda^2 L}{2\gamma^2 ce}\left[\frac{\Delta\nu_q^e}{\Delta\Omega}\right]_{sp}J_0\ , \tag{5.3}$$

where J_0 is the current density. The experimental data in the cited experiment (Andersen *et al.*, 1981) was $\gamma=9$, $\Delta\Omega\approx0.64\times10^{-6}$ ster, $L=1$ μm, $\Delta\nu_q^e\approx0.5\times10^{-8}$ *photons*. Using this data, Eq. (5.3) yields

$$G\approx0.54\times10^{-15}J_0(A/\text{cm}^2)\ .$$

A more important equation may be the gain as a function of the electron beam brightness $(dI/dA\,d\Omega)$, since the acceptance angle of the crystal channel is limited and not all electrons entering at arbitrary entrance angles can channel and emit coherently. In a planar channeling experiment the coherent emission acceptance angle in the dimension parallel to the channel plane is $\sqrt{\lambda/L}$. The acceptance angle in the dimension perpendicular to the crystal channel within which the electrons are injected into the upper transverse energy level is 1.2 mrad. This parameter is deduced out of the reported data on the angular dependence of the measured emission as function of the crystal orientation (Andersen *et al.*, 1981). Thus the total acceptance solid angle in this experiment is estimated to be $\Delta\Omega=9.6\times10^{-5}$ ster. The gain dependence on the electron beam brightness under the conditions of Andersen's experiment is therefore

$$G=5.2\times10^{-20}\left[\frac{dI}{dA\,d\Omega}\right]\ .$$

This result corresponds to a requirement for an electron source that is much brighter than that of a cathode temperature-limited source, if a reasonable gain of at least a few percent is to be obtained. This is, of course, a discouraging result (before considering yet any other technological limitations such as material damage and crystal heating). However, we do not rule out the possibility of obtaining more favorable predictions under different experimental conditions (possibly at longer wavelength and lower electron energies).

C. General (off-axis) gain equations for the magnetic bremsstrahlung free-electron laser and cyclotron resonance maser

In order to calculate the spontaneous emission spectral radiant intensity, we use a known standard formula (Jackson, 1975) for radiation from a moving point charge. The energy emitted per electron per unit frequency per steradian is

$$\frac{d^2I^e}{d\omega\, d\omega}=\frac{e^2\omega^2}{16\pi^3}\left|\int dt\,\hat{e}_q\times(\hat{e}_q\times\hat{e}_\beta)\beta e^{i\omega[t-\hat{e}_q\cdot\mathbf{r}(t)/c]}\right|^2 . \tag{5.4}$$

We assume that only the components of the electron velocity that are perpendicular to the wiggler direction in a FEL, or to the axial magnetic field in a CRM, contribute to the radiation. We change the integration variable from t to z using $t=t_{0j}+z/v_z$,

$$\frac{d^2I^e}{d\omega\, d\omega}=\frac{e^2}{4\pi\lambda^2}\left[\frac{\mu_0}{\varepsilon_0}\right]^{1/2}\sin^2\Theta_q^v\left|\int_0^L dz\frac{v_\perp}{v_z}e^{i(\omega/v_z)z-i(\omega/c)\hat{e}_q\cdot\mathbf{r}_\perp(z)-i(\omega/c)\hat{e}_q\cdot\hat{e}_z z}\right|^2 , \tag{5.5}$$

where Θ_q^v is the angle between the radiation wave number q and the transverse velocity of the electron $\mathbf{v}_\perp$. For undulator radiation (periodic magnetic bremsstrahlung), the transverse velocity is

$$\mathbf{v}_\perp=\tfrac{1}{2}(\bar{\mathbf{v}}_w e^{-i\mathbf{k}_w\cdot\mathbf{r}}+\bar{\mathbf{v}}_w^* e^{i\mathbf{k}_w\cdot\mathbf{r}}) . \tag{5.6}$$

For a CRM the transverse velocity is

$$\mathbf{v}_\perp=\tfrac{1}{2}(\bar{\mathbf{v}}_w e^{-i\omega_c t}+\bar{\mathbf{v}}_w^* e^{i\omega_c t}) . \tag{5.7}$$

Substitution of (5.6) or (5.7) into (5.5) and multiplying by the electron injection rate I_0/e in order to get the spectral radiant intensity of an electron beam results in the same equation for both cases:

$$\frac{d^2P}{d\omega\, d\Omega}=\frac{e^2}{4\pi\lambda^2}\frac{I_0}{e}\left[\frac{\mu_0}{\varepsilon_0}\right]^{1/2}\frac{L^2}{4}\sin^2\Theta_q^v\left|\frac{\bar{v}_w}{v_z}\right|\mathrm{sinc}^2\frac{\bar{\theta}}{2} , \tag{5.8}$$

where $\bar{\theta}$ is the detuning parameter, given by Eq. (3.81) for the magnetic bremsstrahlung FEL,

$$\bar{\theta}=[\omega-(\mathbf{q}+\mathbf{k}_w)\cdot\bar{\mathbf{v}}]\frac{L}{\bar{v}_z} , \tag{5.9}$$

and $\bar{\mathbf{v}}$ is the average electron velocity. For the CRM case the detuning parameter $\bar{\theta}$ is

$$\bar{\theta}=\left[\frac{\omega-\omega_c}{v_z}-q_z\right]L . \tag{5.10}$$

Note that in (5.9) an assumption $v_z=\bar{v}_z=$const was used. This is an approximation valid only for $a_w\equiv eB_w/(k_w mc)\ll 1$ in the case of a linear wiggler, but is exact in the case of a helical wiggler with zero canonical momentum. It is instructive to note that undulator radiation and cyclotron resonance emission have the same spontaneous emission radiation pattern for the same wiggling velocity v_w. The electron trajectories (which are exactly the same in both cases if the wiggler is helical) completely determine the spontaneous emission radiation pattern.

In order to calculate the gain we use the equations in rows 4 and 6 of the second column in Table V for the bremsstrahlung FEL and the CRM, respectively. The equation for the gain in the first case is

$$G(\omega)=\frac{\pi}{2}\frac{\omega L^3}{cA_{\mathrm{em}}}\frac{I_0}{I_A}\left|\frac{v_w}{v_z}\right|^2\frac{1}{\gamma\bar{\beta}^3}\sin^2\Theta_q^v\left[\frac{1}{\bar{\gamma}^2}+\tan^2\Theta_{\mathrm{rec}}\right]\times\frac{d}{d\bar{\theta}}\mathrm{sinc}^2\frac{\bar{\theta}}{2} , \tag{5.11}$$

where $I_A=4\pi\varepsilon_0 mc^3/e=1.7\times10^4$ A is the Alfvén current constant. This gain formula applies for any arbitrary direction of the electron, wiggler, and radiation. Also, the general tuning equation was restored by replacing the maximum gain point volume, used in the table by the finite-length homogeneous broadening detuning curve [(4.23) and (3.67)]. In the special case in which the electron and the wiggler are aligned, $\Theta_{\mathrm{rec}}=\Theta_q$, $\bar{\gamma}=\gamma_z$, the gain formula reduces to

$$G(\omega)=\frac{\pi}{2}\frac{\omega L^3}{cA_{\mathrm{em}}}\frac{I_0}{I_A}\left|\frac{v_w}{v_z}\right|^2\frac{1}{\gamma\beta_z}\times\sin^2\Theta_q^v[(\gamma_z^2\beta_z^2)^{-1}+\sin^2\Theta_q]\frac{d}{d\bar{\theta}}\mathrm{sinc}^2\frac{\bar{\theta}}{2} . \tag{5.12}$$

In the even simpler case, when also the radiation is on axis ($\Theta_q=0$), Eq. (5.12) reduces to the well-known gain formula (Madey, 1971)

$$G(\omega)=\frac{\pi}{2}\frac{\omega L^3}{cA_{\mathrm{em}}}\frac{I_0}{I_A}\left|\frac{v_w}{v_z}\right|^2\frac{1}{\gamma\gamma_z^2\beta_z^3}\frac{d}{d\bar{\theta}}\mathrm{sinc}^2\frac{\bar{\theta}}{2} . \tag{5.13}$$

In the CRM case the resulting equation for the gain at arbitrary emission angle is

$$G(\omega)=-\frac{\pi}{2}\frac{\omega_{c0}^2L^3}{\omega cA_{\mathrm{em}}}\frac{I_0}{I_A}\left|\frac{v_w}{v_z}\right|^2\frac{1}{\gamma^3\beta_z}\sin^2\Theta_q^v\frac{\sin^2\Theta_q}{1-\beta_z\cos\Theta_q}\times\frac{d}{d\bar{\theta}}\mathrm{sinc}^2\frac{\bar{\theta}}{2} . \tag{5.14}$$

This result indicates that one should not expect net gain terms that scale as L^3 on axis for CRM-based devices (Ride and Colson, 1979; Gell *et al.*, 1982). As was discussed in Sec. II, there are still gain terms that scale as L^2 that may not cancel on axis, but these terms are only significant for a short CRM device and were not included in the present derivation.

APPENDIX A: THE CYCLOTRON RESONANCE MASER ENERGY LEVELS

The total energy of a relativistic electron in a uniform axial magnetic field B_z, which is the positive eigenvalue of the Klein-Gordon equation, is

$$\mathcal{E}=mc^2\left[1+\left[\frac{p_z}{mc}\right]^2+\left[\frac{\mathbf{p}_\perp}{mc}\right]^2\right]^{1/2} . \tag{A1}$$

As in the nonrelativistic limit (Landau, 1930) the transverse momentum is quantized:

$$\mathbf{p}_\perp^2=(n+\tfrac{1}{2})2m\hbar\omega_{c0} , \tag{A2}$$

where $\omega_{c0}=eB_z/m$ and m is the particle rest mass.

In the relativistic regime there is no particular advantage in separating the electron energy into longitudinal and transverse components, as was done in Sec. II.D, since we have an explicit equation for the total energy dispersion relation (A1) and it does not split (as it does in the nonrelativistic limit) into pure transverse and longitudinal components.

To calculate the classical cyclotron emission frequency at any harmonic Δn, it is sufficient to expand $\mathcal{E}_f$ to first order in $\hbar$ and substitute in the equations for conservation of *total* energy (2.10) and longitudinal momentum [(2.11), with $m=0$ (2.50)]. Using $\partial\mathcal{E}/\partial k_{zi}=\hbar v_{gz}$ and $\partial\mathcal{E}/\partial n=\hbar\omega_{c0}m^2c^2/\gamma$, one obtains

$$\omega_0=(\Delta n)\frac{\omega_{c0}/\gamma}{1-\beta_{gz}\cos\Theta_q} . \tag{A3}$$

In order to find the difference between the absorption and emission frequencies we expand $\mathcal{E}_{n_fk_{zf}}$ to second order in $\hbar$ around (n_i,k_{zi}):

$$\begin{aligned}\mathcal{E}_{n_fk_{zf}}-\mathcal{E}_{n_ik_{zi}}\approx&\left.\frac{\partial\mathcal{E}}{\partial k_{zi}}\right|_{n_ik_{zi}}(k_{zf}-k_{zi})+\left.\frac{\partial\mathcal{E}}{\partial n}\right|_{n_ik_{zi}}(n_f-n_i)\\&+\frac{1}{2}\left.\frac{\partial^2\mathcal{E}}{\partial k_z^2}\right|_{n_ik_{zi}}(k_{zf}-k_{zi})^2+\left.\frac{\partial^2\mathcal{E}}{\partial k_z\partial n}\right|_{n_ik_{zi}}(n_f-n_i)(k_{zf}-k_{zi})+\frac{1}{2}\left.\frac{\partial^2\mathcal{E}}{\partial n^2}\right|_{n_ik_{zi}}(n_f-n_i)^2 .\end{aligned} \tag{A4}$$

Again, using the conservation of energy and longitudinal momentum conditions and the relations

$$\frac{\partial^2\mathcal{E}}{\partial k_z^2}=\frac{\hbar^2}{m_\parallel^*}=\frac{\hbar^2}{\gamma\gamma_z^2m} ,$$

$$\frac{\partial^2\mathcal{E}}{\partial k_z\partial n}=\hbar^2\frac{\omega_{c0}}{mc\gamma^2}\beta_z ,$$

$$\frac{\partial^2\mathcal{E}}{\partial n^2}=-\hbar^2\frac{\omega_{c0}^2}{mc^2\gamma^3} ,$$

results in

$$\Delta\omega=\omega_a-\omega_e=\frac{\hbar\omega_{c0}^2}{mc^2\gamma^3}\left[\frac{1}{\gamma_z^2}\frac{\cos^2\Theta_q}{(1-\beta_z\cos\Theta_q)^2}-2\beta_z\frac{\cos\Theta_q}{1-\beta_z\cos\Theta_q}-1\right] . \tag{A5}$$

Equation (A5) is composed of three terms that can be traced to originate, respectively, from (1) pure longitudinal momentum change (recoil), (2) combined longitudinal and transverse-state change, and (3) pure transverse-state change, with each change taking place during the emission and absorption processes. It can be simplified into a compact form when the three different contributions are lumped together:

$$\Delta\omega=-\frac{\hbar\omega_{c0}}{mc^2\gamma^3}\frac{\sin\Theta_q}{(1-\beta_z\cos\Theta_q)^2} . \tag{A6}$$

APPENDIX B: THE CLASSICAL LIMITS OF AN ELECTRON WAVE PACKET

An electron can be defined to be in the classical limit if throughout the entire interaction region it can be well localized relative to the typical variation parameters of the force wave with which it interacts. In order to determine when this condition is satisfied, we write the electron wave function at time $t=0$ as a Gaussian with width σ,

$$\psi(z,t=0)=f(z)e^{ik_iz} , \tag{B1}$$

where

$$f^2(z)=\frac{1}{\sqrt{2\pi}\sigma}e^{-z^2/2\sigma^2} . \tag{B2}$$

The wave function at time t is

$$\psi(z,t)=\frac{1}{\sqrt{2\pi}}\int dk\,\chi(k-k_i)e^{i[kz-(\mathcal{E}/\hbar)t]} , \tag{B3}$$

where $\chi(k)$ is the Fourier transform of the initial wave function:

$$\chi(k)=\frac{1}{\sqrt{2\pi}}\int dz\,f(z)e^{-ikz}=\frac{\sqrt{2\sigma}}{(2\pi)^{1/4}}e^{-\sigma^2k^2} . \tag{B4}$$

We expand the energy of the electron $\mathcal{E}_k$ to second order around k_i,

$$\mathcal{E}_k\approx\mathcal{E}_{k_i}+\hbar v_g(k-k_i)+\frac{1}{2}\hbar^2\frac{1}{m_\parallel^*}(k-k_i)^2 . \tag{B5}$$

Substituting (B5) in (B3), and performing the integration, we find

$$\psi(z,t)\approx f_t[z-v_g t,\sigma_t(t)]e^{i[k_i z-(\mathcal{E}_{k_i}/\hbar)t]}, \tag{B6}$$

where

$$|f_t[z-v_g t,\sigma_t(t)]|^2=\frac{1}{(2\pi\sigma_t^2)^{1/2}}e^{-(z-v_g t)^2/2\sigma_t^2},$$
$$\sigma_t^2=\frac{\sigma^4+(\hbar t/2m_\parallel^*)^2}{\sigma^2}. \tag{B7}$$

The wave function in (B6) is a Gaussian pulse, moving with velocity v_g. The width of this pulse increases with time in a diffusionlike way.

The minimum possible value for σ_t (varying σ for fixed t) is

$$\sigma_{t_{\min}}^2=\frac{\hbar t}{m_\parallel^*}. \tag{B8}$$

The time when the pulse arrives at the end of the interaction length L is $t=L/v_g$. The condition for the electron to be classical, is that at the end of the interaction length, where the full width of the electron wave packet is taken to be $\sqrt{2}\,\sigma_{t_{\min}}$, it is still smaller than the wavelength of the ponderomotive potential (see Fig. 5). This results in the inequality condition

$$\frac{\hbar L}{2\pi m_\parallel^* v_g}(q_z+k_w)^2\ll\pi. \tag{B9}$$

Equation (B9) can be written in a more practical form using the equation for the effective mass (2.47),

$$\frac{\lambda_{\rm pm}^2}{L}>\frac{1}{\pi}\frac{\lambda_c}{\gamma_z^2\gamma\beta_z}, \tag{B10}$$

where $\lambda_{\rm pm}\equiv 2\pi/(q_z+k_w)$ and $\lambda_c=\hbar/mc$ is the Compton wavelength.

1. Transverse classical limit

In order to find the condition for the transverse classical limit we follow a similar procedure and start at $t=0$ with a wave packet of infinite extent in the longitudinal dimensions and finite width:

$$\psi(x,z,t=0)=f(x)e^{i(k_{zi}z+k_{xi}x)}, \tag{B11}$$

where $f^2(x)$ is again a Gaussian (B2) with width $\sigma_\perp$.

In analogy to (B6), the time-dependent wave function is

$$\psi(x,z,t)=f_t(x-v_{gx}t,\sigma_{\perp t})e^{i[k_{zi}z+k_{xi}x-(\mathcal{E}_i/\hbar)t]}, \tag{B12}$$

where $|f_t(x)|^2$ is a Gaussian similar to (B7). The minimal possible width of the Gaussian, sustainable within an interaction time t [analogous to (B8)] is

$$\sigma_{\perp t_{\min}}^2=\frac{\hbar t}{m_\perp^*}. \tag{B13}$$

We assume that the interaction time is the longitudinal transit time L/v_{gz}, and we require that the minimal full transverse width of the electron at the end of the interaction length $\sqrt{2}\,\sigma_{\perp t_{\min}}$ will be smaller than the electromagnetic field transverse variation (see Fig. 6). In characterizing the transverse variation of the radiation field we distinguish between two cases: (1) The radiation mode propagates at an angle to the electron wave packet. In this case the electron wave-packet width has to be smaller than the transverse wavelength of the radiation mode. This results in the condition

$$\frac{\lambda^2}{2\sin^2\Theta_q}>\frac{1}{\pi}\frac{\lambda_c}{\beta_z\gamma}. \tag{B14}$$

(2) The radiation wave propagates collinearly with the electron. Thus the electron wave-packet width has to be smaller than the radiation beamwidth. If we assume a Gaussian radiation mode, then the minimum diffraction-limited width of the mode for a given propagation length L is $\sqrt{\lambda L\pi}$. This results in the transverse classical limit condition

$$\lambda>\frac{\lambda_c}{\beta_z\gamma}. \tag{B15}$$

APPENDIX C: A DETAILED DERIVATION OF THE TRANSITION RATE EQUATION FOR VARIOUS CASES OF TRANSVERSE STATES

1. The transversely discrete (quantum) case

In order to keep convenient account of the electrons number normalization, we describe the electrons, even in the longitudinal quantum limit, as a finite-length longitudinal wave packet, which is distributed around a single longitudinal eigenstate function with a very narrow spectral width. We thus express the initial wave function as

$$\psi_i(\mathbf{r},t)=\sqrt{2\pi}\,\varphi_{\mathbf{k}_{\perp i}k_{zi}}(\mathbf{r},t)f_z(z-z_0), \tag{C1}$$

where $\varphi_{\mathbf{k}_{\perp i}k_{zi}}(\mathbf{r})=|\mathbf{k}_i\rangle$ is a single state function normalized according to (3.14)

$$\int\varphi_{\mathbf{k}_\perp k_z}(\mathbf{r})\varphi^*_{\mathbf{k}'_\perp k'_z}(\mathbf{r})d^3r=\delta(k_z-k'_z)\delta_{\mathbf{k}_\perp\mathbf{k}'_\perp},$$

and $f_z(z-z_0)$ is a real envelope function, which is substantially longer (in the z dimension) than the interaction length. Thus this envelope function seems constant as long as the classical electron location (wave-packet center) $z_0=v_{gz}(t-t_0)$ is within the interaction region.

We can keep the original volume normalization of the total wave function $\int|\psi|^2d^3r=1$ [see Eq. (3.13)], if we assign to the function $f_z(z-z_0)$ the constant value $1/\sqrt{L}$ within the entire interaction region $(0<z<L)$. This assertion can be verified by substituting (C1) in (3.13) and using the relation

$$(1/L)\int_0^L\int\int_{-\infty}^{\infty}|\varphi_{k_{\perp i}k_{zi}}|^2d^3r=1/(2\pi),$$

which applies to eigenstates of infinitely long systems with symmetry of axial translation or axial periodicity [specifically for an axially uniform system explicitly $\varphi_{\mathbf{k}_i}=\varphi_{\mathbf{k}_{\perp i}}(\mathbf{r}_\perp)e^{ik_{zi}z}/\sqrt{2\pi}$, where $\int_{-\infty}^{\infty}|\varphi_{\mathbf{k}_{\perp i}}(\mathbf{r}_\perp)|^2 d^3r=1$].

The total initial wave function can now be written within the interaction region as

$$|\psi\rangle=\sqrt{2\pi/L}\,\exp\left[-i\frac{E_{\mathbf{k}_i\nu_i}}{\hbar}t\right]|\mathbf{k}_i\nu_i\rangle\ . \tag{C2}$$

Comparison of this equation with the general expansion of the wave function (3.12) results in the explicit equation for the initial expansion coefficient: $C^0_{k\nu}=\delta_{\nu\nu_i}\delta_{ll_i}\delta(k_z-k_{zi})\sqrt{2\pi/L}$ [see Eq. (3.18)].

Once we derived the explicit expression for $C^0_{\mathbf{k}\nu}$, we can substitute it in Eq. (3.17) to obtain a compact expression for the transition rate. The symbolic summation over final states is replaced by an explicit integration over the continuous-final-states wave numbers k_{zf}. Substitution of (3.18) in (3.17) results in

$$W_{\nu_f}=2\pi n_L\frac{t}{\hbar^2}\int_{-\infty}^{\infty}dk_{zf}\,|\langle n_f l_f k_{zf}\nu_f|H'|\nu_i k_{zi}l_i n_i\rangle|^2\,\mathrm{sinc}^2\left[\frac{\Delta Et}{2\hbar}\right]\ , \tag{C3}$$

where $n_L\equiv N_e/L$ is the longitudinal electron density, and where

$$\Delta E\equiv\mathcal{E}^*_{k_{zi}l_i n_i}-\mathcal{E}_{k_{zf}l_f n_f}-\hbar(\nu_f-\nu_i)\omega_q\ . \tag{C4}$$

We assumed here that the radiation into the particular radiation mode $\mathbf{q},\sigma$ is possible only by transition into a single transverse mode n_f,l_f. If the transverse-states energies are spaced closely enough so that the emission into the radiation mode $\mathbf{q},\sigma$ may involve more than one final transverse state, one must keep the summation over the final transverse states in (C3).

The temporal dependence of (C3) is eliminated when we assume that the interaction time t is long enough (longer than the electron transit time[19]), so that the sinc^2 function may be replaced by a delta function (note, however, that at the same time t must also be kept short enough to satisfy the first-order approximation condition $-P^e_{\nu'\neq\nu}\ll 1$). Under these conditions,

$$\mathrm{sinc}^2\frac{\Delta Et}{2\hbar}\rightarrow 2\pi\frac{\hbar}{t}\delta(\Delta E)\ . \tag{C5}$$

Substitution of (C4) and (C5) into (C3) results in Eq. (3.20) and, consequently, (3.21).

2. The transversely continuous (inherently quantum) case

In analogy to the previous case, we start with an electron wave packet that is distributed around a single eigenstate with a very narrow spectral width. This time, however, the single eigenstate is of infinite extent in all three dimensions, and in order to keep convenient account of the electron number normalization we choose to take a finite (but large) extent wave packet in both the longitudinal and transverse dimensions. In analogy to Eq. (C1) in the previous case, we write the initial wave function as

$$\psi_i(\mathbf{r},t)=(2\pi)^{3/2}\varphi_{\mathbf{k}_i}f(\mathbf{r}-\mathbf{r}_0)\ , \tag{C6}$$

where $\varphi_{\mathbf{k}_i}(\mathbf{r})=|\mathbf{k}_i\rangle$ is a single state function normalized according to (3.15),

$$\int\varphi_{\mathbf{k}}\varphi^*_{\mathbf{k}'}d^3r=\delta(\mathbf{k}-\mathbf{k}')\ , \tag{C7}$$

and where the envelope function f is assumed to have much larger dimensions than the interaction region. Thus it looks constant as long as the classical electron location (the wave-packet spatial center) $\mathbf{r}_0=\mathbf{v}_g(t-t_0)$ is within the interaction region.

As a consequence of these assumptions and the normalization relations for the initial function $\int|\psi_i|^2d^3r=1$ [see Eq. (3.13)] and the eigenstate function $(1/V)\int_V|\varphi_{\mathbf{k}_i}|^2d^3r=(2\pi)^{-3}$, it is possible to assign to the function $f(\mathbf{r}-\mathbf{r}_0)$ in (C6) the constant value $1/\sqrt{V}$, within the interaction region and interaction time. Comparison of (C6) with the definition of the initial function mode expansion (3.12) results in the explicit equation for the initial eigenfunction amplitude $C^0_{k\nu}=\delta_{\nu\nu_i}\delta(\mathbf{k}-\mathbf{k}_i)\sqrt{(2\pi)^3/L}$ [see Eq. (3.22)]. This equation can be substituted into the generic equation for the

[19]To show that the interaction time for which the transient effects may be neglected, is a time longer than the electron transit time, we first estimate the frequency bandwidth that is associated with a finite interaction time. This bandwidth is calculated by relaxing the conservation of energy condition (2.13) and writing it as an inequality $|\mathcal{E}_{k_{zi}}-\mathcal{E}_{k_{zf}}-\hbar\omega|<\hbar\pi/t$. This inequality together with the conservation of momentum condition (2.14), results in the bandwidth

$$\Delta\omega_t=\frac{v_z}{1-\beta_z\cos\Theta_q}2\pi/(tv_z)\ .$$

In order to be able to neglect the line broadening due to finite interaction time, this linewidth must be much smaller than the linewidth due to finite interaction length (2.31) $\Delta\omega_t\ll\Delta\omega_L$. This yields the condition $t\gg t_{\mathrm{tr}}$, where $t_{\mathrm{tr}}=L/v_z$ is the transit time of the electron through the interaction region.

transition rate (3.17), resulting in Eq. (3.23), where we replaced the symbolic summation over $\mathbf{k}$ in (3.17) by a three-dimensional integration in $\mathbf{k}$ space, and again we made use of relation (C5) for time t large with respect to the transit time.

In special cases such as a laminated structure, we can proceed from Eq. (3.23) by developing further the matrix element in the integrand and performing the integration over $\mathbf{k}_{\perp f}$. The transverse coordinates integration implied by the matrix element in Eq. (3.23) is performed over the interaction region with the electron wave function [(3.25) and (3.33)] and the perturbation Hamiltonian (3.28). This results in sinc function dependencies on the transverse momentum mismatches:

$$\frac{1}{(2\pi)^2}\int_{-L_x/2}^{L_x/2}dx\int_{-L_y/2}^{L_y/2}dy\,\exp[i(\mathbf{k}_{\perp i}\pm\mathbf{q}_\perp-\mathbf{k}_{\perp f})\cdot\mathbf{r}_\perp]=\frac{L_xL_y}{(2\pi)^2}\mathrm{sinc}\frac{(k_{xi}\pm q_x-k_{xf})L_x}{2}\mathrm{sinc}\frac{(k_{yi}\pm q_y-k_{yf})L_y}{2}\ . \tag{C8}$$

When substituted in (3.23), the resulting sinc^2 functions would behave as very narrow functions when L_x, L_y are large. We may replace them with delta functions, if the line broadening they introduce is small in comparison to the longitudinal finite-interaction length broadening (see Sec. III.D). Hence substituting in (3.23) Eq. (C8) and the limit relation

$$\mathrm{sinc}^2(k_{x,y_i}\pm q_{x,y}-k_{x,y_f})L_{x,y}/2\rightarrow 2\pi\delta(k_{x,y_i}\pm q_{x,y}-k_{x,y_f}) \tag{C9}$$

and subsequently performing the integration over the final transverse states $\mathbf{k}_{\perp f}$ in (3.23) leaves finally a factor $(L_xL_y)^2/(L_xL_y)=L_xL_y$ on the right-hand side of the transition rate equation which makes it dependent only on the longitudinal density $n_L=L_xL_yn_v$. The only $\mathbf{k}$ space integration left (over k_{zf}) can now be replaced by integration over $\mathcal{E}_{k_{zf}}$, from which the delta function dependence on the final energy leads directly to the Fermi golden rule equations for this case [(3.23),(3.30),(3.31)] in complete analogy to the derivation of (3.20) and (3.21).

3. The transversely continuous classical case

The initial wave packet we take in this case is (3.32),

$$\psi_i(\mathbf{r}^e,0)=(2\pi)^{3/2}/L^{1/2}\varphi_{\mathbf{k}^e_{\perp 0}k^e_{zi}}(\mathbf{r}^e)f_\perp[\mathbf{r}^e_\perp-\mathbf{r}^e_{\perp\mathrm{cl}}(z)]\ .$$

This wave packet should be compared with the corresponding expansion in case (1) [see Eq. (C1)] and case (2) [see Eq. (C6)]. It is essentially the same wave packet as (C6), but based on our previous experience we factorized out the longitudinal envelope function and assigned to it the constant value $1/\sqrt{L}$, as in case (1). Contrary to case (2), the transverse envelope function is a narrow function that represents a composition of many transverse eigenstates. The initial total wave-function normalization $\int|\psi_i|^2d^3r=1$ and the eigenmode normalization

$$(1/L)\int_0^L|\varphi_{\mathbf{k}_{\perp 0}k_z}(\mathbf{r})|^2dz=(2\pi)^{-3}$$

[implied by (3.15)] lead to the conclusion that $f_\perp$ is normalized according to $\int_{-\infty}^{\infty}f_\perp^2d^2r^e_\perp=1$.

In order to propagate the wave packet in time, we expand it in terms of transverse eigenfunctions by substituting in a Fourier integral decomposition of the envelope function $f(\mathbf{r}^e_\perp)$,

$$\begin{aligned}f_\perp(\mathbf{r}^e_\perp)&=\frac{1}{2\pi}\int_{-\infty}^{\infty}d^2k^e_\perp\chi(\mathbf{k}^e_\perp)e^{i\mathbf{k}^e_\perp\cdot\mathbf{r}^e_\perp}\ ,\\ \chi(\mathbf{k}^e_\perp)&=\frac{1}{2\pi}\int_{-\infty}^{\infty}d^2r^e_\perp f(\mathbf{r}^e_\perp)e^{-i\mathbf{k}^e_\perp\cdot\mathbf{r}^e_\perp}\ .\end{aligned} \tag{C10}$$

Substituting $f_\perp$ in the initial wave-function Eq. (3.32) and comparing to the eigenstates expansion definition (3.12) results in

$$C_{\mathbf{k}^e\nu}(0)=\sqrt{2\pi/L}\ \delta(k^e_z-k^e_{zi})\chi(\mathbf{k}^e_\perp)e^{i\mathbf{k}^e_\perp\cdot\mathbf{r}^e_{\perp\mathrm{cl}}(z)}\delta_{\nu\nu_i}\ . \tag{C11}$$

This equation is identical with the approximate Eq. (3.35) only in the rather limited case, in which the transverse wave packet can still be considered wide enough to assume a single transverse state, so that $\chi(\mathbf{k}^e_\perp)=2\pi\delta(\mathbf{k}^2_\perp)$. Note that $\mathbf{k}^e_{\perp i}=0$ due to the definition of the electron coordinate frame. Substitution of (C11) in (3.17), again replacing the symbolic summation over $\mathbf{k}$ by three-dimensional integration over the initial and final $\mathbf{k}$ spaces, results in

$$W_{\nu_f}=\frac{t}{\hbar^2}(2\pi)n_L\int_{-\infty}^{\infty}d^3k^e_f\left|\int_{-\infty}^{\infty}d^2k^e_\perp\langle\nu_f\mathbf{k}^e_f|H'\chi(\mathbf{k}^e_\perp)e^{i\mathbf{k}^e_\perp\cdot\mathbf{r}^e_{\perp\mathrm{cl}}(z)}|\mathbf{k}^e\nu_i\rangle\mathrm{sinc}\left[\frac{\mathcal{E}_{\mathbf{k}}-\mathcal{E}_{\mathbf{k}_f}-\hbar\omega(\nu_f-\nu_i)}{2\hbar}t\right]\right|^2, \tag{C12}$$

where $n_L\equiv N_e/L$ is the longitudinal electron density.

Because of the choice of coordinates, for which $v_{g\perp}=(1/\hbar)\nabla_{\mathbf{k}_\perp}\mathcal{E}_{\mathbf{k}}=0$, the equality $\mathcal{E}_{\mathbf{k}}\approx\mathcal{E}_{\mathbf{k}^e_{\perp 0}k^e_{zi}}$ is maintained up to first order in $\hbar$. Thus the sinc function can be taken out of the $\mathbf{k}^e_\perp$ integration in (C12). What is left, then, is the integral over $\chi(\mathbf{k}^e_\perp)$ times $\exp[i\mathbf{k}^e_\perp\cdot\mathbf{r}^e_{\perp\mathrm{cl}}(z)]$ times the initial transverse eigenfunctions (which are transverse plane waves in our model). This integral is simply the inverse Fourier transform of $\chi(\mathbf{k}_\perp)$ [see Eq. (C10)] displaced by $\mathbf{r}^e_{\perp\mathrm{cl}}(z)$, and it yields the initial envelope function $f_\perp[\mathbf{r}^e_\perp-\mathbf{r}^e_{\perp\mathrm{cl}}(z^e)]$. Hence Eq. (C12) becomes

$$W_{\nu_f}=\frac{t}{\hbar^2}(2\pi)^3 n_L\int_{-\infty}^{\infty}d^3k_f^e\,|\langle\nu_f k_{zf}^e\mathbf{k}_{\perp f}^e\,|\,H'f[\mathbf{r}_\perp^e-\mathbf{r}_{\perp\mathrm{cl}}^e(z^e)]\,|\,\mathbf{k}_{\perp 0}^e k_{zi}^e\nu_i\rangle\,|^2\mathrm{sinc}^2\left[\frac{\mathcal{E}_{\mathbf{k}_i}-\mathcal{E}_{\mathbf{k}_f}-\hbar\omega(\nu_f-\nu_i)}{2\hbar}\right]. \quad \text{(C13)}$$

Taking advantage of the narrowness of the envelope function relative to the interaction Hamiltonian results in

$$W_{\nu_f}=\frac{t}{\hbar^2}(2\pi)^3 n_L\int_{-\infty}^{\infty}d^3k_f^e\,|\langle\nu_f k_{zf}^e\,|\,H'[\mathbf{r}_{\perp\mathrm{cl}}^e(z^e),z^e]\,|\,k_{zi}^e\nu_i\rangle\,|^2\,|\langle\mathbf{k}_{\perp f}^e\,|\,f[\mathbf{r}_\perp^e-\mathbf{r}_{\perp\mathrm{cl}}^e(z^e)]\,|\,\mathbf{k}_{\perp 0}^e\rangle\,|^2$$
$$\times\mathrm{sinc}^2\left[\frac{\mathcal{E}_{\mathbf{k}_i}-\mathcal{E}_{\mathbf{k}_f}-\hbar\omega(\nu_f-\nu_i)}{2\hbar}t\right]^2. \quad \text{(C14)}$$

In Eq. (C14) we used the assumption that $f_\perp(\mathbf{r}_\perp^e-\mathbf{r}_{\perp\mathrm{cl}}^e)$ is a narrow function relative to H' in the transverse dimensions. Thus it forces the value $\mathbf{r}_\perp^e=\mathbf{r}_{\perp\mathrm{cl}}^e$ in the transverse coordinates dependence of H'. We also assumed that $\mathbf{r}_{\perp\mathrm{cl}}^e(z^e)$ changes as a function of z^e much slower than the interaction Hamiltonian H'. Consequently the spatial integration implied in the matrix element definition was factorized, and the envelope function together with the transverse coordinates integration were taken out of the perturbation Hamiltonian matrix element, which is then left only with z^e integration. The transverse coordinates integration implied in the envelope function matrix element in (C14) is nothing else but the Fourier transform of the envelope function $\chi(\mathbf{k}_\perp)$ (C10). The integration over $\mathbf{k}_{\perp f}^e$ of the envelope function matrix element can now be executed explicitly even without knowledge of χ, simply by applying Parsewal's theorem:

$$\int_{-\infty}^{\infty}d^2k_\perp^2\,|\,\chi(\mathbf{k}_\perp^e)\,|^2=\int_{-\infty}^{\infty}d^2r_\perp^e\,|\,f(\mathbf{r}_\perp^e)\,|^2=1\,. \quad \text{(C15)}$$

This results in the transition rate equation for the transversely classical case, Eq. (3.36).

APPENDIX D: SECOND QUANTIZATION OF THE KLEIN-GORDON EQUATION

The Klein-Gordon equation for a relativistic particle is

$$\left[i\hbar\frac{\partial}{\partial t}+eV\right]^2\psi=c^2(-i\hbar\nabla+e\,\mathbf{A})^2\psi+m^2c^4\psi\,. \quad \text{(D1)}$$

The Hamiltonian that leads to this equation is (Schweber, 1961)

$$H=\int d^3r\{\hbar^2\dot\psi^*\dot\psi-e^2V^2\psi^*\psi+c^2[(i\hbar\nabla+e\,\mathbf{A})\psi^*]\cdot[(-i\hbar\nabla+e\,\mathbf{A})\psi]+m^2c^4\psi^*\psi\}\,. \quad \text{(D2)}$$

This Hamiltonian has two canonical variables ψ and ψ^*. Following the ordinary procedure of second quantization, the corresponding canonical momenta are found to be

$$\pi=i\hbar\left[-i\hbar\frac{\partial}{\partial t}+eV\right]\psi^* \quad \text{(D3)}$$

and π^*.

We are interested in problems where the electromagnetic potentials are the sum of static wiggler potentials V_w, $\mathbf{A}_w$ and radiation potentials V_s, $\mathbf{A}_s$. Hence the Hamiltonian can be divided into three parts:

$$H=H_{\mathrm{free}}+H_w+H_{\mathrm{int}}\,, \quad \text{(D4)}$$

where H_{free} is the Hamiltonian that describes a free-space particle:

$$H_{\mathrm{free}}=\int d^3r[\hbar^2\dot\psi^*\dot\psi+\psi^*(-c^2\hbar^2\nabla^2+m^2c^4)\psi]\,; \quad \text{(D5)}$$

H_w is the Hamiltonian describing the interaction between a charged Klein-Gordon particle and the wiggler field in the absence of the radiation field:

$$H_w=\int d^3r\,\psi^*\mathcal{H}_w\psi\,,$$
$$\mathcal{H}_w\equiv-e^2V_w^2+c^2[-i\hbar\nabla\cdot e\,\mathbf{A}_w+e\,\mathbf{A}_w\cdot(-i\hbar\nabla)+e^2\mathbf{A}_w^2]\,; \quad \text{(D6)}$$

and H_{int} is the Hamiltonian that describes the integration between the charged Klein-Gordon particle and the radiation field in the presence of the wiggler field:

$$H_{\mathrm{int}}=\int d^3r\,\psi^*\mathcal{H}_{\mathrm{int}}\psi\,,$$
$$\mathcal{H}_{\mathrm{int}}\equiv 2ec^2\left[-\frac{e}{c^2}V_wV_s+\frac{-i\hbar\nabla\cdot\mathbf{A}_s+\mathbf{A}_s\cdot(-i\hbar\nabla)}{2}+e\,\mathbf{A}_w\cdot\mathbf{A}_s\right]+e^2(c^2\mathbf{A}_s^2-V_s^2)\,. \quad \text{(D7)}$$

We follow the ordinary second quantization procedure, as carried out, for example, by Bjorken and Drell (1965) for a particle in free space. In order to quantize the Hamiltonian, one replaces the field ψ by a field operator, so that it will satisfy the commutation relation

$$[\psi(\mathbf{r},t),\pi(\mathbf{r}',t)]=i\hbar\delta(\mathbf{r}-\mathbf{r}')\,. \quad \text{(D8)}$$

As in the standard second quantization procedure (Bjork-

en and Drell, 1965), we choose to write the field operator in the momentum representation

$$\psi(\mathbf{r},t)=\frac{1}{(2\pi)^{3/2}}\int d^3k\frac{1}{\sqrt{2\mathcal{E}_{\mathbf{k}}}}(e^{-i(\mathcal{E}_{\mathbf{k}}/\hbar)t+i\mathbf{k}\cdot\mathbf{r}}a_{\mathbf{k}} +e^{i(\mathcal{E}_{\mathbf{k}}/\hbar)t+i\mathbf{k}\cdot\mathbf{r}}b_{\mathbf{k}}^{\dagger}) . \quad \text{(D9)}$$

Here $\mathcal{E}_{\mathbf{k}}$ is the energy of a free electron or positron with momentum $\hbar\mathbf{k}$, $a_{\mathbf{k}}$ is the annihilation operator of a free-electron state $|\mathbf{k}\rangle$, and $b_{\mathbf{k}}^{\dagger}$ is the creation operator of a free-positron state $|\mathbf{k}\rangle$. These operators obey the following commutation relations:

$$\begin{aligned}&[a_{\mathbf{k}},a_{\mathbf{k}'}^{\dagger}]=[b_{\mathbf{k}},b_{\mathbf{k}'}^{\dagger}]=\delta(\mathbf{k}-\mathbf{k}') ,\\ &[a_{\mathbf{k}},a_{\mathbf{k}'}]=[a_{\mathbf{k}}^{\dagger},a_{\mathbf{k}'}^{\dagger}]=[b_{\mathbf{k}},b_{\mathbf{k}'}]=[b_{\mathbf{k}}^{\dagger},b_{\mathbf{k}'}^{\dagger}]=0 ,\\ &[a_{\mathbf{k}},b_{\mathbf{k}'}]=[a_{\mathbf{k}},b_{\mathbf{k}'}^{\dagger}]=[a_{\mathbf{k}}^{\dagger},b_{\mathbf{k}'}^{\dagger}]=[a_{\mathbf{k}}^{\dagger},b_{\mathbf{k}'}]=0 .\end{aligned} \quad \text{(D10)}$$

It can be shown that this representation of the field operator ψ (D9) satisfies the commutation relation (D8) for any potential V. The momentum representation (D9) is an intermediate picture representation.[20] In this picture the time derivatives in the Hamiltonian (D2) can be explicitly executed.

Substitution of (D9) in (D5) and (D6) and going back to the Schrödinger picture by eliminating the time dependence of all operators results in equations for the quantized Hamiltonians,

$$\begin{aligned}H_{\text{free}}&=\int d^3k\ \mathcal{E}_k(a_{\mathbf{k}}^{\dagger}a_{\mathbf{k}}+b_{\mathbf{k}}b_{\mathbf{k}}^{\dagger}) ,\\ H_w&=\int\int d^3k\,d^3k'(h_{w_{\mathbf{k}'\mathbf{k}}}a_{\mathbf{k}'}^{\dagger}a_{\mathbf{k}}+h_{w_{\mathbf{k}'\mathbf{k}}}^{*}b_{\mathbf{k}'}b_{\mathbf{k}}^{\dagger} +h_{w_{\mathbf{k}'(-\mathbf{k})}}a_{\mathbf{k}'}^{\dagger}b_{\mathbf{k}}^{\dagger}+h_{w_{(-\mathbf{k})\mathbf{k}'}}^{*}b_{\mathbf{k}'}a_{\mathbf{k}}) ,\end{aligned} \quad \text{(D11)}$$

where

$$h_{w_{\mathbf{k}'\mathbf{k}}}=\frac{1}{(2\pi)^3}\frac{1}{2\sqrt{\mathcal{E}_{\mathbf{k}}\mathcal{E}_{\mathbf{k}'}}}\int d^3r\,e^{-i\mathbf{k}'\cdot\mathbf{r}}\mathcal{H}_w e^{i\mathbf{k}\cdot\mathbf{r}} . \quad \text{(D12)}$$

In order to diagonalize the unperturbed Hamiltonian $H_{\text{free}}+H_w$, one has to find a unitary transformation u that defines a new set of "wiggler states" annihilation operators:

$$\begin{aligned}\tilde{a}_{\tilde{\mathbf{k}}}&\equiv\int d^3k[u_{--}^{*}(\mathbf{k},\tilde{\mathbf{k}})a_{\mathbf{k}}+u_{-+}^{*}(\mathbf{k},\tilde{\mathbf{k}})b_{\mathbf{k}}^{\dagger}] ,\\ \tilde{b}_{\tilde{\mathbf{k}}}^{\dagger}&\equiv\int d^3k[u_{+-}^{*}(\mathbf{k},\tilde{k})a_{\mathbf{k}}+u_{++}^{*}(\mathbf{k},\tilde{\mathbf{k}})b_{\mathbf{k}}^{\dagger}] .\end{aligned} \quad \text{(D13)}$$

The unitary matrix $u(\mathbf{k},\tilde{\mathbf{k}})$ is the Hilbert representation of the transformation u, which diagonalizes the unperturbed Hamiltonian $H_{\text{free}}+H_w$. It can be constructed in principle by a standard diagonalization procedure of the Hermitian matrix $(\mathcal{E}_{\mathbf{k}}\delta_{\mathbf{k}'\mathbf{k}}+h_{w_{\mathbf{k}'\mathbf{k}}})$, the result of which is a diagonal matrix of the wiggler Hamiltonian eigenvalues $(\tilde{E}_{\tilde{\mathbf{k}}})$. Note that the transformation (D13) involves in general mixing of electron and positron states. However, in all relevant practical cases, and in particular when $V_w=0$, the mixing submatrices u_{-+},u_{+-} are negligible or vanishing, which means that the wiggler by itself does not generate pairs.

It can now be shown that the newly defined creation and annihilation operators of "wiggler states" satisfy commutation relations similar to the free-particles commutation relations,

$$[\tilde{a}_{\mathbf{k}},\tilde{a}_{\tilde{\mathbf{k}}'}^{\dagger}]=[\tilde{b}_{\tilde{\mathbf{k}}},\tilde{b}_{\tilde{\mathbf{k}}'}^{\dagger}]=\delta(\tilde{\mathbf{k}}-\tilde{\mathbf{k}}') , \quad \text{(D14)}$$

and all the other combinations commute to zero. This makes it possible to define the wiggler eigenfunction electron occupation states $|\tilde{\mathbf{k}}\rangle\equiv\tilde{a}_{\tilde{\mathbf{k}}}^{\dagger}|0\rangle$ that are orthogonal to each other. The energy of the state $|\tilde{\mathbf{k}}\rangle$ is $\tilde{\mathcal{E}}_{\tilde{\mathbf{k}}}$—one of the eigenvalues of the unperturbed Hamiltonian $H_{\text{free}}+H_w$. Using this new set of eigenstates one can follow the first-order perturbation procedure outlined in Sec. III.A to calculate the transition rate into the photon state $|\nu_f\rangle$. Since we already concluded that the wiggler does not mix electron and positron states, and since only one kind of particle (let us say electrons) is injected into the wiggler, we can simplify our analysis and neglect all positron-creating operators in the previous equations (substitute $u_{-+}=u_{+-}=\tilde{b}_{\tilde{\mathbf{k}}}=0$). Substitution of (D9) and (D13) in (D7) results in the representation of the interaction Hamiltonian in the $\tilde{\mathbf{k}}$ space

$$H_{\text{int}}=\int\int d^3\tilde{\mathbf{k}}\,d^3\tilde{\mathbf{k}}'\tilde{h}_{\tilde{\mathbf{k}}'\tilde{\mathbf{k}}}\tilde{a}_{\tilde{\mathbf{k}}}^{\dagger}\tilde{a}_{\tilde{\mathbf{k}}} , \quad \text{(D15)}$$

where

$$\tilde{h}_{\tilde{\mathbf{k}}'\tilde{\mathbf{k}}}=\int\int d^3k'd^3k\,u_{--}(\mathbf{k}',\tilde{\mathbf{k}}')u_{--}^{*}(\mathbf{k},\tilde{\mathbf{k}})\frac{1}{(2\pi)^3} \times\frac{1}{2\sqrt{\mathcal{E}_k'\mathcal{E}_k}}\int d^3r\,e^{-i\mathbf{k}'\cdot\mathbf{r}}\mathcal{H}_{\text{int}}e^{i\mathbf{k}\cdot\mathbf{r}} . \quad \text{(D16)}$$

Using the commutation relations it is straightforward to show that the matrix element of (D15) between states $|\tilde{\mathbf{k}}'\rangle$ and $|\tilde{\mathbf{k}}\rangle$, which is needed for the computation of the radiative transition rate equation (3.17), is

$$\langle\tilde{\mathbf{k}}'|H_{\text{int}}|\tilde{\mathbf{k}}\rangle=\tilde{h}_{\tilde{\mathbf{k}}'\tilde{\mathbf{k}}} . \quad \text{(D17)}$$

In order to obtain a more explicit equation for the matrix element computation we define the wiggler

[20] In this picture the time development of an operator is

$$\hat{O}(t)=e^{i(H_{\text{free}}/\hbar)t}\hat{O}(0)e^{-i(H_{\text{free}}/\hbar)t} .$$

We do not refer to this picture as the interaction picture, since H_w is not regarded here as a perturbation. For a free electron, this representation is nothing but the Heisenberg representation.

eigenwave function of the electron

$$\frac{1}{\sqrt{\mathcal{E}_{\mathbf{k}}}}\varphi_{\mathbf{k}}(\mathbf{r})\equiv\frac{1}{(2\pi)^{3/2}}\int d^3k\frac{1}{\sqrt{\mathcal{E}_k}}u^*_{--}(\mathbf{k},\tilde{\mathbf{k}})e^{i\mathbf{k}\cdot\mathbf{r}}\ . \tag{D18}$$

This wave function diagonalizes the unperturbed first quantization Hamiltonian, and therefore it is the eigenmode solution of the Klein-Gordon equation (D1) in the absence of the radiation field. Using this definition the matrix element is

$$\tilde{h}'_{\tilde{\mathbf{k}}'\tilde{\mathbf{k}}}=\frac{1}{2\sqrt{\tilde{\mathcal{E}}_{\tilde{\mathbf{k}}'}\tilde{\mathcal{E}}_{\tilde{\mathbf{k}}}}}\int d^3r\,\varphi^*_{\tilde{\mathbf{k}}'}\mathcal{H}_{\rm int}\varphi_{\tilde{\mathbf{k}}}\ . \tag{D19}$$

In order to obtain an explicit equation for the energy $\tilde{\mathcal{E}}_{\tilde{\mathbf{k}}}$ and complete the computation of the radiative transition rate, one has to solve explicitly the Klein-Gordon equation in the wiggler and, in general, match boundary conditions for the electron wave function at the entrance and exit from the wiggler. However, in practical calculations we will assume that an incoming free-space electron excites predominantly a single wiggler state with $\tilde{\mathcal{E}}_{\tilde{\mathbf{k}}}=\mathcal{E}_{\mathbf{k}_i}=\gamma_i mc^2$, and after interaction the electron exits with a single state energy $\mathcal{E}_{\tilde{\mathbf{k}}'}=\mathcal{E}_{\mathbf{k}_f}=\gamma_f mc^2$. As in Sec. III.A we now choose the sourceless radiation modes to be described in the transverse gauge ($\nabla\cdot\mathbf{A}_s=0=V_s$). Hence the first-order perturbation Hamiltonian matrix element [(D19), (D7)] can be written as

$$\tilde{h}'_{\tilde{\mathbf{k}}'\tilde{\mathbf{k}}}=\int d^3r\frac{1}{\sqrt{\gamma_i\gamma_f}}\varphi^*_{\tilde{\mathbf{k}}'}H'_{\rm NR}\varphi_{\tilde{\mathbf{k}}}\ , \tag{D20}$$

where $H'_{\rm NR}$ is the nonrelativistic Schrödinger equation interaction Hamiltonian as given in Eq. (3.3). Equation (D20) is identical to the matrix element of the relativistic perturbation Hamiltonian (3.47), which was derived in this paper in an alternative less rigorous way.

One can conclude that the perturbation procedure based on the Schrödinger equation, which we formulated in Secs. III.A–III.D is extendable to the relativistic regime. In the relativistic regime the entire formulation remains valid with the introduction of two modifications to the perturbation Hamiltonian matrix element calculation: (a) The functions to be used in the overlap integral of the matrix element are the Klein-Gordon eigenfunctions, instead of the Schrödinger equation solutions. (b) The perturbation Hamiltonian should be multiplied by the factor $(\gamma_i\gamma_f)^{-1/2}$.

APPENDIX E: FIRST-ORDER EXPANSION OF THE EMISSION AND ABSORPTION DETUNING PARAMETERS

In order to calculate the explicit dependence of the emission detuning parameter $\bar{\theta}_e$ in Eq. (3.69) on ω and k_{zi} in the case of general recoil (continuous transverse states), one has to use the conservation of energy and the conservation of transverse momentum conditions,

$$\mathcal{E}_{\mathbf{k}_i}-\mathcal{E}_{\mathbf{k}_e}=\hbar\omega\ , \tag{E1}$$

$$\mathbf{k}_{\perp i}-\mathbf{k}_{\perp e}=\mathbf{q}_\perp+\mathbf{k}_{w\perp}\ . \tag{E2}$$

As in Sec. II.G, these two equations can be solved by expanding the final electron energy to second order around the initial electron energy,

$$\mathcal{E}_{\mathbf{k}_e}\approx\mathcal{E}_{\mathbf{k}_i}-\hbar\bar{v}_z(k_{zi}-k_{ze})-\hbar\bar{\mathbf{v}}_\perp\cdot(\mathbf{k}_{\perp i}-\mathbf{k}_{\perp f})+\tfrac{1}{2}\hbar^2\sum_{ij}(\mathbf{k}_i-\mathbf{k}_e)_i\left[\frac{1}{m^*}\right]_{ij}(\mathbf{k}_i-\mathbf{k}_e)_j\ , \tag{E3}$$

where

$$\bar{\mathbf{v}}\equiv\frac{1}{\hbar}\frac{\partial\mathcal{E}_{\mathbf{k}}}{\partial\mathbf{k}}\bigg|_{\mathbf{k}=\mathbf{k}_i}$$

[see Eq. (2.81)] and

$$\left[\frac{1}{m^*}\right]_{ij}=\frac{1}{\hbar^2}\frac{\partial^2\mathcal{E}_{\mathbf{k}}}{\partial k_i\partial k_j}\bigg|_{\mathbf{k}=\mathbf{k}_i}$$

[see Eq. (2.88)]. We now substitute (E3) and (E2) in (E1) and solve for $(k_{zi}-k_{ze})$. The substitution of this in the equation for $\bar{\theta}_e$ (3.69) results in the first-order expansion in $\hbar-\bar{\theta}_e=\bar{\theta}+\varepsilon/2$ (3.72), where $\bar{\theta}$, the classical detuning parameter, and ε, the recoil parameter, are given by (3.80) and (3.81). The first-order expansion of $\bar{\theta}_a=\bar{\theta}-\varepsilon/2$ (3.72) is obtained by following the same procedure, starting from (3.70).

We supplement this proof by an alternative derivation of $\bar{\theta}$ and ε, which also reveals the explicit dependence of the detuning parameters $\bar{\theta}_e,\bar{\theta}_a,\bar{\theta}$ on ω (third column of Table I). This derivation ties up to the kinematic considerations analysis of Sec. II.G and takes advantage of the equation for $\delta\omega=\omega_a-\omega_e$ (2.87), which we derived there for the case on which we presently focus, namely, the case of transversely continuous states with general transverse recoil.

The alternative derivation starts by expanding k_{ze} and q_z to first order in $\omega-\omega_e$ (and not in $\hbar$, as we expanded before). The expansion is around ω_e, the center of the emission line, which is defined by $\bar{\theta}_e(\omega_e)=0$. Substituting this expansion in $\bar{\theta}_e$ (3.69) results in

$$\bar{\theta}_e=-\left[\frac{dk_{ze}}{d\omega}+\frac{dq_z}{d\omega}\right]\bigg|_{\omega=\omega_e}L(\omega-\omega_e)\ . \tag{E4}$$

The dependence of k_{ze} on ω is defined implicitly by (E1) and (E2) and the dispersion relation $\mathcal{E}_{\mathbf{k}_e}=\mathcal{E}(k_{ze},\mathbf{k}_{\perp e})$. Using the rules for derivatives of implicit functions, we can write the derivative of k_{ze}, with respect to ω, as

$$\frac{dk_{ze}}{d\omega}=\frac{\partial k_{ze}}{\partial\mathcal{E}_{\mathbf{k}_e}}\frac{d\mathcal{E}_{\mathbf{k}_e}}{d\omega}+\frac{\partial k_{ze}}{\partial\mathbf{k}_{\perp e}}\cdot\frac{d\mathbf{k}_{\perp e}}{d\omega}\ , \tag{E5}$$

where

$$\frac{\partial k_{ze}}{\partial\mathcal{E}_{\mathbf{k}_e}}=\frac{1}{\hbar v_{ze}}\quad\text{and}\quad\frac{\partial k_{ze}}{\partial\mathbf{k}_{\perp e}}=-\frac{\mathbf{v}_{\perp e}}{v_{ze}}\ . \tag{E6}$$

We note that $\mathbf{v}_e \equiv 1/\hbar\,\partial\mathcal{E}_{\mathbf{k}}/\partial\mathbf{k}\,|_{\mathbf{k}=\mathbf{k}_e}$ is not (necessarily) the electron velocity, but it is the synchronism velocity corresponding to the exact solution of the conservation of energy and total momentum conditions at emission [(2.76) and (2.77)]. Assuming the plane-wave radiative dispersion relation $\mathbf{q}=\hat{e}_{\mathbf{q}}\omega/c$ (2.20) in the conservation of energy and transverse momentum conditions [(E1) and (E2)] we obtain

$$\frac{dk_{ze}}{d\omega} = -\frac{1}{v_{ze}}(1-\boldsymbol{\beta}_{\perp e}\cdot\hat{e}_{q\perp}) \ . \tag{E7}$$

Thus the emission detuning parameter is

$$\bar{\theta}_e = \frac{1}{v_{ze}}(1-\boldsymbol{\beta}_e\cdot\hat{e}_q)L(\omega-\omega_e) \ . \tag{E8}$$

Equation (E8) is an exact first-order equation (in terms of $\omega-\omega_e$) for the emission detuning parameter $\bar{\theta}_e$. The parameters $\underline{\beta}_e,\omega_e$ are found from the exact solution of the *full* 3D momentum conservation and energy conservation conditions (2.76) and (2.77), and can be computed in principle to any order of $\hbar$. In order to get practical equations, second-order expansion (in terms of $\hbar$) is employed around $\mathcal{E}_{\mathbf{k}_i}$ in Eq. (2.76) in exactly the same manner as in (E3), except that in the present case the expansion is of $\mathcal{E}_{\mathbf{k}_e}$ around $\mathcal{E}_{\mathbf{k}_i}$. Substitution of the 3D conservation of momentum condition (2.77) results in

$$\omega_e = \frac{v_{ze}k_w}{1-\boldsymbol{\beta}_e\cdot\hat{e}_{\mathbf{q}}} + \frac{\delta\omega}{2} \ . \tag{E9}$$

This equation is correct to first order in $\hbar$. Since this equation is written in terms of the "center *emission* velocity" $\underline{\beta}_e$, it can be directly used in (E8) to eliminate the $\underline{\beta}_e$ terms resulting in

$$\bar{\theta}_e = \frac{k_w L}{\omega_0-\delta\omega}(\omega-\omega_e) = 2\pi\frac{\omega-\omega_e}{\Delta\omega_L}\left[1+\frac{\delta\omega}{\omega_0}\right] \ . \tag{E10}$$

Following the same procedure for the absorption detuning parameter results in

$$\bar{\theta}_a = \frac{k_w L}{\omega_0+\delta\omega}(\omega-\omega_a) = 2\pi\frac{\omega-\omega_a}{\Delta\omega_L}\left[1-\frac{\delta\omega}{\omega_0}\right] , \tag{E11}$$

where $\omega_e=\omega_0=\delta\omega/2$, $\omega_a=\omega_0+\delta\omega/2$ [see Eqs. (2.85) and (2.86)].

Equations (E10) and (E11) can be interpreted as the modifications to the approximate equations (3.89) and (3.90), stemming from the small difference in linewidth between the emission and absorption lines $\Delta\omega_{Le}\approx\Delta\omega_L(1-\delta\omega/\omega_0)$, $\Delta\omega_{La}\approx\Delta\omega_L(1+\delta\omega/\omega_0)$. Written in terms of the classical detuning parameter $\bar{\theta}=2\pi(\omega-\omega_0)/\Delta\omega_L$ and the recoil parameter ε [as in the corresponding Eqs. (3.71) and (3.72)], the modified Eqs. (E10) and (E12) appear as

$$\bar{\theta}_e = \bar{\theta}+\frac{\varepsilon}{2}\left[1+2\frac{\omega-\omega_0}{\omega_0}\right] , \tag{E12}$$

$$\bar{\theta}_a = \bar{\theta}-\frac{\varepsilon}{2}\left[1+2\frac{\omega-\omega_0}{\omega_0}\right] . \tag{E13}$$

In all practical cases, we are interested in frequencies that are within the linewidth,

$$\left|\frac{\omega-\omega_0}{\omega_0}\right| \lesssim \frac{\Delta\omega}{\omega_0} \ll 1 \ .$$

Thus the modifying terms in (E12) and (E13) may be neglected, resulting in the practical equations for the emission and absorption detuning parameters [(3.71),(3.72)] and [(3.89),(3.90)].

APPENDIX F: THE RECOIL PARAMETER AND ITS SYMMETRY PROPERTIES

The recoil parameter ε is defined in Eq. (3.80). For an electron in a uniform wiggler field, the mass tensor elements are given by Eqs. (2.90). Evidently, in the average electron coordinates, the mass tensor forms a diagonal matrix

$$\left[\frac{1}{m^*}\right] = \frac{1}{m\gamma}\begin{bmatrix} 1 & 0 & 0 \\ 0 & 1 & 0 \\ 0 & 0 & \dfrac{1}{\bar{\gamma}^2} \end{bmatrix} . \tag{F1}$$

Thus there is symmetry preference to the axis of average electron motion, and the coordinate system (x^e,y^e,z^e), which is aligned with this axis, is the principal coordinate system of the mass tensor. The equations that define the mass tensor (2.90) are covariant (form invariant) under coordinate rotational transformations. To prove this we examine the mass tensor (2.90) for the case of a coordinate system that is misaligned with respect to the average motion axis (see Fig. 7). Hence $\beta_x\neq 0\neq\beta_z$. For simplicity we choose the special case where $\beta_y=0$, so that the mass tensor is described by a scalar $m^*_{yy}=m\gamma$ and a 2D tensor:

$$\left[\frac{1}{m^*}\right] = \frac{1}{m\gamma}\begin{bmatrix} \dfrac{1}{\gamma_x^2} & -\beta_x\beta_z \\ -\beta_x\beta_z & \dfrac{1}{\gamma_z^2} \end{bmatrix} . \tag{F2}$$

The eigenvalues of this matrix should be the diagonal terms of the mass tensor, once it is diagonalized by performing a coordinate rotational transformation into its principal coordinate system. Indeed the eigenvalue equation of the matrix in (F2) is

$$\left[\frac{1}{m\gamma\gamma_z^2}-\lambda\right]\left[\frac{1}{m\gamma\gamma_x^2}-\lambda\right]-\frac{\beta_x^2\beta_z^2}{(m\gamma)^2}=0 \ , \tag{F3}$$

and using the relations $1/\gamma_{x,z}^2=1-\beta_{x,z}^2$, it is straightforwardly solved to result in

$$\lambda_1=(1-\beta_x^2-\beta_z^2)/(m\gamma), \quad \lambda_2=1/(m\gamma) \ . \tag{F4}$$

These eigenmass tensor components are identical to the ones obtained in (F1) by direct substitution $\beta_x^e=\beta_y^e=0$ in (2.90) in the averaged electron coordinates.

The recoil parameter (3.80) can be expressed in a more explicit way by substituting in the mass tensor $1/m^*$, given in the principal coordinates system (F1). This results in Eq. (3.82), which demonstrate the partition of the recoil parameter ε into a longitudinal and transverse term (with respect to the average motion axis vector $\hat{e}_e \equiv \hat{e}_z e$). Yet an alternative equation for ε can be found by pulling out the term $(q_z^e+k_{wz}^e)^2$ from the parentheses in (3.82) and substituting the synchronism condition $q_z^e+k_{wz}^e=\omega_0/\bar{v}$, where ω_0 is the classical synchronism frequency $[\bar{\theta}(\omega_0)=0]$,

$$\varepsilon=\frac{\hbar L}{\bar{v}}\frac{1}{m\gamma}\frac{\omega_0^2}{\bar{v}^2}\left[\frac{1}{\bar{\gamma}^2}+\frac{(\mathbf{q}_\perp^e+\mathbf{k}_{w\perp}^e)^2}{(q_z^e+k_{wz}^e)^2}\right] . \tag{F5}$$

The second term in large parentheses can be identified as the tangent of the angle between the recoil vector $\mathbf{q}+\mathbf{k}_w$ and the electron motion axis $\hat{e}_e$ [defined in (3.85)]. Both the recoil parameter ε and the detuning parameter $\bar{\theta}$ can thus be written in terms of this angle $\Theta_{\rm rec}$, resulting in Eqs. (3.84) and (3.86), respectively.

It is instructive to note that, as in many scattering problems (e.g., Bragg diffraction from the crystal lattice), the relevant dynamic parameters depend on the *total* recoil momentum, which in our case is $\mathbf{q}+\mathbf{k}_w$ (see footnote 15). Nevertheless, for practical applications it is convenient to express ε and $\bar{\theta}$ in terms of the separate wave number amplitudes $|\mathbf{q}|=\omega/c$ and $|\mathbf{k}_w|=k_w$, their angles with respect to the electron average motion angle $\Theta_{\rm rec}$ to these angles (3.87), providing a most general equation for $\bar{\theta}$ and ε for arbitrary electron motion axis, wiggler axis, and radiation direction.

The general equation for ε [(3.84),(3.87)] and $\bar{\theta}$ (3.88) can be easily reduced to the most common case of "on-axis propagation and emission," for which $\Theta_{\rm rec}=0=\Theta_q^e$, $\Theta_w^e=\pi=\Theta_w^a$, and consequently $\varepsilon=\hbar L\omega_0^2/(m\gamma\bar{v}^3\bar{\gamma}^3)$, $\bar{\theta}=(\omega(1-\bar{\beta})-k_w\bar{v})L/\bar{v}$. It is also instructive in this limit to present explicitly the velocity parameter for the case of the magnetic bremsstrahlung FEL. In this case the energy dispersion relation of an electron in a uniform transverse wiggler is

$$\mathcal{E}_{\mathbf{k}}=c[(\hbar k)^2+(mc)^2(1+\bar{a}_w^2)]^{1/2}(=\gamma mc^2) ,$$

where $\bar{a}_w=e\bar{A}_w/(mc)$ is the average wiggler strength parameter (Steinberg *et al.*, 1986), and the wiggler period oscillating terms were averaged out. The electron canonical momentum $\mathbf{p}_e=\hbar\mathbf{k}$ indicates the average electron propagation direction. Its transverse components are constant in a uniform wiggler, and its longitudinal component is the wiggler period averaged longitudinal momentum $\bar{p}_z$. In the case of on-axis propagation, the electron average motion axis and the wiggler axis coincide and $\mathbf{p}_{c\perp}=0$. The calculation of the average motion velocity and the mass tensor components proceeds on as in Sec. II.G, resulting in $\bar{v}\equiv\bar{v}_z=\bar{p}_z/(\gamma m)$, where $\bar{p}_z=mc(\gamma^2-1-\bar{a}_w^2)^{1/2}$, and $\bar{\gamma}\equiv\gamma_z=(1-\bar{\beta}_x^2)^{-1/2}=\gamma/\gamma_\perp$, where $\gamma_\perp\equiv(1+\bar{a}_w^2)^{1/2}$. These results and the subsequent equations for spontaneous and stimulated emission are completely consistent with the conventional classic derivation of a uniform wiggler FEL in the on-axis propagation and emission limit (Sprangle and Smith, 1980).

In conclusion of this appendix we try to gain deeper insight into the emission problem by expressing the detuning and recoil parameters in terms of the electron rest frame coordinates and by examining the Lorentz covariance of the parameter equations. Using the Lorentz transformation relations applied for transformation into the rest frame of the electron average motion,

$$\begin{aligned} t_{\rm tr}&=\bar{\gamma}t'_{\rm tr} ,\\ \mathbf{q}_\perp^e+\mathbf{k}_{w\perp}^e&=\mathbf{q}'_\perp+\mathbf{k}'_{w\perp} ,\\ q_z^e+k_{wz}^e&=\bar{\gamma}(q'_z+k'_{wz}) . \end{aligned} \tag{F6}$$

Equation (3.82) reduces into (3.83),

$$\varepsilon=\frac{\hbar t'_{\rm tr}}{m\gamma'}(q'+k'_w)^2=\delta\omega' t'_{\rm tr} , \tag{F7}$$

where

$$\delta\omega'/2=\omega'_0-\omega'_w=\mathcal{E}'_f/\hbar=\hbar(\mathbf{q}'+\mathbf{k}6'_w)^2/(2m\gamma')$$

is the Compton recoil frequency shift of a photon scattered by an electron in rest, with effective mass $m\gamma'$, and $t'_{\rm tr}=L_z^e/(\bar{\gamma}\bar{v})$ is the wiggler transit time (and therefore the electron oscillation time) in the electron rest frame (Gover, 1984). We also use the relations

$$\omega'=\bar{\gamma}(\omega-\mathbf{q}\cdot\bar{\mathbf{v}}),\quad \omega'_0=\bar{\gamma}\mathbf{k}_w\cdot\bar{\mathbf{v}} , \tag{F8}$$

to express (3.86) in terms of the rest frame coordinates:

$$\theta=2\pi(\omega-\omega'_0)t'_{\rm tr} . \tag{F9}$$

Evidently $\bar{\theta}$ and ε are scalar quantities that can be evaluated in any Lorentz frame. The detuning parameter $\bar{\theta}$ is the relative phase measured in the electron rest frame between the radiation frequency ω' and the electron "wiggling" frequency ω'_0 during an oscillation period $t'_{\rm tr}$. The recoil parameter $\varepsilon=\delta\omega t'_{\rm tr}$ is the shift in this phase due to the doppler shift associated with the quantum recoil effect.

Both (F7) and (F9) could have been proved also in an alternative, simpler way, by evaluating Eq. (3.75) for ε and (3.91) for $\bar{\theta}$ directly in the electron rest frame. This is permissible, since these equations are covariant and can be evaluated at *any* Lorentz frame. To prove the covariance we use the Lorentz transformation formula

$$\Delta\omega=\gamma(\Delta\omega'+\beta_L c\Delta q'_z) \tag{F10}$$

and the dispersion relation

$$\Delta q_z=\frac{\Delta\omega}{v_{qgz}} , \tag{F11}$$

where β_L is the axial velocity of an arbitrary Lorentz

frame and v_{qgz} is the group velocity of the electromagnetic mode (for plane waves $v_{qgz}=c\cos\Theta_q$). Using (F10) and (F11), we see that the factors in the numerator and the denominator cancel each other out in both (3.75) and (3.91), resulting in, respectively, $\varepsilon=(\omega'_a-\omega'_e)/\Delta\omega'_L$ and $\bar{\theta}=2\pi(\omega'-\omega'_0)/\Delta\omega'_L$.

The main explicit equations that we derived for ε and $\bar{\theta}$ [(3.80)–(3.82)] were shown above to be covariant under rotational transformations, but they are not covariant under general Lorentz transformations. The reason for this lack of covariance is that we limited our analysis to static wigglers, so that $\omega_w=0$ (but in any other frame different from the laboratory frame, $\omega'_w\neq 0$). Fully Lorentz invariant equations may be recovered by repeating the classical limit expansion procedure of this appendix and of Sec. II.G, but replacing the emission and absorption frequencies ω_e,ω_a in the conservation of energy conditions [(2.76),(2.78)] with $\omega_e-\omega_w$ and $\omega_a-\omega_w$. This further generalization will not be carried out here.

APPENDIX G: THE INHOMOGENEOUS BROADENING REGIME AND HOLE-BURNING EFFECT

If the homogeneous broadening line-shape function is much narrower than the inhomogeneous line-shape function, then the convolution integral inferred in (4.26) picks out of the electron distribution function $f(k_z)$ only electrons with initial wave numbers in the regions $k_{zu}-\Delta k_{zh}/2<k_{zi}<k_{zu}+\Delta k_{zh}/2$ and $k_{zd}-\Delta k_{zh}/2<k_{zi}<k_{zd}+\Delta k_{zh}/2$, where k_{zu},k_{zd} are the exact solutions of the energy and momentum conservation conditions (4.29) *for a given frequency* ω. This result in Eqs. (4.27) and (4.28) for the inhomogeneous broadening emission rate. The electrons in the two wave-number regions are essentially the upper- and lower-level populations of a two-level quantum system. They are represented by the shaded area in the electron distribution function shown in Fig. 10(a). The figure and Eq. (4.27) illustrate that the net gain in this limit is proportional to the population inversion between the levels, and that in the classical limit [Fig. 10(b)] the population inversion condition $f(k_{zu})>f(k_{zd})$ is equivalent to the "slope condition" for plasma instabilities $f'(k_{zi}=p_{z\mathrm{ph}}/\hbar)>0$ and to the Čerenkov condition $v_{z0}\equiv(1/\hbar)(d\mathcal{E}/dk_z)\,|\,k_{z0}>v_{\mathrm{ph}}\equiv\omega/(q_z+k_w)$ (Gover and Yariv, 1975).

The initial wave number width due to the homogeneous broadening $-\Delta k_{zh}$ is the range of initial wave numbers k_{zi} around k_{zu} and k_{zd}, which for a *fixed* ω and *exact conservation of energy condition* conserve momentum in the transition, within the momentum uncertainty $\Delta k_z=\Delta\theta\equiv\Delta\bar{\theta}/L$ allowed by the homogeneous broadening process [for finite-length homogeneous broadening (3.67), $\Delta\theta=2\pi/L$, and for Lorentzian broadening function (3.65), $\Delta\theta=2\pi\kappa$]. The wave number width Δk_{zh} illustrated in Fig. 10(a) should be distinguished from the wave number mismatch widths $\Delta k_{ze}=\Delta k_{za}=2\pi/L$, which are illustrated in Fig. 3. The latter wave number width parameters, contrary to the definition given above for Δk_{zh}, are the final electron wave number uncertainties of an electron *for a given initial wave number,* emitting or absorbing a photon in a finite-length interaction region, whereas *the emission and absorption frequencies are not prescribed.*

To calculate Δk_{zh}, one should solve the equations

$$\mathcal{E}_{\mathbf{k}_{\perp u}k_{zu}+\Delta k_{zu}/2}-\mathcal{E}_{\mathbf{k}_{\perp d}k_{zd}+\Delta k_{zd}/2}=\hbar\omega\ , \tag{G1}$$

$$k_{zu}+\frac{\Delta k_{zu}}{2}-k_{zd}-\frac{\Delta k_{zd}}{2}=q_z+k_w+\frac{\Delta\theta}{2}\ , \tag{G2}$$

which are obtained from the conservation of energy and momentum conditions in the general case of continuous transverse states, assuming that the homogeneous broadening is due to longitudinal wave-number uncertainty ($\Delta\theta$). Expansion of $\mathcal{E}_{\mathbf{k}_\perp k_z}$ to first order in $\hbar$ around $\mathcal{E}_{\mathbf{k}_{\perp u}k_{zu}}$ and $\mathcal{E}_{\mathbf{k}_{\perp d}k_{zd}}$ in (G1) and using Eqs. (4.30), which defines the expansion centers $\mathbf{k}_u,\mathbf{k}_d$, results in

$$\frac{\Delta k_{zu}}{v_{zu}}=\frac{\Delta k_{zd}}{v_{zd}}\ , \tag{G3}$$

$$\Delta k_{zu}-\Delta k_{zd}=\Delta\theta\ , \tag{G4}$$

where

$$v_{zu}=\frac{1}{\hbar}\frac{\partial\mathcal{E}}{\partial k_z}\bigg|_{\mathbf{k}_u}\quad\text{and}\quad v_{zd}=\frac{1}{\hbar}\frac{\partial\mathcal{E}}{\partial k_z}\bigg|_{\mathbf{k}_d}\ .$$

This results in

$$\Delta k_{zu}=\Delta\theta\frac{v_{zu}}{v_{zu}-v_{zd}}=\frac{v_{zu}}{v_{zd}}\Delta k_{zd}\ . \tag{G5}$$

Since v_{zu} is very close to v_{zd}, we have $\Delta k_{zu}\approx\Delta k_{zd}\equiv\Delta k_{zh}$. The difference between v_{zu} and v_{zd} can be found by using the relation

$$k_z=\frac{p_z}{\hbar}=\frac{\mathcal{E}v_z}{c^2\hbar}\ . \tag{G6}$$

Differentiation of (G6) results in

$$\begin{aligned}\Delta v_z&=v_{zu}-v_{zd}\\&\approx\frac{1}{\mathcal{E}^{(0)}}[\hbar c^2(k_{zu}-k_{zd})-v_z^{(0)}(\mathcal{E}_u-\mathcal{E}_d)]\ .\end{aligned} \tag{G7}$$

We now substitute in (G7) the energy-momentum conservation conditions [Eqs. (4.29) in the intrabranch transition case or Eqs. (4.30) in the case of continuous transverse states]. This results in

$$v_{zu}-v_{zd}=\frac{\hbar}{m\gamma^{(0)}}\left[(q_z+k_{wz})-\beta_z\frac{\omega}{c}\right]\ . \tag{G8}$$

For the intrabranch transitions case one can use the relations $k_{wz}=k_w$, $v_z^{(0)}=v_{z\mathrm{ph}}=\omega/(q_z+k_w)$. This results in

$$v_{zu}-v_{zd}=\frac{\hbar\omega}{m\gamma_{\mathrm{ph}}\gamma_{z\mathrm{ph}}^2v_{z\mathrm{ph}}}\ , \tag{G9}$$

where $\gamma_{\mathrm{ph}}=\gamma^{(0)}$. In the case of continuous transverse

states the difference between v_{zu} and v_{zd} is calculated in the coordinate system, which is aligned with the average electron trajectory ($\hat{e}_z = \hat{e}_e$). Thus we substitute in Eq. (G8) the relation $v_z^{e(0)} = v_{z\mathrm{ph}}^e = \omega/(q_z^e + k_{w,z}^e)$, where q_z^e, k_{wz}^e are the radiation and wiggler longitudinal wave numbers in this coordinates system. This results in

$$v_{zu}^e - v_{zd}^e = \frac{\hbar\omega}{m\gamma_{\mathrm{ph}}\gamma_{z\mathrm{ph}}^{e2} v_{z\mathrm{ph}}^e} . \tag{G10}$$

Both the case of intrabranch transition and the case of continuous transverse states can be described in a unified way by defining $\bar{\gamma}_{\mathrm{ph}}, \bar{v}_{\mathrm{ph}}$ as $\gamma_{z\mathrm{ph}}, v_{z\mathrm{ph}}$ in the first case and, respectively, as $\gamma_{z\mathrm{ph}}^e, v_{z\mathrm{ph}}^e$ in the latter case. Using (G5) the electron wave-number homogeneous width then reads for both of these cases:

$$\Delta k_{zh} = \Delta\theta \frac{m\gamma_{\mathrm{ph}}\bar{\gamma}_{\mathrm{ph}}^2 \bar{v}_{\mathrm{ph}}^2}{\hbar\omega} . \tag{G11}$$

In both cases the *radiative emission can be in an arbitrary direction.* By inspecting (G11), we note that Δk_{zh} would be much wider than $\Delta\theta$ in all practical cases.

The wave number width parameter Δk_{zh} provides a measure of the number of electrons participating in the interaction, in the upper and lower levels, between which transitions take place. This width would become, in principle, an observable parameter if one can measure the electron distribution function after interaction, whence significant energy extraction is assumed to have taken place. At these conditions (nonlinear or saturation regime), there is an effect in the distribution function of "hole burning" around k_{zu} and "pile heaping" around k_{zd} until, at saturation, the bottom of the hole and the top of the pile are at the same levels (population inversion depletion). This repopulation process is illustrated by the dotted areass of Fig. 10(a). The widths of the "hole" and the "pile" are Δk_{zh}, and their areas give a measure of the maximum radiative energy extraction efficiency possible in the warm beam limit (Gover, 1980b; Gover and Sprangle, 1981).

This inhomogeneous saturation mechanism of the FEL in the quantum limit is completely analogous to the known hole-burning effect in inhomogeneously broadened atomic lasers (Yariv, 1975). However, in the classical limit, the saturation characteristics of inhomogeneously broadened free-electron lasers are different than their atomic counterparts. In this limit ($\varepsilon \ll 2\pi$) it is straightforward to show that the homogeneous wave number width (G11) is much wider than the entire recoil momentum (wave number):

$$\Delta k_{zh} \gg q_z + k_w . \tag{G12}$$

All of the electrons in the region $p_{z\mathrm{ph}} - \hbar\Delta k_{zh}/2 < p_z < p_{zh} + \hbar\Delta k_{zh}/2$ can then perform both stimulated emission and absorption transitions with almost equal probability. Consequently, the net emission process saturates only when the electrons redistribute evenly in k_z space within the homogeneous broadening region, and the number of photo-emitting and photo-absorbing electrons becomes the same. This situation is depicted in Fig. 10(b), which indicates how the hole-burning mechanism turns in the classical limit into a process of "plateau formation" on the electron distribution function.

In a FEL oscillator, where many longitudinal modes at many frequencies may develop, this saturation mechanism may lead to a peculiar process of "mode cooperation" [a term coined in extension of the "mode competition" effect in atomic lasers (Yariv, 1975)] and to processes of continuous widening of both the electron beam and optical spectrum (white light lasing). These processes, which have been described in more detail (Gover, 1980b; Gover and Sprangle, 1981), result from the fact that the plateau formation increases the electron distribution slope (and consequently the gain) at wave numbers near the edges of the plateau, and from the fact that in the classical limit a multiphoton emission process is possible.

For the calculation of the inhomogeneous broadening linewidth in Sec. IV.D [Eq. (4.36)] one needs to evaluate $(\partial\theta/\partial k_{zi})$. This parameter can be deduced directly from Eq. (G11):

$$\frac{\partial\bar{\theta}}{\partial k_{zi}} = \frac{\partial\theta}{\partial k_{zi}} \frac{\partial\bar{\theta}}{\partial\theta} \approx L^e \frac{\Delta\theta}{\Delta k_{zh}} = \frac{\hbar\omega L^e}{m\gamma_{\mathrm{ph}}\bar{\gamma}_{\mathrm{ph}}^2 \bar{v}_{\mathrm{ph}}^2} . \tag{G13}$$

The interaction length L^e is measured along the electron beam averaged motion axis.

APPENDIX H: EINSTEIN RELATIONS BETWEEN SPONTANEOUS AND STIMULATED EMISSION

As was delineated in Appendix G, in the quantum limit the free-electron radiator described by (4.15), in the homogeneous broadening regime, or (4.27), in the inhomogeneous regime, is a two-level quantum system. In this sense it is analogous to an atomic radiator or a laser, which are based on transitions between two atomic quantum levels.

Einstein relations between spontaneous emission, stimulated emission, and stimulated absorption, were developed for such a system in a historical paper published in 1917 (Einstein, 1917). It is instructive to understand the correspondence between Einstein's famous A,B coefficients and the radiation parameters that were derived in Sec. IV for the quantum free-electron radiator. In doing that we have to resolve difficulties associated with three differences between the atomic case treated by Einstein and the case of a free-electron radiator treated here. (1) Contrary to the free-electron radiator, the transition energy levels of the atomic radiator are inherent properties of the atom and are independent of the radiation frequency and emission direction. (2) The radiation frequency in the atomic radiator is isotropic (independent of emission direction), contrary to the free-electron case. (3) In Einstein's formulation, both the spontaneous and stimulated emission are discussed in terms of a continuum of radiation modes. This was needed for the indirect proof (based on equating the calculated equilibrium

blackbody distribution to Planck's formula), which was used by Einstein. By contrast, our Eqs. (4.15) and (4.27), derived from modern quantum-electrodynamics theory, refer to a single radiation mode.

Einstein's A,B coefficients are defined in terms of $(W_{21})_{st}$, the stimulated emission radiative transition rate of a single radiator (atom) from upper level 2 to lower level 1, the corresponding inverse transition rate $(W_{12})_{st}$ (stimulated absorption rate) and the spontaneous emission rate $(W_{21})_{sp}$. These rates define the A,B coefficients:

$$(W_{21})_{st}=B_{21}\rho_E(\omega) , \tag{H1}$$

$$(W_{12})_{st}=B_{12}\rho_E(\omega) , \tag{H2}$$

$$(W_{21})_{sp}=A_{21} , \tag{H3}$$

where $\rho_E(\omega)$ is the energy density of the radiation modes, which, in terms of the formulation of this paper, would be interpreted as

$$\rho_E(\omega)=\hbar\omega[\nu_s+(e^{\hbar\omega/kT}-1)^{-1}]\rho(\omega) , \tag{H4}$$

where for box quantization of the radiation modes

$$\rho(\omega)=\frac{\omega^2 V}{\pi^2 c^3} . \tag{H5}$$

Here $\rho(\omega)$ is the total mode density in both polarization states per unit radiation frequency. It is derived by multiplying $(d^2N/d\omega\, d\Omega)_\sigma$ [see Eq. (4.2)] by a factor $2\times 4\pi$, where $\Omega=4\pi$ is the full space solid angle, and 2 stands for the two polarization states.

Einstein's A,B coefficients relations are (Yariv, 1975)

$$B_{21}=B_{12} , \tag{H6}$$

$$\frac{A_{21}}{B_{21}}=\hbar\omega\rho(\omega) . \tag{H7}$$

These relations were derived by Einstein by simply equating at equilibrium the total emission $[(W_{21})_{st}+(W_{21})_{sp}]$ and absorption rate $(W_{12})_{st}$ given by (H1) and then comparing the resultant distribution to Planck's distribution. With present-day basic QED theory, Einstein's relations can of course be derived directly (without resorting to equilibrium limit consideration). This can be shown for atomic radiators by simply comparing the coefficients of the emission terms in a transition rate equation analogous to (4.27), which can be derived for an atomic radiator. However, for a free-electron radiator, this comparison cannot be done straightforwardly. The differences, listed above, between an atomic and a free-electron radiator require some care in the definition of the emission rate parameters $(W_{21})_{st}$, $(W_{12})_{st}$, $(W_{21})_{sp}$ in the latter case.

Since Einstein's transition rates refer to a single radiator (atom) in either the upper or lower level, we define also for the free-electron case $\Gamma^0_{sp}=\Gamma_{sp}/N_e$, which is the single mode spontaneous emission rate per radiator (electron). Furthermore, considering stimulated emission into a continuum of radiation modes, we multiply the emission rate per radiation mode by the number of radiation modes within the solid angle $\Delta\Omega$ and frequency bandwidth $\Delta\omega$ defined by the linewidth for emission around a certain emission frequency center ω_e and emission direction $\hat{e}_{qe}$,

$$W_{21}=\Gamma^0_{sp}[\nu_s+(e^{\hbar\omega/kT}-1)^{-1}]2\frac{d^2N_{q\sigma}}{d\Omega\, d\omega}\Delta\Omega\,\Delta\omega , \tag{H8}$$

$$W_{12}=\Gamma^0_{sp}[\nu_s+(e^{\hbar\omega/kT}-1)^{-1}]2\frac{d^2N_{q\sigma}}{d\Omega\, d\omega}\Delta\Omega\,\Delta\omega . \tag{H9}$$

These equations result from the stimulated emission and absorption parts of Eq. (4.15), in the homogeneous broadening case, when we assume first a single electron in the upper state [for which in the quantum limit $F(\bar{\theta}_{e2})\approx 1$, $F(\bar{\theta}_{a2})\approx 0$], and then a single electron in the lower state [for which $F(\bar{\theta}_{e1})\approx 0$, $F(\bar{\theta}_{a1})\approx 1$]. The parameters $\Delta\Omega$and $\Delta\omega$ can be derived from the linewidth formula. For example, for the finite-length homogeneous broadening line-shape function $F(\bar{\theta})=\mathrm{sinc}^2(\bar{\theta}/2)$ (3.68) with a periodic structure radiator—$\Delta\omega/\omega_0=1/N_w$ and for on-axis radiation $\Delta\Omega=\pi\lambda/L_w$. Alternatively, in the homogeneous regime, Eq. (4.27) or, more generally, Eq. (4.43), would result in similar equations to (H8) and (H9), but with the inhomogeneous broadening linewidth and the corresponding (larger) $\Delta\Omega$ and $\Delta\omega$.

Using definitions (H4), (H5), and (4.2), Eqs. (H8) and (H9) can now be compared with Einstein's transition rate (H1) and (H2), yielding explicit equations for the Einstein B coefficients and proving directly Einstein's first relation in the case of a free-electron radiator:

$$B_{21}=\frac{\Gamma^0_{sp}}{\hbar\omega}\frac{\Delta\Omega}{4\pi}\Delta\omega=B_{12} . \tag{H10}$$

More care must be exercised in the definition of the spontaneous emission rate. Einstein's definition (H3) can be understood as the total spontaneous emission rate in all radiation directions. This parameter can be calculated for free-electron radiators by multiplying the spontaneous emission part of (4.15) by the density of radiation modes (4.2) and integrating over all frequencies and angles:

$$(W_{21})_{sp,tot}=\int_0^\infty \oint \Gamma^0_{sp}F(\bar{\theta})2\frac{d^2N_{q\sigma}}{d\Omega\, d\omega}d\Omega\, d\omega . \tag{H11}$$

For the most practical case of a linewidth function given by $F(\bar{\theta})=\mathrm{sinc}^2(\bar{\theta}/2)$ and a detuning parameter of a periodic structure FEL given by $\bar{\theta}=(\omega/v_z-q_z-k_w)L$, the integration can be carried out explicitly, resulting in the interesting formula

$$(W_{21})_{sp,tot}=\Gamma^0_{sp}\frac{V}{\pi}\frac{k_w^3}{N_w}\beta_{0z}^6\gamma_{0z}^4 . \tag{H12}$$

This is the equation for the total spontaneous emission rate of a free electron in all frequencies and direction, and it is the quantum-mechanical analogue of Larmour's formula (Jackson, 1975).

Evidently the total spontaneous emission rate (H12) is proportional to the stimulated emission rates (H8) and

(H9) and Γ_{sp}^0 cancels out when their ratio is calculated (which is the essence of Einstein relations). However, in order to get a complete formal agreement with Einstein's second relation (H7), and in lieu of the fact that the emission frequency is nonisotropic, it would be preferable to define the Einstein A coefficient of a free-electron radiator in a differential way (as was done in Sec. IV.A). Defining the free-electron spontaneous emission rate $(W_{21})_{sp}$ to correspond to the spontaneous emission rate only into the differential solid angle and frequency segments $\Delta\Omega, \Delta\omega$ [the same ones used in the estimate of the stimulated emission rates (H8) and (H9)], and equating the result with Einstein's A coefficient definition (H3), one obtains the explicit equation for the free-electron radiator A coefficient:

$$A_{21}=(W_{21})_{sp}=\Gamma_{sp}^0 2\frac{d^2N_{q\sigma}}{d\Omega\, d\omega}\Delta\Omega\,\Delta\omega$$

$$=\Gamma_{sp}^0\rho(\omega)\frac{\Delta\Omega}{4\pi}\Delta\omega\ . \qquad \text{(H13)}$$

The ratio between (H13) and (H10) results directly in Einstein's second relation (H7).

REFERENCES

Agdur, B., 1961, in *Crossed-Field Microwave Devices,* edited by E. Okress, G. Mourier, J. Feinstein, and E. Kettlewell (Academic, New York/London), Vol. 11, p. 93.

Andersen, J. U., 1986, private communication with G. Kurizki.

Andersen, J. U., E. Bonderuo, and R. H. Pantell, 1983, Annu. Rev. Nucl. Part. Sci. **33**, 453.

Andersen, J. U., K. R. Eriksen, and E. Laegsgaard, 1981, Phys. Scr. **24**, 588.

Arakawa, Y., and H. Sakaki, 1982, Appl. Phys. Lett. **40**, 939.

Arakawa, Y., H. Sakaki, M. Nishioka, and N. Miura, 1983, IEEE Trans. Electron Devices **30**, 330.

Bachheimer, J. P., 1972, Phys. Rev. B **6**, 2985.

Becker, W., 1980, Opt. Commun. **33**, 69.

Becker, W., and J. K. McIver, 1982, Phys. Rev. A **25**, 956.

Becker, W., and J. K. McIver, 1983, Phys. Rev. A **28**, 1838.

Bekefi, G., 1966, *Radiation Processes in Plasmas* (Wiley, New York).

Bekefi, G., and R. E. Shefer, 1979, J. Appl. Phys. **50**, 5158.

Beloshitskii, V. V., and F. F. Komarov, 1982, Phys. Rep. **93**, 117.

Beloshitskii, V. V., and M. A. Kumakhov, 1978, Zh. Eksp. Teor. Fiz. **74**, 1244 (Sov. Phys. JETP **47**, 652).

Bjorken, J. D., and S. D. Drell, 1965, *Relativistic Quantum Fields* (McGraw-Hill, New York).

Bonifacio, R., 1980, Opt. Commun. **32**, 440.

Bosco, P., W. Colson, and R. A. Freedman, 1983, IEEE J. Quantum Electron. **19**, 272.

Bratman, V. L., G. G. Denisov, N. S. Ginzburg, and M. I. Petelin, 1983, IEEE J. Quantum Electron. **19**, 282.

Bucksbaum, P. H., M. Bashkansky, and T. J. McIlrath, 1987, Phys. Rev. Lett. **58**, 349.

Burdette, E. L., and G. Hughes, 1976, Phys. Rev. A **14**, 1766.

Chu, K. R., and J. L. Hirshfield, 1978, Phys. Fluids **21**, 461.

Chu, A. N., M. A. Piestrup, T. W. Barbee, Jr., and R. H. Pantell, 1980, J. Appl. Phys. **51**, 1290.

Chu, A. N., M. A. Piestrup, R. H. Pantell, and F. R. Buskirk, 1981, J. Appl. Phys. **52**, 22.

Coleman, P. D., and C. Enderby, 1960, J. Appl. Phys. **31**, 1695.

Collin, R. E., 1960, *Field Theory of Guided Waves* (McGraw-Hill, New York).

Datta, S., and A. E. Kaplan, 1985, Phys. Rev. A **31**, 790.

Dattoli, G., J. C. Gallardo, A. Renieri, M. Richeta, and A. Torre, 1985, *Proceedings of the 1984 FEL Conference,* Castelgandolfo, Italy (North-Holland, Amsterdam), p. 93.

Dattoli, G., and A. Renieri, 1983, J. Phys. (Paris) Colloq. **C1**, 125.

Dattoli, G., and A. Renieri, 1985, in *Laser Handbook,* Vol. IV, edited by M. L. Stitch and M. Bass (North-Holland, Amsterdam), p. 1.

Deacon, D. A., L. R. Elias, J. M. J. Madey, G. L. Ramian, H. A. Schwettman, and T. F. Smith, 1977, Phys. Rev. Lett. **38**, 892.

Dekker, H., 1977, Physica C **90**, 283.

Einstein, A., 1917, Phys. Z. **18**, 121.

Elias, L. R., W. Fairbank, J. Madey, H. A. Schwettman, and T. Smith, 1976, Phys. Rev. Lett. **36**, 717.

Fassum, H. J., and B. Ancker-Johnson, 1973, Phys. Rev. B **8**, 2850.

Felch, K. L., K. O. Busby, R. W. Layman, D. Kapilow, and J. H. Walsh, 1981, Appl. Phys. Lett. **38**, 601.

Feynman, R. P., 1961, *Quantum Electrodynamics* (Benjamin, New York).

Fruchtman, A., and L. Friedland, 1983, IEEE J. Quantum Electron. **19**, 328.

Fujiwara, K., 1961, J. Phys. Soc. Jpn. **17**, 2226.

Gea-Banacloche, J., G. T. Moore, and M. O. Scully, 1983, *Free-Electron Generators of Coherent Radiation,* SPIE Proceedings (IEEE, New York), Vol. 453, p. 393.

Gell, Y., J. R. Torstensson, H. Wilhelmsson, and B. Levush, 1982, Appl. Phys. B **27**, 15.

Gover, A., 1976, Ph.D. thesis (California Institute of Technology).

Gover, A., 1980a, in *Free-Electron Generators of Coherent Radiation,* Physics of Quantum Electronics Vol. 7, edited by S. Jacobs, H. Pilloff, M. Sargent III, M. O. Scully, and R. Spitzer (Addison-Wesley, Reading, MA), p. 701.

Gover, A., 1980b, Opt. Lett. **5**, 525.

Gover, A., 1984, in *Free Electron Generation of Extreme Ultraviolet Coherent Radiation,* AIP Conference Proceedings No. 118, edited by J. M. J. Madey and C. Pellegrini (AIP, New York), p. 144.

Gover, A., H. K. Burrell, and A. Yariv, 1974, J. Appl. Phys. **45**, 4847.

Gover, A., P. Dvorkis, and U. Elisha, 1984, J. Opt. Soc. Am. B **1**, 723.

Gover, A., and A. Friedman, 1986, unpublished.

Gover, A., and Z. Livni, 1978, Opt. Commun. **26**, 375.

Gover, A., and P. Sprangle, 1981, IEEE J. Quantum Electron. **17**, 1196.

Gover, A., and A. Yariv, 1975, J. Appl. Phys. **46**, 3946.

Gover, A., and A. Yariv, 1978a, Appl. Phys. **16**, 121.

Gover, A., and A. Yariv, 1978b, in *Novel Sources of Coherent Radiation,* Physics of Quantum Electronics Vol. 5, edited by S. Jacobs, M. Sargent III, and M. Scully (Addison-Wesley, Reading, MA/Palo Alto/London), p. 197.

Grossman, A., T. C. Marshall, and S. P. Schlesinger, 1983, Phys. Fluids **26**, 337.

Hirshfield, J. L., I. B. Bernstein, and J. M. Wachtel, 1965, IEEE J. Quantum Electron. **1**, 237.

Hirshfield, J. L., and V. L. Granatstein, 1977, IEEE Trans. Microwave Theory Tech. **25**, 522.
Hirshfield, J. L., and J. M. Wachtel, 1964, Phys. Rev. Lett. **12**, 533.
Jackson, J. D., 1975, *Classical Electrodynamics,* 2nd ed. (Wiley, New York).
Jelly, J. V., 1958, *Čerenkov Radiation and Its Application* (Pergamon, New York).
Kimura, W. D., D. Y. Wang, M. A. Piestrup, A. M. Fauchet, J. A. Edighhoffer, and R. H. Pantell, 1982, IEEE J. Quantum Electron. **18**, 239.
Kincaid, B. M., 1977, Appl. Phys. **48**, 2684.
Korneyenkov, V. K., and V. P. Shestopalov, 1977, Radio Eng. Electron. Phys. (USSR) **22**, 148.
Kreischer, K. E., and R. J. Temkin, 1983, in *Infrared and Millimeter Waves,* edited by Kenneth J. Button (Academic, New York), p. 372.
Krinsky, S., 1983, IEEE Trans. Nucl. Sci. **30**, 3078.
Krinsky, S., J. M. Wang, and P. Luchini, 1982, J. Appl. Phys. **53**, 5453.
Kroll, N. M., 1982, in *Free-Electron Generators of Coherent Radiation,* Physics of Quantum Electronics Vol. 8, edited by S. Jacobs, G. Moore, H. Pilloff, M. Sargent III, M. Scully, and R. Spitzer (Addison-Wesley, Reading, MA), p. 315.
Kroll, N. M., P. L. Morton, and M. N. Rosenblum, 1981, IEEE J. Quantum Electron. **8**, 1436.
Kumakhov, M. A., 1976, Phys. Lett. **57**, 17.
Kumakhov, M. A., 1977, Phys. Status Solidi B **84**, 41.
Kumakhov, M. A., and R. Wedell, 1977, Phys. Status Solidi B **84**, 581.
Kurizki, G., and J. K. McIver, 1982, Phys. Lett. A **89**, 43.
Kurizki, G., and J. K. McIver, 1984, Nucl. Instrum. Methods B **2**, 67.
Kurizki, G., and J. K. McIver, 1985, Phys. Rev. B **32**, 4358.
Landau, L., 1930, Z. Phys. **64**, 629.
Lau, Y. Y., K. R. Chu, L. R. Barnet, and V. L. Granatstein, 1981, Int. J. Infrared **2**, 373.
Lawson, J. D., 1977, *The Physics of Charged-Particle Beams* (Clarendon, Oxford).
Levush, B., T. M. Antosen, W. M. Manheimer, and P. Sprangle, 1985, Phys. Fluids **28**, 2273.
Madey, J. M. J., 1971, J. Appl. Phys. **42**, 1906.
Madey, J. M. J., 1979, Nuovo Cimento **50**, 64.
Madey, J. M. J., and D. Deacon, 1977, in *Cooperative Effects in Matter and Radiation,* edited by C. M. Bowden, D. W. Howgate, and Hermann R. Robl (Plenum, New York), p. 313.
Marcuse, D., 1980, *Principles of Quantum Electronics* (Academic, New York/London).
McIver, J. K., and M. V. Federov, 1979, Zh. Eksp. Teor. Fiz. **76**, 1996 (Sov. Phys. JETP **49**, 1012).
McMullin, W. A., and G. Bekefi, 1981, Appl. Phys. Lett. **39**, 845.
Mizuno, K., S. Ono, and Y. Shibata, 1973, IEEE Trans. Electron Devices **20**, 749.
Motz, H., 1951, J. Appl. Phys. **22**, 527.
Pantell, R. H., 1980, Phys. Quantum Electron. **7**, 1.
Pantell, R. H., and M. J. Alguard, 1979, J. Appl. Phys. **50**, 798.
Pantell, R. H., G. Soneini, and H. E. Puthoff, 1968, IEEE J. Quantum Electron. **4**, 905.
Philips, R. M., 1960, IRE Trans. Electron Devices **7**, 231.
Pierce, J. R., 1950, *Travelling Wave Tubes* (Van Nostrand, Princeton).
Piestrup, M. A., and P. F. Finman, 1983, IEEE J. Quantum Electron. **19**, 357.
Piestrup, M. A., R. H. Pantell, E. H. Puthoff, and G. B. Rithbart, 1973, J. Appl. Phys. **44**, 5160.
Raman, C. W., and N. S. Nath, 1936, Proc. Indian Acad. Sci. **2**, 406.
Reif, F., 1965, *Fundamentals of Statistical and Thermal Physics* (McGraw-Hill, New York).
Renieri, A., 1984, in *Free Electron Generation of Extreme Ultraviolet Coherent Radiation,* AIP Conference Proceedings No. 118, edited by J. M. J. Madey and C. Pellegrini (AIP, New York), p. 1.
Ride, S. K., and W. B. Colson, 1979, Appl. Phys. **20**, 41.
Rusin, F. S., and G. D. Bogomolov, 1969, Proc. IEEE **57**, 720.
Salisbury, W. W., 1970, J. Opt. Soc. Am. **60**, 1279.
Schiff, L., 1971, *Quantum Mechanics,* 3rd ed. (McGraw-Hill, New York).
Schneider, J., 1959, Phys. Rev. Lett. **2**, 504.
Schnitzer, I., and A. Gover, 1985, Nucl. Instrum. Methods Phys. Res. A **237**, 124.
Schweber, S., 1961, *An Introduction to Relativistic Quantum Field Theory* (Row, Peterson, Evanston/New York).
Shraga, I., Y. Goren, C. Leibovitch, S. Eckhause, and A. Gover, 1986, Appl. Phys. Lett. **49**, 1412.
Smith, S. J., and E. M. Purcell, 1953, Phys. Rev. **92**, 1069.
Solimar, A., and E. Ash, 1966, Int. J. Electron. **20**, 127.
Soln, J., 1981, J. Appl. Phys. **52**, 6882.
Spence, J. C. H., G. Reese, N. Yamamoto, and G. Kurizki, 1983, Philos. Mag. B **48**, L39.
Sprangle, P., and R. Smith, 1980, Phys. Rev. A **21**, 293.
Sprangle, P., J. L. Vonworidis, and W. M. Manheimer, 1981, Phys. Rev. A **73**, 3127.
Steinberg, B., A. Gover, and S. Ruschin, 1986, Phys. Rev. A **33**, 421.
Stenholm, S. T., and A. Bambini, 1981, IEEE J. Quantum Electron. **17**, 1363.
Sumi, M., 1966, Appl. Phys. Lett. **9**, 251.
Terhune, R. W., and R. H. Pantell, 1977, Appl. Phys. Lett. **30**, 265.
Tsu, R., and L. Esaki, 1973, Appl. Phys. Lett. **22**, 562.
Twiss, R. Q., 1958, Aust. J. Phys. **11**, 564.
Uberal, H., 1956, Phys. Rev. **103**, 1055.
Ultrich, R., 1967, Z. Phys. **199**, 171.
Van den Berg, P. M., 1973, J. Opt. Soc. Am. **63**, 1588.
Von Laven, S., J. Branscum, J. Golub, R. Layman, and J. Walsh, 1982, Appl. Phys. Lett. **41**, 408.
Walker, R. L., B. L. Berman, and S. D. Bloom, 1975, Phys. Rev. A **11**, 736.
Weibel, E. S., 1959, Phys. Rev. Lett. **2**, 83.
Wortman, D. E., H. Dropkin, and R. P. Leavitt, 1981, IEEE J. Quantum Electron. **17**, 1341.
Yariv, A., 1975, *Quantum Electronics,* 2nd ed. (Wiley, New York).